CRCLEME
Cooperative Research Centre for
Landscape Evolution & Mineral Exploration

CSIRO
EXPLORATION
AND MINING

AMIRA
Australian Mineral Industries Research Association Limited ACN 004 448 266

OPEN FILE
REPORT
SERIES

SPECTRAL PROPERTIES OF SOIL OVERLYING THE SITES OF THE BOUNTY AND NORTH BOUNTY GOLD MINES, FORRESTANIA REGION, WESTERN AUSTRALIA

T.J. Cudahy, M.J. Lintern and A.R. Gabell

CRC LEME OPEN FILE REPORT 67

February 1999

(CSIRO Division of Exploration Geoscience Report 169R, 1992.
Second impression 1999)

AMIRA
Australian Mineral Industries Research Association Limited ACN 004 448 266

CRCLEME
Cooperative Research Centre for Landscape Evolution & Mineral Exploration

CSIRO
EXPLORATION AND MINING

SPECTRAL PROPERTIES OF SOIL OVERLYING THE SITES OF THE BOUNTY AND NORTH BOUNTY GOLD MINES, FORRESTANIA REGION, WESTERN AUSTRALIA

T.J. Cudahy, M.J. Lintern and A.R. Gabell

CRC LEME OPEN FILE REPORT 67

February 1999

(CSIRO Division of Exploration Geoscience Report 169R, 1992.
Second impression 1999)

CRC LEME is an unincorporated joint venture between The Australian National University, University of Canberra, Australian Geological Survey Organisation and CSIRO Exploration and Mining
Headquarters: CRC LEME c/o CSIRO Exploration and Mining, Private Bag, PO Wembley, Western Australia, 6014

RESEARCH ARISING FROM CSIRO/AMIRA REGOLITH GEOCHEMISTRY PROJECTS 1987-1993

In 1987, CSIRO commenced a series of multi-client research projects in regolith geology and geochemistry which were sponsored by companies in the Australian mining industry, through the Australian Mineral Industries Research Association Limited (AMIRA). The initial research program, "Exploration for concealed gold deposits, Yilgarn Block, Western Australia" (1987-1993) had the aim of developing improved geological, geochemical and geophysical methods for mineral exploration that would facilitate the location of blind, buried or deeply weathered gold deposits. The program included the following projects:

P240: Laterite geochemistry for detecting concealed mineral deposits (1987-1991). Leader: Dr R.E. Smith.
Its scope was development of methods for sampling and interpretation of multi-element laterite geochemistry data and application of multi-element techniques to gold and polymetallic mineral exploration in weathered terrain. The project emphasised viewing laterite geochemical dispersion patterns in their regolith-landform context at local and district scales. It was supported by 30 companies.

P241: Gold and associated elements in the regolith - dispersion processes and implications for exploration (1987-1991). Leader: Dr C.R.M. Butt.
The project investigated the distribution of ore and indicator elements in the regolith. It included studies of the mineralogical and geochemical characteristics of weathered ore deposits and wall rocks, and the chemical controls on element dispersion and concentration during regolith evolution. This was to increase the effectiveness of geochemical exploration in weathered terrain through improved understanding of weathering processes. It was supported by 26 companies.

These projects represented "an opportunity for the mineral industry to participate in a multi-disciplinary program of geoscience research aimed at developing new geological, geochemical and geophysical methods for exploration in deeply weathered Archaean terrains". This initiative recognised the unique opportunities, created by exploration and open-cut mining, to conduct detailed studies of the weathered zone, with particular emphasis on the near-surface expression of gold mineralisation. The skills of existing and specially recruited research staff from the Floreat Park and North Ryde laboratories (of the then Divisions of Minerals and Geochemistry, and Mineral Physics and Mineralogy, subsequently Exploration Geoscience and later Exploration and Mining) were integrated to form a task force with expertise in geology, mineralogy, geochemistry and geophysics. Several staff participated in more than one project. Following completion of the original projects, two continuation projects were developed.

P240A: Geochemical exploration in complex lateritic environments of the Yilgarn Craton, Western Australia (1991-1993). Leaders: Drs R.E. Smith and R.R. Anand.
The approach of viewing geochemical dispersion within a well-controlled and well-understood regolith-landform and bedrock framework at detailed and district scales continued. In this extension, focus was particularly on areas of transported cover and on more complex lateritic environments typified by the Kalgoorlie regional study. This was supported by 17 companies.

P241A: Gold and associated elements in the regolith - dispersion processes and implications for exploration. Leader: Dr. C.R.M. Butt.
The significance of gold mobilisation under present-day conditions, particularly the important relationship with pedogenic carbonate, was investigated further. In addition, attention was focussed on the recognition of primary lithologies from their weathered equivalents. This project was supported by 14 companies.

Although the confidentiality periods of the research reports have expired, the last in December 1994, they have not been made public until now. Publishing the reports through the CRC LEME Report Series is seen as an appropriate means of doing this. By making available the results of the research and the authors' interpretations, it is hoped that the reports will provide source data for future research and be useful for teaching. CRC LEME acknowledges the Australian Mineral Industries Research Association and CSIRO Division of Exploration and Mining for authorisation to publish these reports. It is intended that publication of the reports will be a substantial additional factor in transferring technology to aid the Australian Mineral Industry.

This report (CRC LEME Open File Report 67) is a Second impression (second printing) of CSIRO, Division of Exploration Geoscience Restricted Report 169R, first issued in 1992, which formed part of the CSIRO/AMIRA Projects P243 and 241A.

Copies of this publication can be obtained from:
The Publication Officer, c/- CRC LEME, CSIRO Exploration and Mining, PMB, Wembley, WA 6014, Australia. Information on other publications in this series may be obtained from the above or from http://leme.anu.edu.au/

Cataloguing-in-Publication:
Cudahy, T.J.
Spectral properties of soil overylying the sites of the Bounty and North Bounty gold mines, Forrestania Region, Western Australia
ISBN 0 642 28285 4
1. Spectrophotometry 2. Remote sensing 3. Soils - Western Australia.
I. Lintern, M.J. II. Gabell, A.R. III. Title
CRC LEME Open File Report 67.
ISSN 1329-4768

PROJECT LEADERS PREFACE

The CSIRO-AMIRA Research Program "Exploration for Concealed Gold Deposits, Yilgarn Craton, Western Australia" has, as its overall aim, the development of improved geological, geochemical and geophysical methods for mineral exploration that will facilitate the location of blind, concealed, or deeply weathered gold deposits. The research has been undertaken by three modules; Laterite Geochemistry (AMIRA Project P240), Weathering Processes (AMIRA Project P241), and Remote Sensing (AMIRA Project P243).

The Remote Sensing Project's primary aim is to develop, evaluate and demonstrate new remote sensing techniques tailored to exploration in the deeply weathered terrains of Western Australia. An important part of this strategy is understanding the spectral characteristics of natural materials. This spectral information is often needed for the selection, processing and interpretation of remotely sensed data. Therefore, some of the activity of the P243 project has examined the spectral behaviour of a wide range of regolith materials including weathered gold alteration systems and unmineralised geology (160R, 169R, 234R, 235R, 240R and 244R). These spectral studies have generally proceeded in conjunction with various mineralogical and geochemical investigations by P240 and P241 scientists so that relationships have been established between spectral reflectance and mineralogical/geochemical/physical information.

This study details the results from one of these collaborative investigations for the Bounty and North Bounty gold deposits in the Forrestania region. This deposit was particularly interesting because of the association between pedogenic carbonate and secondary gold.

A.R. Gabell
Project Leader

September, 1992

SUMMARY

Gold exploration in the Yilgarn Craton using spectral remote sensing is difficult for at least two reasons. Firstly, very deep weathering has changed the complex, fresh rock mineralogy to a surface mantle largely consisting of ferric oxides, clays and quartz. Secondly, there is little detailed knowledge of the spectral properties of these weathered surface materials, of very variable crystallinity, overlying gold mineralisation and background areas. To address these problems, some of the studies in the P243 project have concentrated on the measurement and analysis of the 0.4 to 2.5 μm reflectance spectra of a large range of regolith materials overlying gold deposits (reports 160R, 169R and 234R) and background areas (reports 235R and 240R). This study of the spectral properties of weathered materials overlying gold mineralisation at the Bounty and North Bounty deposits, Forrestania region, was conducted in association with P241 mineralogical and geochemical studies on the same samples which meant that spectral information could be directly compared with other physicochemical data.

The exposed regolith units of the study area comprise saprolite, lateritic duricrust and alluvium/colluvium which have developed over mafic, ultramafic and sedimentary parent rocks. Primary gold mineralisation is hosted by shales and cherts. The collection of samples preceded major disturbance of the surface materials by mining. Approximately 100 samples were measured, including 57 near-surface samples from three east-west profiles spanning primary gold mineralisation and background areas, and 25 samples from drill core and costeans, which provided information from deeper down the regolith profile. Only 6 samples were taken from areas overlying primary gold mineralisation and approximately 12 from areas associated with secondary gold.

The spectral results show no evidence for alteration minerals associated with primary gold mineralisation. Only one spectrum from weathered surface materials showed spectral properties related to primary minerals, including absorptions at 1.1 (ferrous iron), 2.306 and 2.384 μm (Mg-trioctahedral silicate). All the other surface samples were characterised by spectral properties related to the products of weathering, namely the ferric oxides (hematite and goethite) and clays (kaolinite and smectite). The spectral variations associated with these weathering products show poor relationships with primary gold mineralisation, though there is information related to the character of the regolith, and possibly secondary gold.

The associated studies found secondary gold, is in places, associated with pedogenic carbonate in the top metre of the soil profile. However, the spectra of even the most carbonate-rich samples showed no evidence for the CO_3^{2-} absorptions in the 2.3 μm wavelength region. This lack of carbonate absorption was found to be caused by insufficient abundance of carbonate, as a laboratory experiment showed 40% by weight of carbonate is required in a given mineral mixture (less than 75 μm particle size) before the absorption at 2.33 μm is recognisable. The soils from the study area contained less than 30% carbonate by weight.

The reflectance data provide other evidence, albeit indirectly, for the presence of pedogenic carbonate. This includes increased albedo, particularly in the visible wavelengths. Also, an intimate relationship between carbonate and smectite was discovered. The smectite is rcognised by characteristic absorptions at 1.4, 1.46, 1.9 and 2.2 μm. The associated XRD analyses confirmed the presence of smectite only after XRD was performed on clay-rich concentrates. Kaolinite is evident in the spectra of carbonate-poor samples and is recognised by absorption doublets at 1.4 and 2.2 μm.

The spectral data show information related to the hematite-goethite ratio. This information is indicated by shifts in the wavelength of the ferric iron charge transfer shoulder, near 0.6 μm, and the crystal field absorption, near 0.9 μm. As with the smectites, XRD did not provide much information on the iron oxide mineralogy. The reflectance data shows the carbonate-poor soils are related to hematite whereas the carbonate-rich soils are related to goethite. The reasons for these changes in the iron oxide mineralogy are not clear but may be related to the effects of Ca and Mg on pH.

The depth of the 0.9 μm absorption was found to correlate with the Fe_2O_3 content. A few soils from primary gold mineralisation show relatively deep 0.9 μm absorption, though further work is required to establish the wider significance of this result as regolith-related variations appear to be more important.

The depth of the 2.2 μm absorption was examined because it can provide information on the relative clay abundances important for discriminating regolith units and possibly gold mineralisation. The 2.2 μm absorption depth was found to correlate with the Al_2O_3 content but a correction factor had to be applied before the 2.2 μm absorption depth could be related to the total clay abundance. This correction is related to the different proportions of Al^{3+} in the smectite and kaolinite structures. The corrected results show the "clay abundances" in the soils over exposed saprolite and lateritic duricrust are similar and that there are no variations spatially related to primary or secondary gold.

The reflectance data provide information consistent with a model for regolith development (report 243R). Important for the interpretation of the Mt Hope regolith is the recognition that pedogenic carbonate (associated with smectite and hematite) overprinted the earlier-formed laterite mineralogy. According to the regolith model, saprolite is characterised by well-crystalline kaolinite and goethite. However, this mineralogy was overprinted by the enrichment of Ca and Mg and the development of smectite, hematite and carbonate.

Regional geochemical sampling and analysis could be assisted using spectral sensing (remote or proximal) by mapping both the surface distribution of pedogenic carbonate and laterite units. Further work is required to establish the significance of more subtle spectral information to gold mineralisation. This subtle information may have to be interpreted in the context of a quantitative regolith model. If for example, gold mineralisation was found to be related to a small increase in the iron oxide content, then larger iron oxide variations, related to regolith development, would first have to be removed (by normalisation ith a pridcted regolith model) so that more subtle information can be enhanced.

CONTENTS

		page
1.0	INTRODUCTION	1
2.0	OBJECTIVES	2
3.0	LOCATION, GEOLOGY, SOILS AND GEOMORPHOLOGY	2
4.0	FUNDAMENTALS OF SPECTRAL PROPERTIES	6
5.0	SAMPLING AND SAMPLE PREPARATION	11
6.0	SPECTRAL MEASUREMENT AND PROCESSING	11
	6.1 Spectrometer	11
	6.2 Spectral Processing	13
	6.3 Correlation and Other Problems	13
7.0	RESULTS	13
	7.1 Primary Minerals	14
	7.2 Iron Oxides	14
	7.3 Clays	22
	7.4 Carbonate	27
8.0	DISCUSSION	29
	8.1 Regolith Characteristics	29
	8.1.1 Iron Oxides	29
	8.1.2 Clays	30
	8.1.3 Carbonates	30
	8.2 Significance to Gold Exploration	31
9.0	CONCLUSIONS	32
10.0	FURTHER WORK	33
11.0	ACKNOWLEDGEMENTS	34
12.0	REFERENCES	35

1.0 INTRODUCTION

Gold exploration in the Yilgarn Craton, using remote sensing techniques, is made difficult by the deep weathering of the regolith and the few detailed spectral studies on weathered materials from this environment. To address this problem, a significant portion of the P243 research activity has concentrated on determining the 0.4 to 2.5 μm reflectance properties of weathered materials overlying gold deposits and background areas. This wavelength region provides information on two of the three major weathering products, namely the iron oxides and clays, and is covered by a variety of airborne and space-borne remote sensing systems. These remote sensing systems are available, or are soon to be available to the exploration industry and include Landsat Thematic Mapper, Daedalus Airborne Thematic Mapper, Geoscan Mk I and II and JERS-1 data. Therefore, understanding the reflectance characteristics of the weathered surface materials, at high resolution, would help evaluate the utility of these remote sensing systems for gold exploration in the deeply weathered mantle of the Yilgarn Craton.

High-resolution spectral studies of Yilgarn gold deposits have been completed for Beasley Creek in the Laverton area (Cudahy and others, 1992a), Bounty in the Forrestania area (this study) and Panglo in the Ora Banda area (Cudahy and others, 1992b). Unlike most of the known Yilgarn gold deposits, the surface environment of these deposits was undisturbed by mining activity at the time of sample collection so the results from these studies can be applied confidently to remote sensing strategies which only map the surface characteristics. The background spectral investigations have been at Laverton (Cudahy, 1992b), Lawlers (Gozzard and Tapley, 1992) and Ora Banda.

Some of these spectral studies have been in association with Gold Project P240 and P241 mineralogical and geochemical investigations, often on the same samples (for example, Lintern 1989; Lintern and others, 1990). This has allowed a direct comparison between spectral information and other analytical data. These comparisons have been supported by laboratory experiments aimed at establishing quantitative relationships between reflectance behaviour and physicochemistry (mineralogy, geochemistry and physical morphology) (this study; Cudahy, 1992c).

These field and laboratory studies, together with published information, have been incorporated into an empirical model relating spectral-physicochemical properties to regolith characteristics and processes typical of the eastern Yilgarn Craton (Cudahy, 1992a). This model provides a mechanism by which unexpected spectral information can be isolated and enhanced as these may provide potential targets for gold mineralisation.

This study examines the 0.4 to 2.5 μm reflectance properties of the weathered surface materials overlying the Bounty and North Bounty gold deposits and compares this information with other physicochemical data, spectral-physicochemical relationships and a regolith model to determine if reflectance information can be used in a quantitative and thematic way by explorationists for finding similar styles of gold mineralisation. In particular, the study concentrated on pedogenic carbonate as an association had earlier been found between carbonate and secondary gold (Lintern, 1989).

2.0 OBJECTIVES

The main objectives of this study were:

1. To investigate whether spectral techniques can be used to identify minerals related to gold mineralisation at Bounty/North Bounty; and

2. To determine the relationships between spectral information and physicochemical characteristics of the regolith of the Mt Hope area.

3.0 LOCATION, GEOLOGY, SOILS AND GEOMORPHOLOGY

The Bounty and North Bounty gold deposits in the Mt Hope area are located approximately 95 km east-northeast of Hyden and 115 km south-southeast of Southern Cross, in the Forrestania region, Western Australia (Figure 1). The terrain is undulating with 25-50 m of local relief. The natural vegetation reflects the topography with scrub heath in the sandplain ridges, mallee in the middle-slopes covering the largest portion of the area and schlerophyll woodlands in the heavy clay soils of the greenstone belts. The density of the vegetation in the schlerophyll woodlands is evenly distributed with approximately 20% of overstorey (eucalypts) and 30% of understorey (shrubs of melaleuca and grasses). Total vegetation cover is approximately 30-50%. An indication of density of the vegetation over the study area is shown in Plate 1.

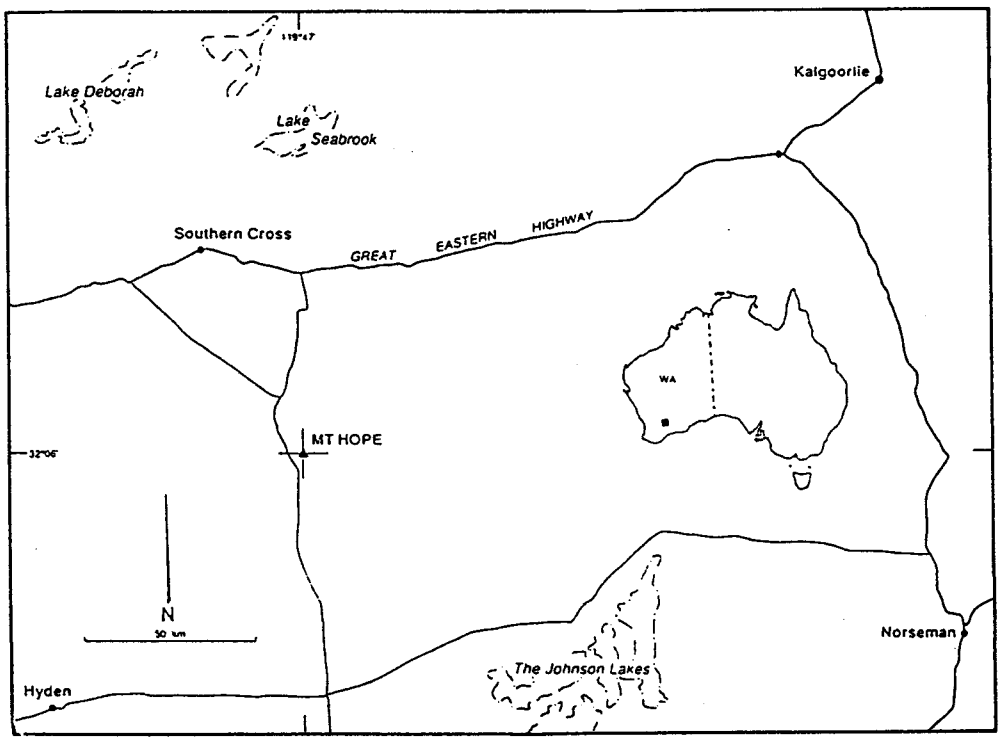

Figure 1: Location map of the Mt Hope study area (after Lintern, 1989).

Plate 1: Young Eucalyptus, small bushes of Acacia and Casia and piles of dry leaf material and branches cover much of the ground.

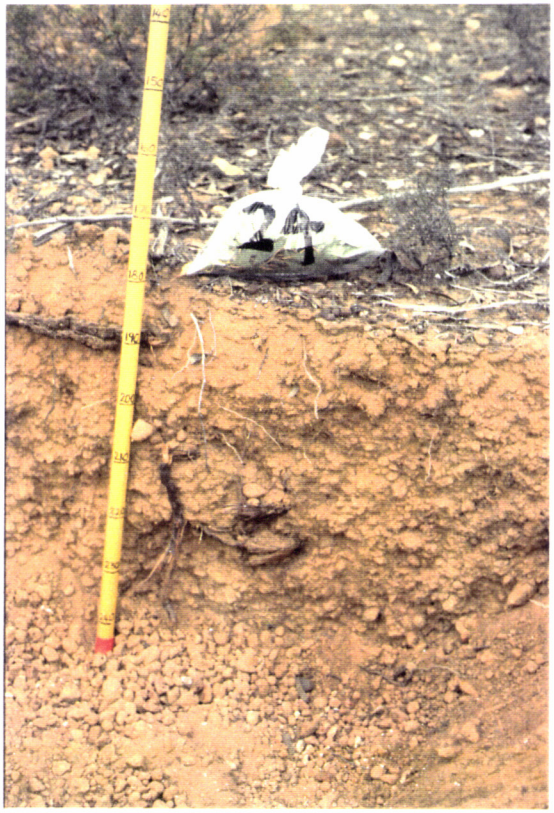

Plate 2: Goethite-rich soil with abundant iron-rich nodules formed over lateritic duricrust.

Plate 3: Hematite-rich soil with pedogenic carbonate (white) formed over saprolite.

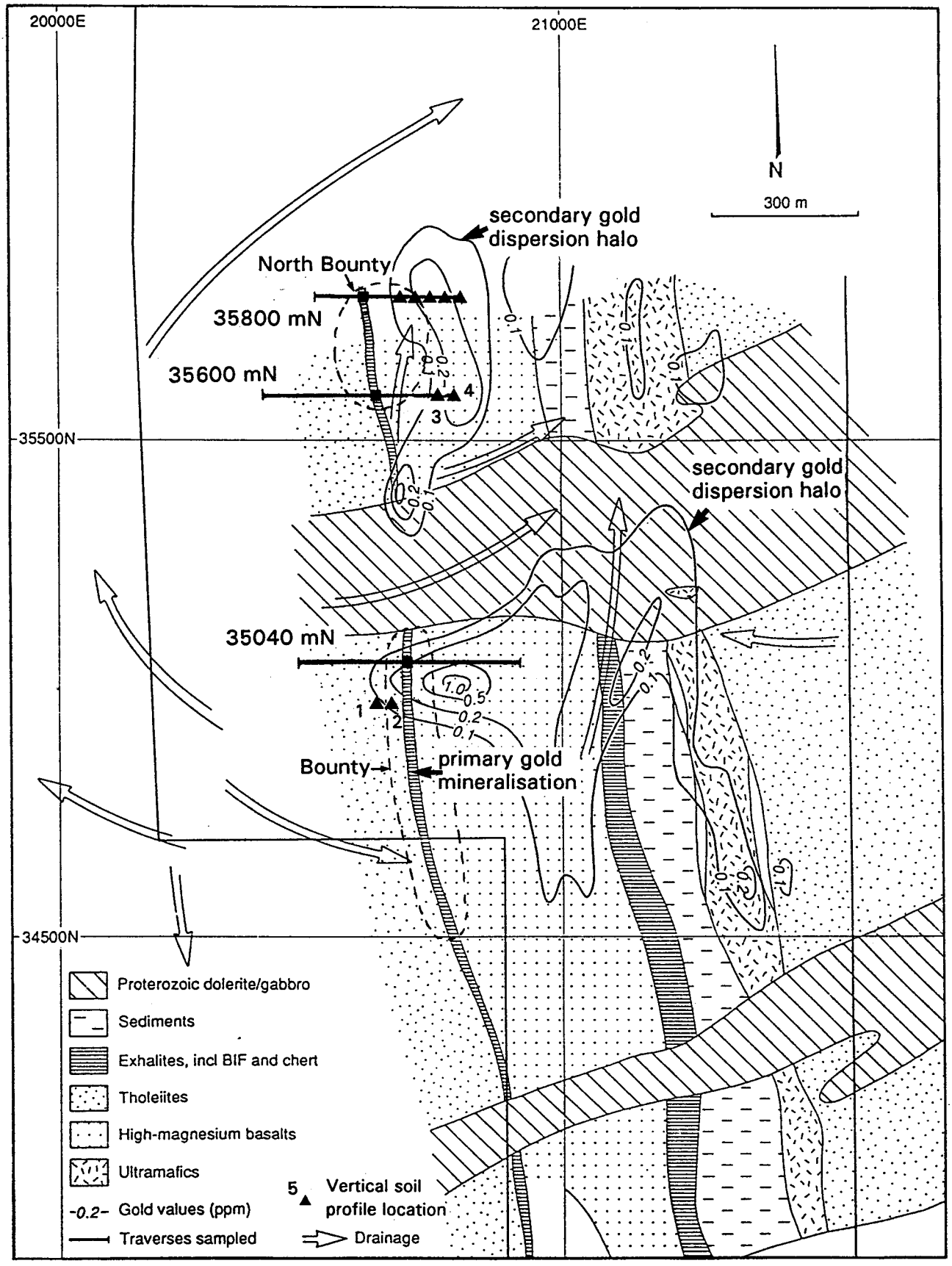

Figure 2: The solid geology of the Mt Hope study area showing the location of the Bounty and North Bounty gold mines, drainage direction, gold dispersion in the soils, the sample traverses and drill core and costean sample sites (after Lintern, 1989).

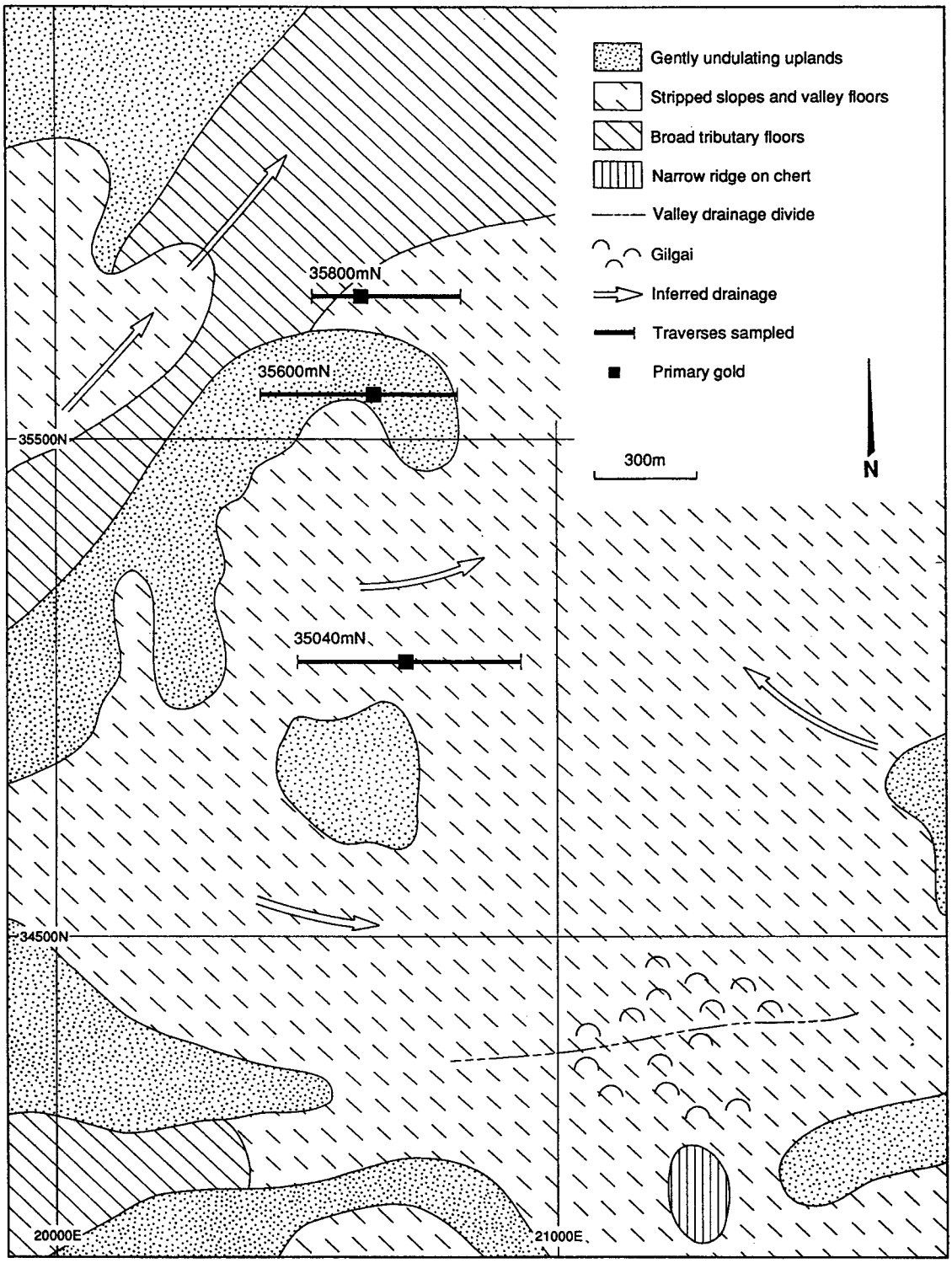

Figure 3: The surface regolith/landform units of the Mt Hope study area (after Lintern and others, 1990).

The region is semi-arid with light winter rains and occasional summer storms averaging 300 mm per annum. Evaporation rates are 1 600 to 1 800 mm per annum and average temperatures range from 17 to 34°C in summer and 4 to 16°C in winter (Chin and others, 1984).

The geology is part of the Forrestania Greenstone Belt which is the southern extension to the Southern Cross Greenstone Belt in the Archaean Yilgarn Craton. The Forrestania Greenstone Belt comprises Archaean rocks of tholeiitic basalts, gabbros, high magnesian-basalts, komatiites, cherts, banded iron formation (BIF), siltstones and sandstones which were structurally deformed into north-south striking fold belts and regionally metamorphosed during the late Archaean (Chin and others, 1984). As all the rocks are metamorphosed to as high as amphibolite grade, the prefix "meta" is implied but not used in this report. Post Archaean geological events included the intrusion of Proterozoic dolerite dykes, Permian glaciation, and Cainozoic deep weathering and lateritisation (Kemp, 1978).

Gold mineralisation within the Bounty and North Bounty deposits is largely restricted to steeply dipping, north-south striking cherts, shales, siltstones and sandstones flanked by non-mineralised dolerite to the west and high Mg-basalts to the east (Figure 2). Komatiites, altered to talc schists, are also found in the area. An east-west striking, 300 m wide, Proterozoic dolerite dyke splits the two zones of mineralisation.

The geomorphology and regolith of the study area comprises uplands typically mantled by deep lateritic cover of preserved duricrust and gravels (Figure 3) with the lower areas showing exposed saprolite and/or alluvium/colluvium. Large areas of calcareous clays occur where erosion has removed the lateritic duricrust (Lintern and others, 1990). Gold mineralisation is located mid-slope on the flank of a broad valley. The soil materials are variable, including, yellow-sandy loams (Plate 2), red loams (Plate 3), grey-brown, sandy clay and red-yellow sand. The transported materials are recognised by gravelly lenses (Lintern and others, 1990).

Pedogenic carbonate developed in the top metre of the soil profile over exposed saprolite and transported cover but not in areas of preserved lateritic duricrust (Lintern, 1989). In places, secondary gold developed with pedogenic carbonate. The secondary gold dispersion halo can be laterally displaced by up to 150 m downslope from the primary mineralisation (Figures 2 and 3).

4.0 FUNDAMENTALS OF SPECTRAL PROPERTIES

The reflectance properties of geological materials, in the 0.4 μm and 2.5 μm, result from electronic/vibrational, atomic/molecular processes and scattering affects. Electronic processes generally involve the movement of electrons associated with transition elements, such as iron, and produce relatively broad absorptions at wavelengths shorter than 1.2 μm (Hunt and others, 1971). Vibrational processes relate to the bending, rotation or stretching of particular anion-cation pairs (such as Al-OH, Mg-OH and H-O-H) and often produce narrow absorptions at wavelengths greater than 1.2 μm.

Scattering affects are generally related to the size of the scattering centres, such as individual crystals (Morris and others, 1985), or collections of crystals joined together as larger particles (Hunt and others, 1971). Scattering can cause changes in the depth and wavelength of absorptions and the albedo (average brightness). Figure 4 shows the affects of scattering on reflectance behaviour caused by changes in the grain sizes. The calcite powder, with less than 75 μm particle size, produces a spectrum with relatively high albedo but relatively shallow CO_3^{2-} absorptions compared to the coarsely crystalline calcite rock spectrum. These scattering effects are approximated by Maxwell's equations (Elachi, 1987).

Iron oxides, clays and carbonates are major products of weathering that have characteristic spectral properties in the 0.4 to 2.5 μm wavelength region. Quartz, another major product of weathering, does not have characteristic absorptions in this wavelength region but there are SiO_2-related features in the mid-infrared (9-14 μm) (Salisbury and D'Aria, in press).

The iron oxides, hematite (αFe_2O_3) and goethite ($\alpha FeHO_2$), possess Fe^{3+} electronic absorptions (Hunt and others, 1971) near 0.5, 0.66 and 0.9 μm (Figures 5a and 5b). The broad absorption band near 0.5 μm is related to a charge transfer effect where electrons are transferred from the ligand to the cation (Hunt and Ashley, 1979). The absorptions at 0.66 and 0.9 μm are related to crystal field effects caused by transitions of the cation's d-shell electrons into different energy levels influenced by the surrounding ligand-field (Hunt and Ashley, 1979).

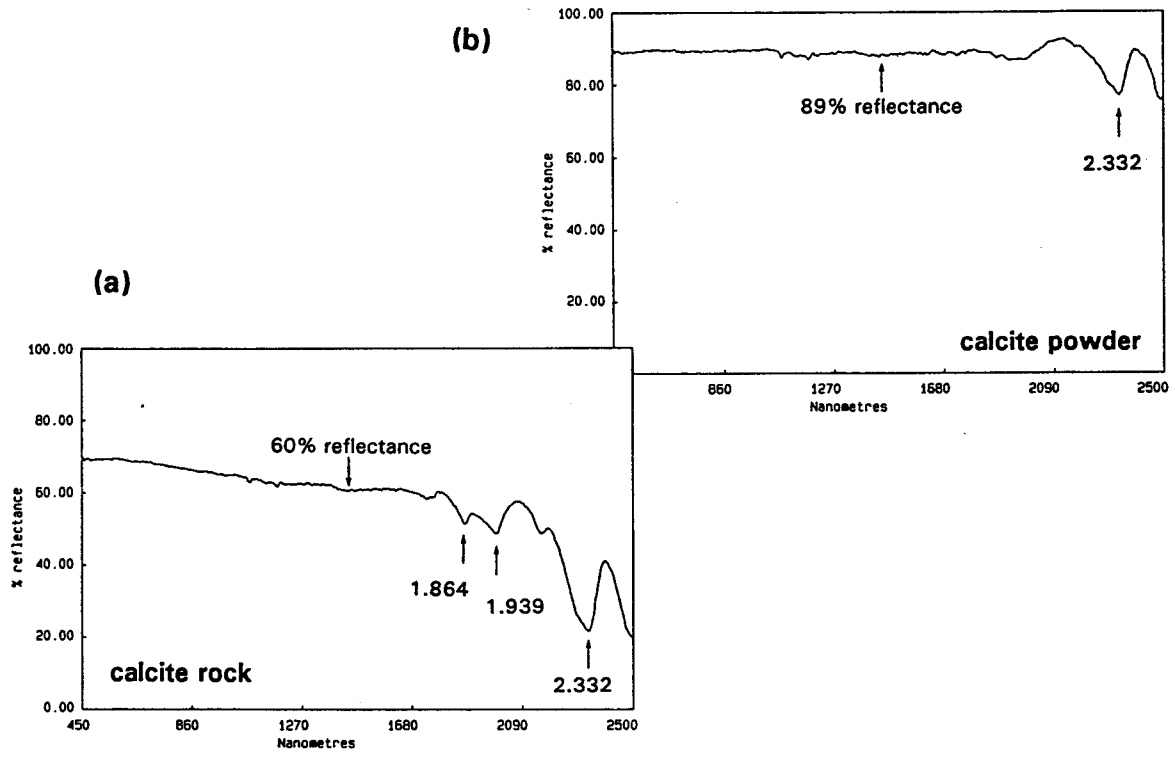

Figure 4: The reflectance spectra of (a) calcite rock, and (b) the same calcite rock but powdered to less than 75 μm particle size.

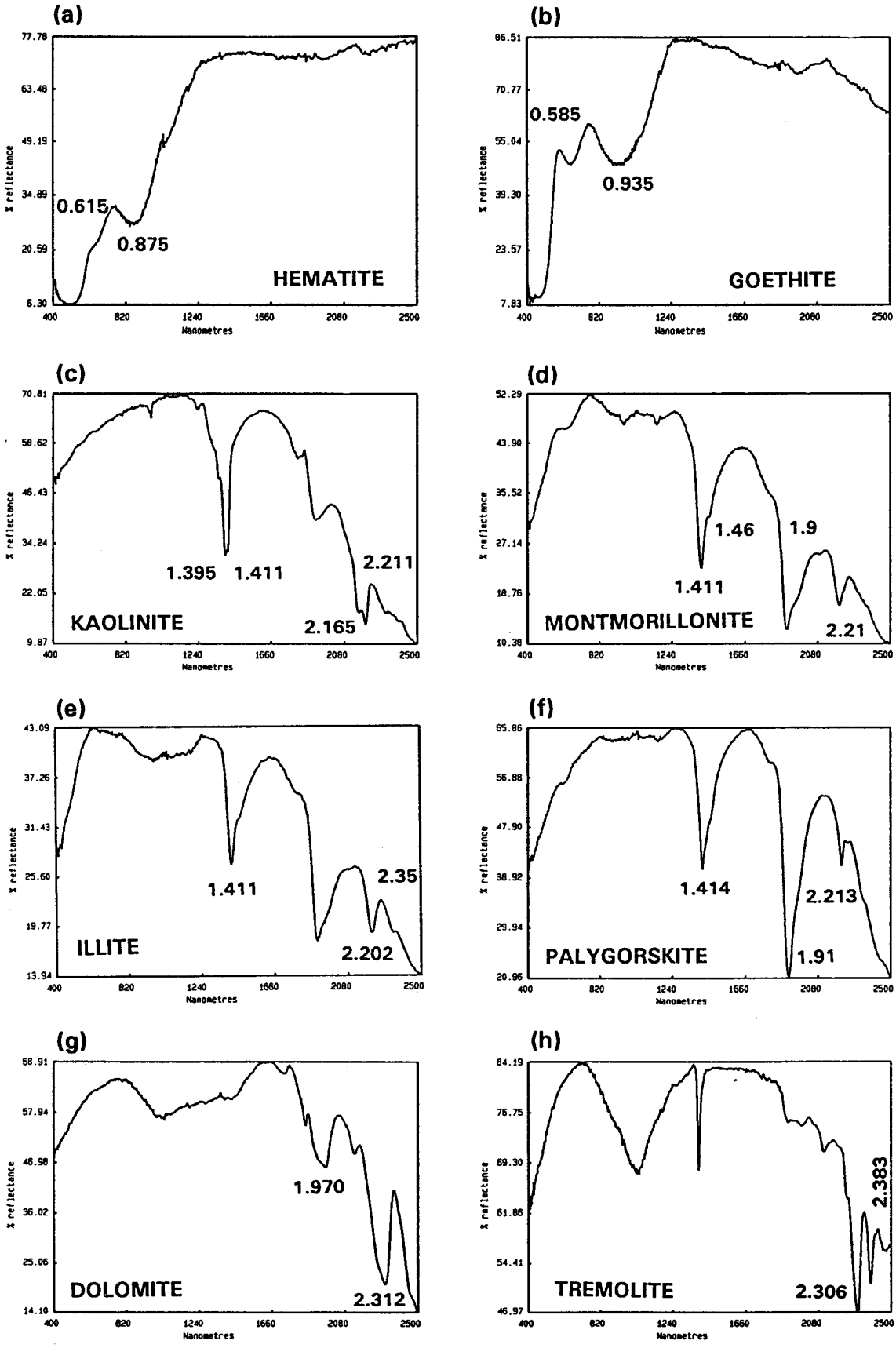

Figure 5: Reflectance spectra of various pure minerals (from the CSIRO Mineral Library).

The Al-bearing clays (kaolinite, smectite and illite) have vibration-related absorptions in the 1.2 to 2.5 μm wavelength region (Figures 5c, 5d and 5e) related to overtones or combination tones of fundamental stretches (ν) or bends (δ) of the Al-OH bonds which absorb at wavelengths greater than 2.5 μm (Farmer, 1974). The spectrum of the Ca/Mg-bearing smectite, montmorillonite (Figure 5d), is characterised by single absorptions at 1.4 μm, 1.9 μm and 2.2 μm which result from the combinations and overtones of molecular H_2O and structural OH. Dioctahedral smectites have high cation exchange capacity in octahedral sites and the interlayers between sheets of SiO_4 tetrahedra (Figure 6) - octahedral substitution of Al^{3+}, Fe^{3+} and Mg^{2+} and interlayer substitution Ca^{2+}, Na^{+}, K^{+}, Mg^{2+} and H_2O are possible. The 2.2 μm absorption is a combination of the fundamental stretching (ν_{OH} = 2.75 μm) and bending (δ_{OH} = 11.8 - 10.9 μm) vibrations of the OH group bonded to the octahedrally coordinated cations (Clark and others, 1990). Interlayer (exchangeable) cation composition and molecular water have little affect on the 2.2 μm band as they exist at a relatively large distance from the structural OH. The deep asymmetric 1.9 μm feature is often typical of smectite clays (Figure 5d) and is a function of two absorptions. The sharp absorption at shorter wavelengths (1.905 - 1.911 μm) is a combination band of fundamental stretching (ν_{water} = 2.76 μm) and bending (δ_{water} = 6.12 μm) vibrations of weakly hydrogen-bonded interlayer water molecules. A broader absorption caused by the fundamental stretching (ν_{water} = 2.92 μm) and bending (δ_{water} = 6.12 μm) of strongly hydrogen bonded water molecules appears at longer wavelengths (1.949 - 1.978 μm). The hydrogen bonding takes place with the exchangeable cations and tetrahedral oxygens (Figure 6). The asymmetric 1.4 μm feature also consists of two distinct combination bands but there is some argument regarding their cause. The longer wavelength band (1.46 μm) appears to

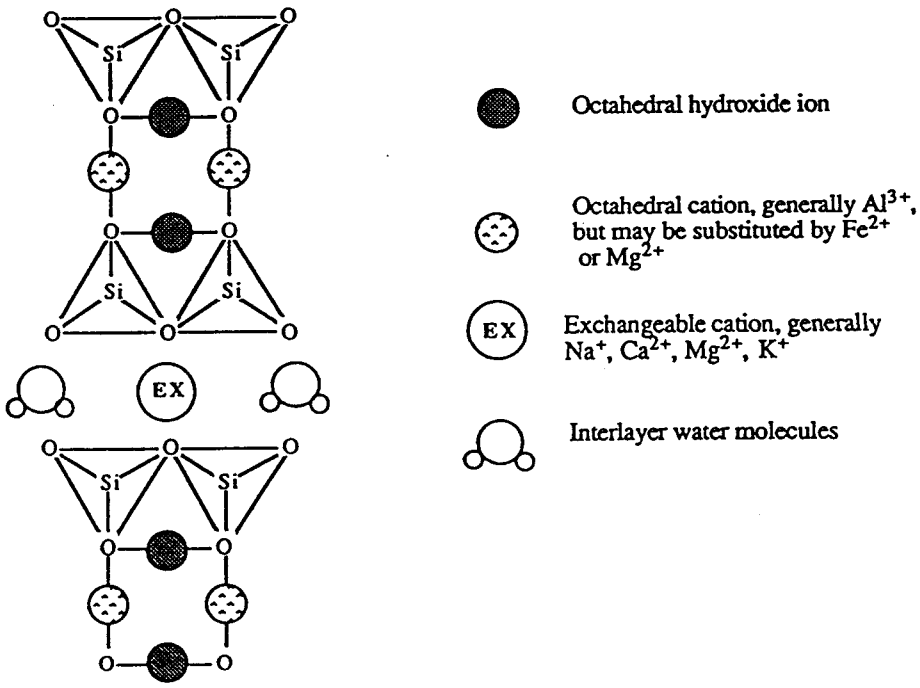

Figure 6: The structure of montmorillonite showing the 2:1 coordination of octahedral sheets and tetrahedral sheets. The interlayer between the SiO_4 tetrahedra may be filled with molecular water and exchangeable cations.

be a combination of the strongly hydrogen-bonded water molecule stretching vibration (ν_{water}) and an overtone of the fundamental stretching vibration, whereas the shorter wavelength band (1.41 μm) appears to be associated with an overtone of the structural OH stretching vibration (ν_{OH}) (Bishop, 1988).

The kaolinite spectrum (Figure 5c) shows overtone or combination-tone absorptions at 1.394, 1.403 and 1.413 (all related to $2\nu_{OH}$), 1.829 μm ($\nu_{OH}+2\delta'_{OH}$), 2.167 μm ($\nu_{OH}+\delta_{OH}$), 2.207 μm ($\nu_{OH}+\delta_{OH}$), 2.32 μm ($\nu_{OH}+\delta'_{OH}$) and 2.387 μm ($\nu_{Al\text{-}O}+\nu_{OH}$) (Clark and others, 1990). The closely spaced absorption pairs at 1.394 and 1.403 μm and 2.165 and 2.207 μm produce the characteristic doublets of the kaolinite spectrum. Weaker 1.394 and 2.165 μm absorptions may be related to more poorly crystalline kaolinite (Crowley and Vergo, 1988) though this behaviour may also be caused by mixing with other Al-bearing dioctahedral silicates.

Carbonates possess vibration-related absorptions between 1.6 μm and 2.5 μm (Figure 5g) caused by overtone and combination tones of stretching and bending vibrations of the CO_3^{2-} radical, or CO_3^{2-} with lattice vibrations (Hunt and Salisbury, 1971). The strongest CO_3-related absorption is located at 2.332 μm caused by an overtone of an antisymmetric stretching mode, ν_3. Other prominent absorptions are located at 1.864 μm, caused by the $2\nu_1 + 2\nu_3$ combination, and at 1.989 μm caused by $\nu_1 + 3\nu_3$ combination (Clark and others, 1990). The replacement of Ca^{2+} by Mg^{2+} or Fe^{2+} changes the wavelength and geometry of these absorptions. Figure 7 summarises the major absorptions discussed above.

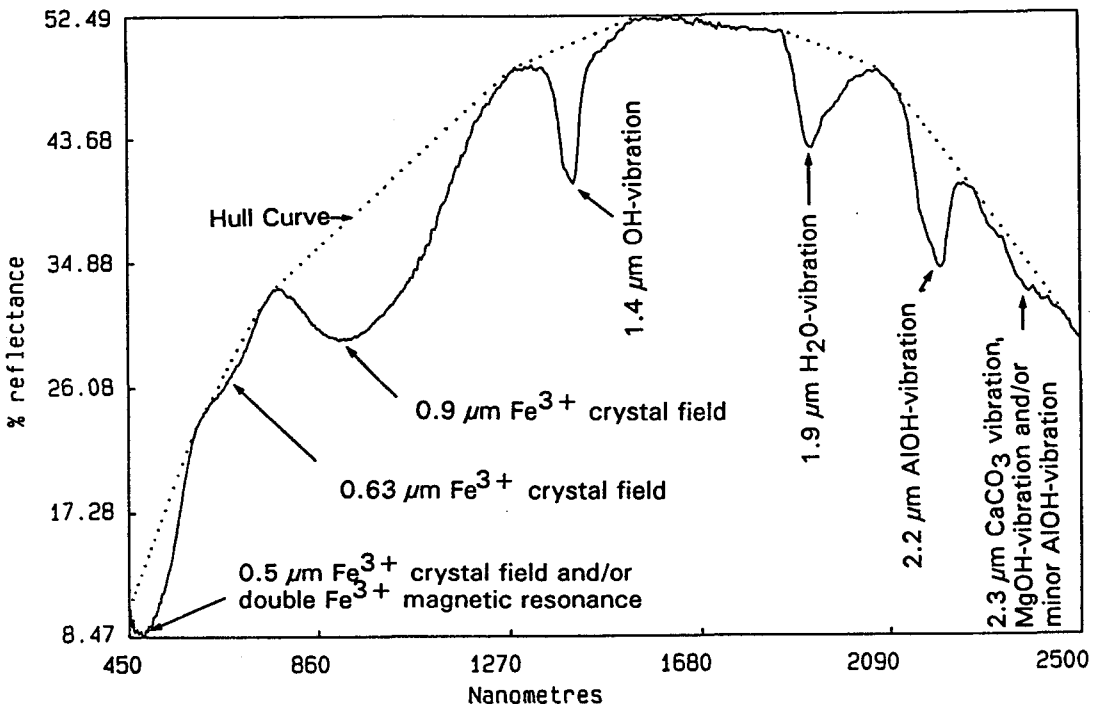

Figure 7: Reflectance spectrum of a typical soil showing the major absorptions with explanations.

5.0 SAMPLING AND SAMPLE PREPARATION

The soil samples for spectral measurement were collected prior to any disturbance by mining activity of the surface materials. These samples were from:

1. Three east-west traverses spanning the ore zones at Bounty and North Bounty and extending into background areas; and

2. Nine vertical profiles (Figure 2).

The surface sample spacing ranged from 10 to 50 m intervals with the closer spacing located over the ore zone. The samples from lines 35600 mN and 35800 mN were collected from the top one metre of the soil profile. Both of these lines span the North Bounty mineralisation with line 35600 mN positioned over preserved lateritic duricrust and line 35800 mN positioned over transported materials and exposed saprolite (Figure 3). The XRF oxide analyses of soil from line 35600 mN (Figure 8a) show low SiO_2 (<60%), variable Al_2O_3 (3-30%) and Fe_2O_3 (7-35%) contents (Lintern, 1989). The XRF oxide analyses of soil from line 35800 mN (Figure 8b) showed high SiO_2 (60-78%) and low Al_2O_3 (9-13.5%) and Fe_2O_3 (4-9%) contents (Lintern, 1989). The soils from line 34050 mN were collected from the upper 5 mm of the soil horizon. This line transects Bounty mineralisation in an area of exposed saprolite (Figures 2 and 3). Limited geochemical/mineralogical data are available for this line.

There was no preparation of the soil samples prior to the initial measurement of the soil reflectance spectra, though sample preparation was required for later experiments, including:

1. The addition of powdered calcite to a sample; and

2. The addition of HCl to remove carbonate from samples;

These experiments are described in more detail in Appendix 2.

6.0 SPECTRAL MEASUREMENT AND PROCESSING

6.1 Spectrometer

The bi-directional reflectance spectra of the soil samples were measured using an "Infrared Intelligent Spectrometer" (IRIS) manufactured by Geophysical Environmental Research Limited (GER). The IRIS measures 875 separate channels between 0.35-3.0 μm. The sampling intervals are approximately 0.002 μm (2 nm) over the 0.35-1.0 μm region, 0.004 μm (4 nm) over the 1.0-1.8 μm region and 0.005 μm (5 nm) over the 1.8-3.0 μm region. The spectral resolution is approximately 0.010-0.012 μm (10-12 nm) in the 2.0 to 2.5 μm region.

(a)

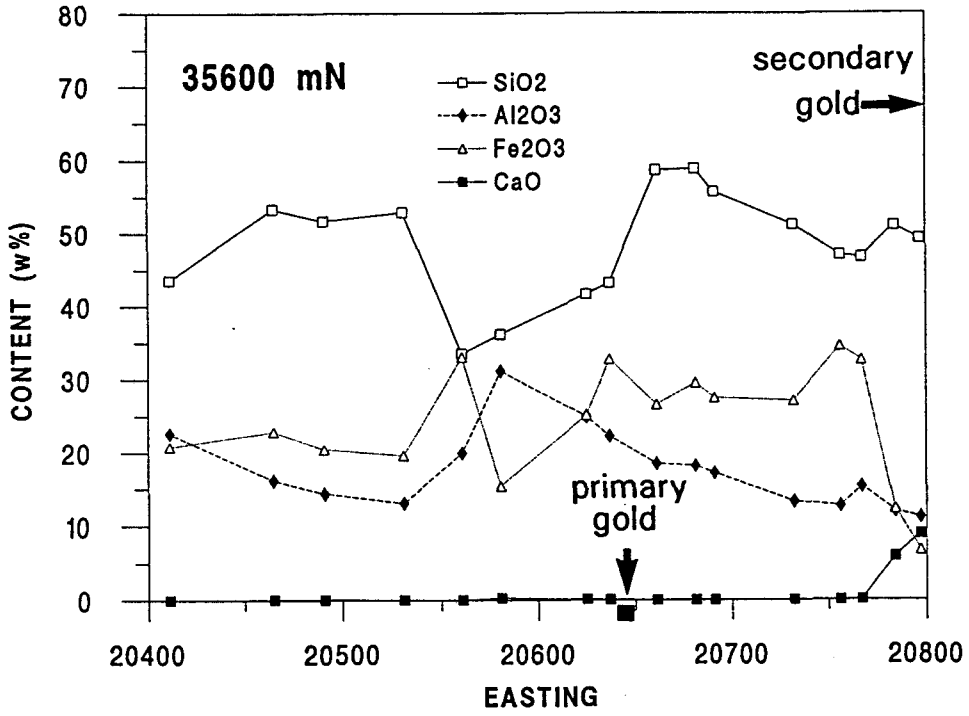

(b)

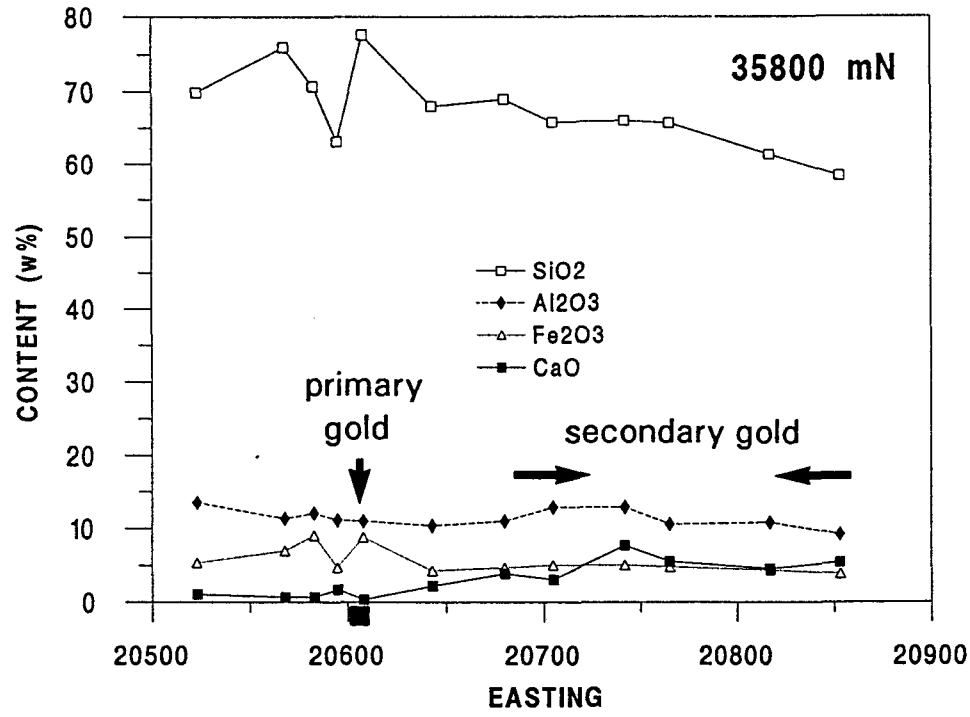

Figure 8: The SiO_2, Al_2O_3, Fe_2O_3, and CaO analyses plotted against the sample location for traverses (a) 35600 mN and (b) 35800 mN. The locations of primary gold mineralisation and the secondary gold dispersion are indicated (after Lintern, 1989).

The IRIS is a dual-beam instrument which simultaneously measures both the target and reference plates. This reduces the effects of instrument drift and any variations in lighting and humidity. Three diffraction gratings mounted on a motor-driven axis disperse the light into the different wavelengths. Silicon detectors measure the first 460 channels and lead sulphide detectors measure the remaining channels.

Barium sulphate or Spectralon (polytetraflouroethylene or PTFE) plates were used as reflectance standards. A quartz-halogen photoflood light provided the source of illumination angled approximately 20° to the vertical and positioned 800 mm from the target/reference. The target and reference plates were located approximately 400 mm from the IRIS optical head such that the area sensed was approximately the 20 by 40 mm. The soil and lag samples were presented to the IRIS in washed petri dishes.

6.2 Spectral Processing

Each spectrum was assigned a unique 9 character code describing all the attributes for that measurement (Appendix 1). The reflectance data were processed using CSIRO's PCSpectra software where the wavelength, symmetry and depth of absorptions were measured to provide information about the composition, abundance and crystallinity of minerals. In addition to reflectance spectra, hull quotient curves (HQ) were also investigated because absorption features are enhanced using this technique (Green and Craig, 1985). Ratios of reflectances were also used to measure the relative depth and geometry of selected absorptions and to measure changes in the wavelength of particular spectral features. However, ratios can be affected by changes in albedo (Cudahy, 1992c) and so care was taken when using this information.

6.3 Correlation and Other Problems

A major problem in relating reflectance information to other analytical data is knowing what part of the sample has been measured. For example, spectral reflectance and scanning electron microscope (SEM) techniques measure the outer few microns of a material (surface) whereas techniques such as X-ray diffraction (XRD), inductively coupled plasma (ICP) and X-ray fluorescence (XRF) measure a bulk property (volume). No compensation was made for this problem.

Two variables were considered correlated if their correlation coefficient (r^2) exceeded the 99% confidence level for the number of samples considered in the analysis (assuming gaussian distribution).

7.0 RESULTS

The reflectance spectra of approximately 70 surface soil samples and 15 subsurface samples, together with associated tables, are presented in Appendix 4. Descriptions and grid locations for these samples are provided in Appendix 3. Some of the general properties of the spectra are described first, then details of the relationships between spectral properties and physicochemical information are described later.

The spectra of the surface soil are plotted together for the different traverses in Figure 9. These data show consistent spectral information for each traverse but considerable differences between traverses. These differences are related to the wavelengths, geometries and depths of absorptions at 0.5, 0.9, 1.4, 1.9, and 2.2 μm. These absorptions are characteristic of ferric oxides and clays which appear to be consistent in composition for each traverse.

The reflectance spectra of the materials from deeper in the weathering profile are plotted together for each drill hole and costean in Figure 10. These data show considerable variation down the weathering profile. The deepest samples (>35 m depth) show absorption over a wide wavelength range, causing low albedo. This character is related to ferrous iron, possibly within magnetite and/or amphibole. Samples from higher in the profile show brighter albedo (no ferrous iron) and absorptions related to ferric oxides (0.4 to 1.1 μm absorptions) and clays (2.2 μm absorptions).

Therefore, the spectra show information related to primary minerals (Section 7.1), iron oxides (Section 7.2) and clays (Section 7.3), Carbonate spectral properties are not apparent (Section 7.4).

7.1 Primary Minerals

The spectra of the near surface materials (upper 10 m of the profile) show little information related to primary minerals. Only one sample, AFLSAA.217 (Appendix 4.1), shows absorptions related to primary minerals. These absorptions are located at 1.1 (related to ferrous iron), 2.306 and 2.385 μm (related to MgOH-bearing trioctahedral silicate). XRD analyses found tremolite-actinolite in this sample which accounts for these Fe^{2+} and MgOH-related absorptions (Figure 5h). The broad Fe^{2+} absorption, centred at 1.1 μm, also causes a distinctive right-handed asymmetry to the spectrum.

The presence of amphibole indicates incomplete chemical weathering of a mafic- and/or ultramafic-derived soil (discussed in Section 8.1). Locally, mafic saprock float is found over exposed Proterozoic dykes.

7.2 Iron Oxides

This section examines, in greater detail, the reflectance data for iron oxide information, including the hematite-goethite ratio and ferric oxide abundance.

Changes in the proportion of hematite to goethite were measured using the wavelengths of the charge transfer long-wavelength shoulder, near 0.6 μm, and the crystal field absorption near 0.9 μm (Figures 5a and 5b). In theory, the charge transfer shoulder is located closer to 0.585 μm for goethite-rich materials and closer to 0.620 μm for hematite-rich materials. Similarly, the crystal field absorption is located closer to 0.86 μm for hematite-rich materials and 0.94 μm for goethite-rich materials. Cudahy (1992c) found that variations with the wavelengths of these parameters provided a quantitative

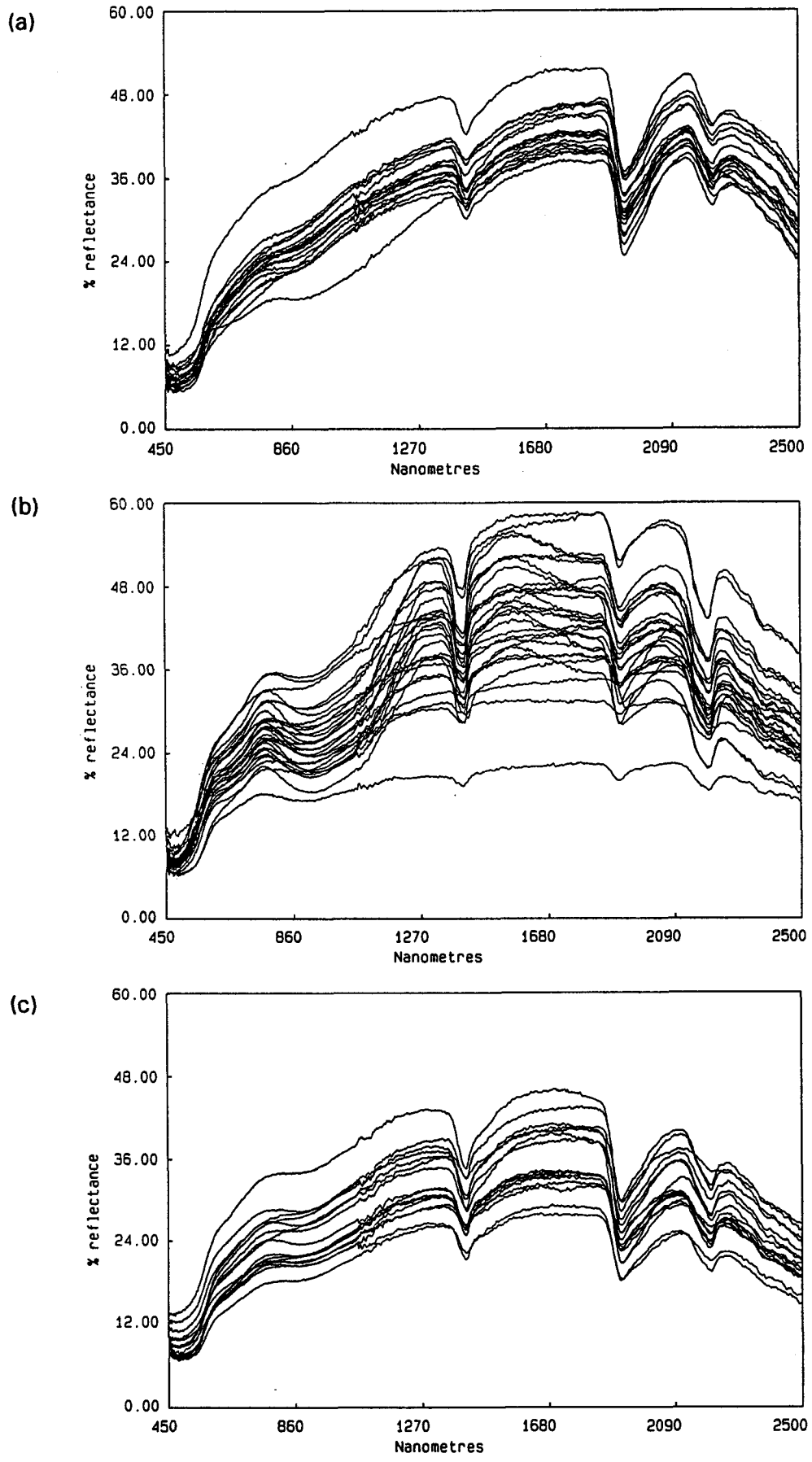

Figure 9: The reflectance spectra from soils taken from lines (a) 35040 mN, (b) 35600 mN, and (c) 35800 mN.

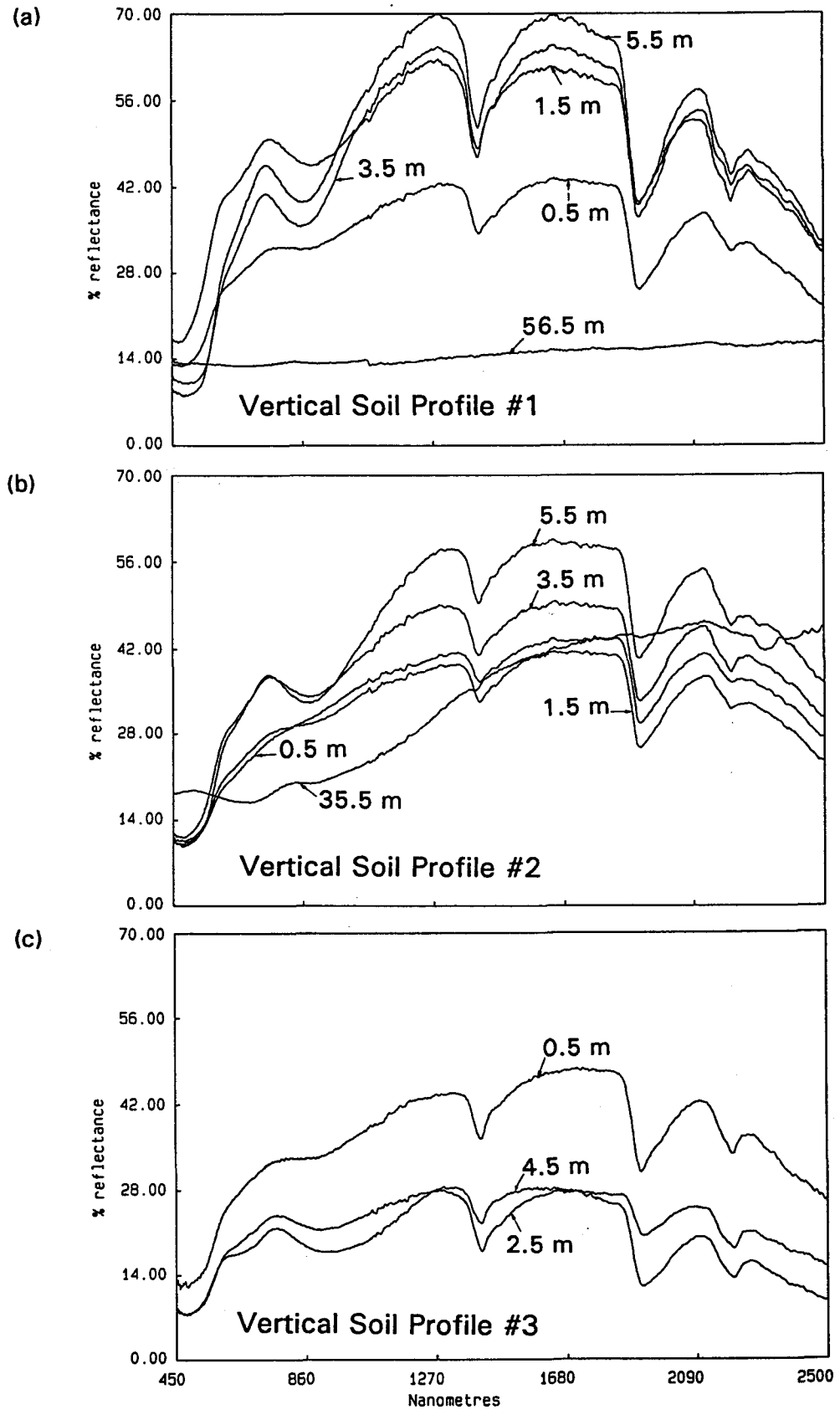

Figure 10: The reflectance spectra of subsurface samples from (a) drill core from 34960 mN - 20645 mE, (b) drill core from 34960 mN - 20676 mE, (c) drill core from 35600 mN - 20797 mE, (d) drill core from 35600 mN - 20784 mE, (e) surface samples from a costean located along 35800 mN, and (f) samples collected from 3-4 m depth along the same costean as (e).

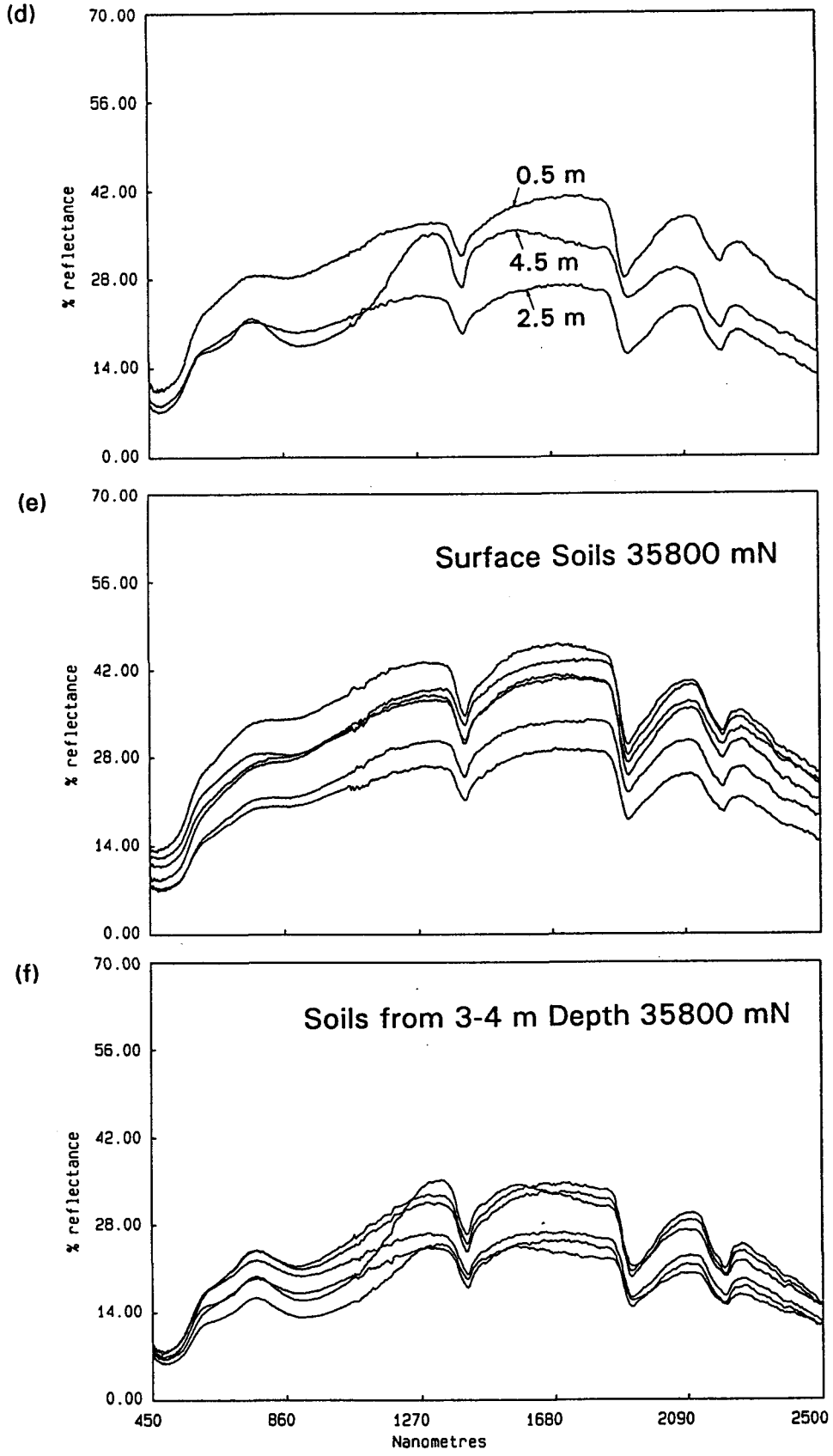

Figure 10 (cont.): The reflectance spectra of subsurface samples from (a) drill core from 34960 mN - 20645 mE, (b) drill core from 34960 mN - 20676 mE, (c) drill core from 35600 mN - 20797 mE, (d) drill core from 35600 mN - 20784 mE, (e) surface samples from a costean located along 35800 mN, and (f) samples collected from 3-4 m depth along the same costean as (e).

estimate for the hematite-goethite ratio, given certain constraints. These constraints are related to the degree of Al^{3+}-substitution in the iron oxide lattice (Buckingham and Sommer, 1983), the crystal size (Morris and others, 1985), possibly the particle size and the state of hydration (Cudahy, 1992c).

The wavelengths of the charge transfer long-wavelength shoulder and crystal field absorption minima were visually determined from both reflectance and hull quotient spectra. A better technique for calculating these parameters involves fitting mathematical functions to the spectral curves (segments) and using derivative information to determine the wavelength of the absorption minimum and the shoulder edge (Cudahy, 1992c). This technique was tested for a few spectra and compared with the visually determined results which showed high correlation.

The results for the wavelengths of the charge transfer shoulder and crystal field absorption of the surface soil spectra are presented in Figure 11. The soils from line 35600 mN are goethite-rich and the soils from line 35040 mN are hematite-rich. Variations across the traverses (Figures 12b, 12c and 12d) are small, except for line 35600 mN (Figure 12b), which shows a change from goethite-rich to hematite-rich from west to east. This enrichment in hematite to the east is associated with an enrichment in smectite (Section 7.3) and carbonate (Section 7.4).

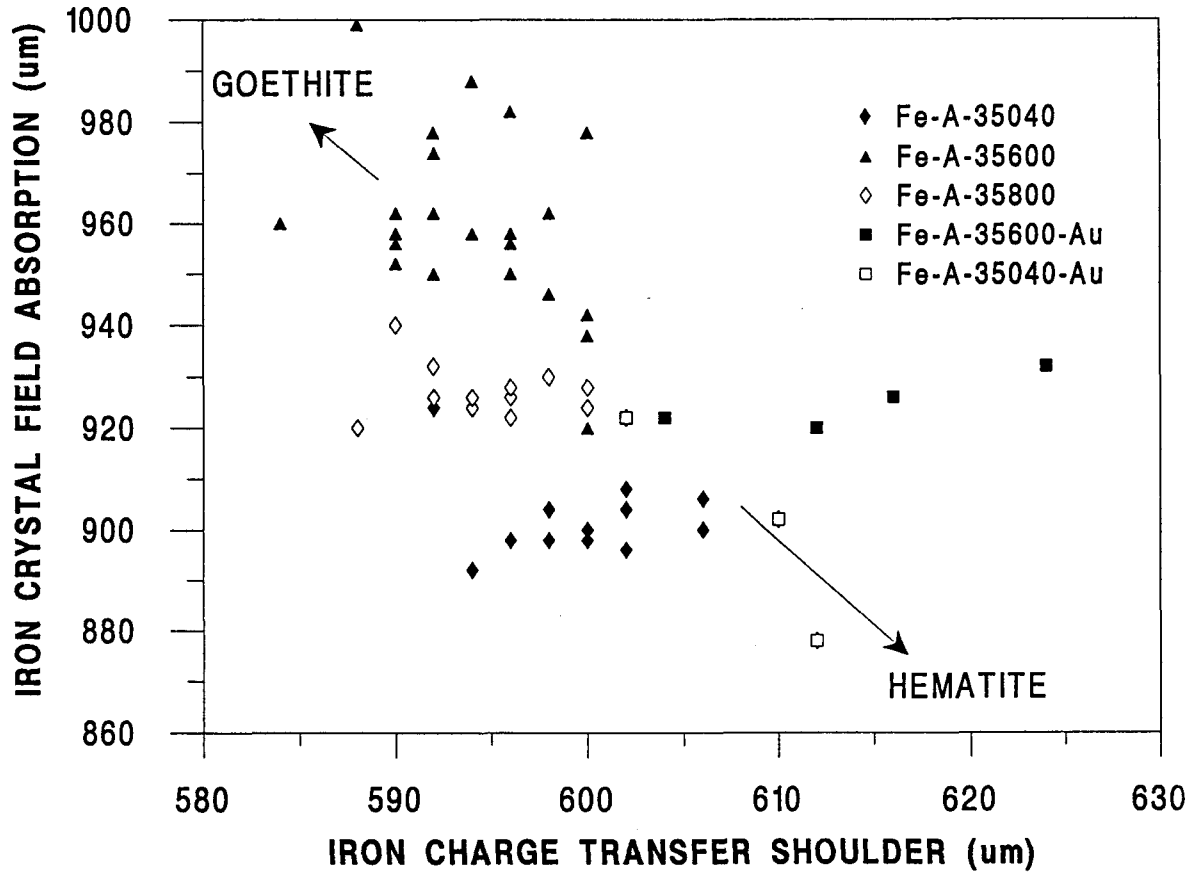

Figure 11: The wavelengths of the Fe^{3+} charge transfer shoulder and crystal field absorption plotted against each other for the surface soils.

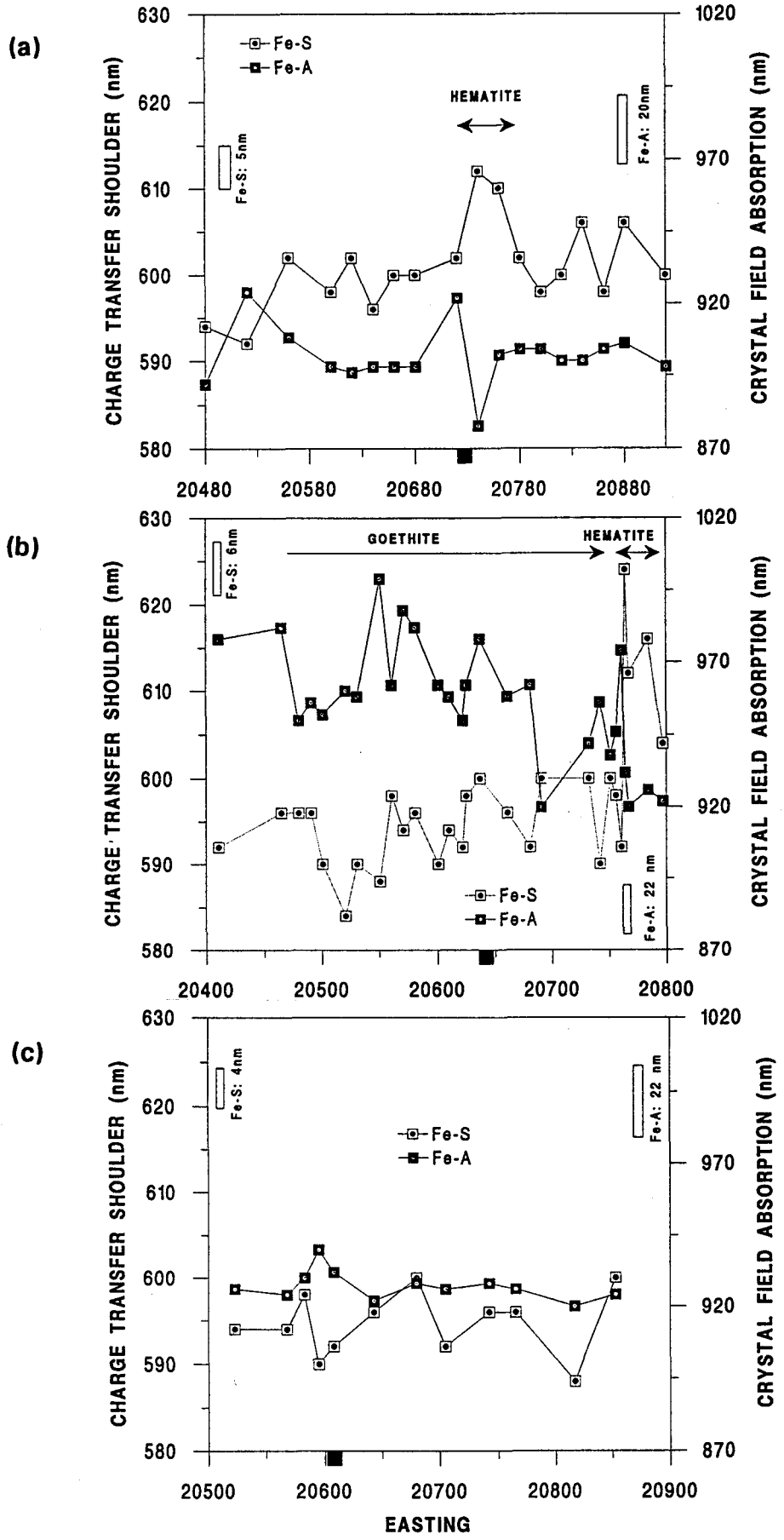

Figure 12: The wavelengths of the Fe^{3+} charge transfer shoulder and crystal field absorption plotted against the traverse location for the surface soils. The location of the primary gold is located as a small box.

The hematite-goethite ratio changes considerably down the weathering profile. The subsurface materials from 34960 mN (Figures 10a and 10b) generally become more hematite-rich with increasing depth down to 5.5 m. Conversely, the subsurface materials from 35600 mN and 35800 mN (Figures 10c to 10f) appear to be more goethite-rich with increasing depth down to approximately 4m. The reasons for these opposite relationships are not clear (Section 8.2).

The XRD analyses of these samples (Lintern, 1989) found little evidence for iron oxides. This lack of discrimination is related to the small concentrations of iron oxide in these materials and suggests that reflectance techniques may be better for deriving iron oxide information. An attempt was made to quantify the hematite-goethite ratio using the relationships established by Cudahy (1992c) but the results were unsatisfactory, possibly because of the types of problems discussed above.

The iron oxide abundances were tested using the relative depth of the 0.9 μm crystal field absorption. Cudahy (1992c) found the reflectance from the top of the reflectance peak near 0.76 μm, divided by the reflectance from the crystal field absorption minima was correlated with the iron oxide content and not significantly affected by the particle size or the hematite-goethite ratio. The iron oxide reflectance ratio, when applied to the Bounty soil spectra, shows significant correlation with the Fe_2O_3 abundances (Figure 13). There is a weak increase with the value of the reflectance ratio associated with gold mineralisation. However, this increase is small compared to the iron oxide-rich soils overlying lateritic duricrust in contrast to the soils mantling exposed saprolite (Figure 14) (discussed in Section 8.1). The subsurface materials (Figure 10) generally show the depth of the 0.9 μm crystal field absorption is deeper compared to the spectra of the soils overlying them. This suggests that pedogenesis in this area involves a process of relative and/or absolute depletion of iron oxide.

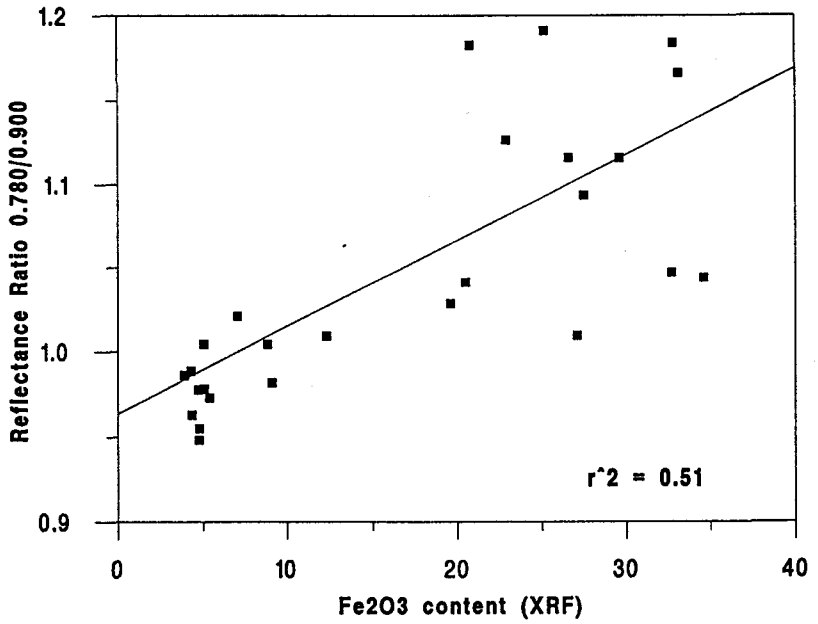

Figure 13: The reflectance ratio (0.78/0.90), sensitive to the depth of the 0.9 μm absorption, plotted against the Fe_2O_3 content for the surface soils.

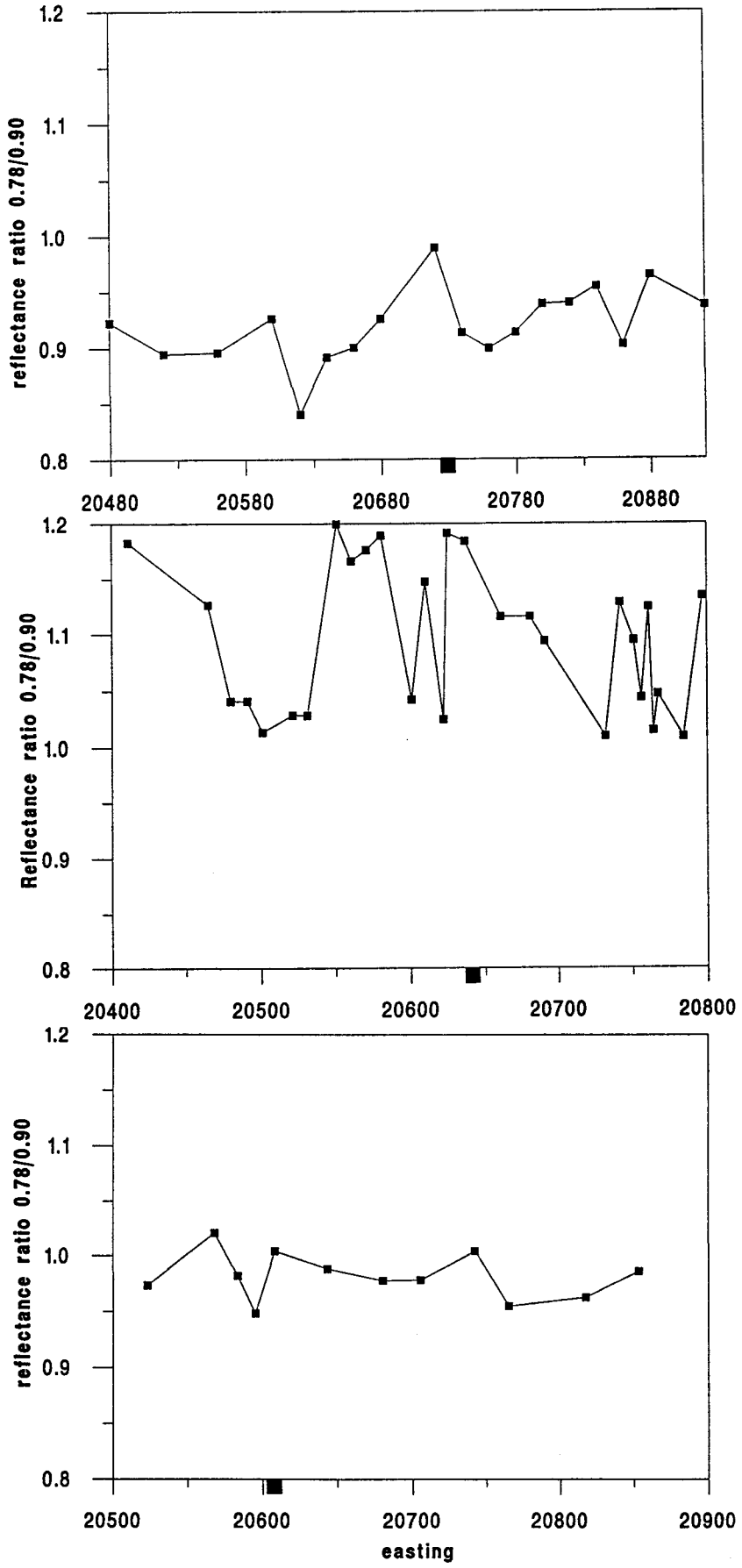

Figure 14: The reflectance ratio (0.78/0.90), sensitive to the depth of the 0.9 μm absorption, plotted against the traverse location. The location of the gold mineralisation is located as a small box.

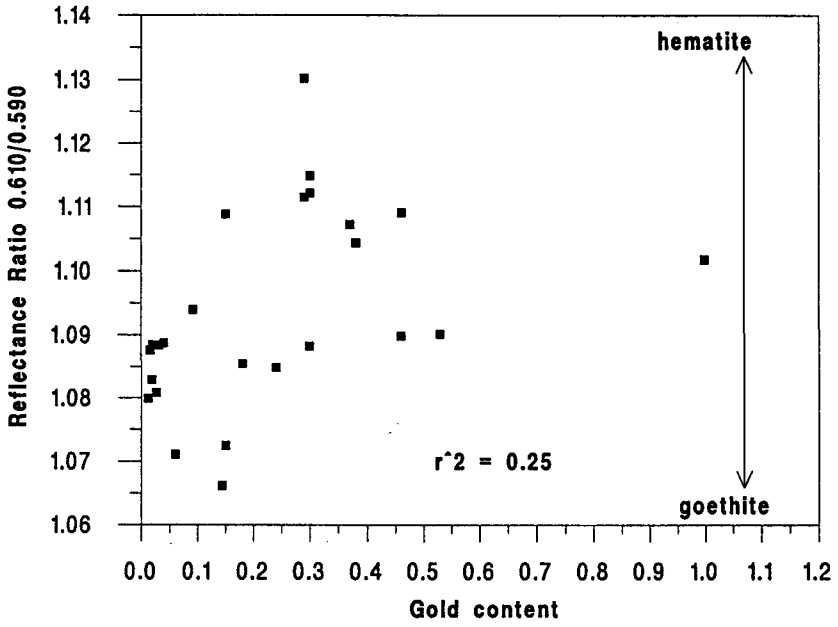

Figure 15: The reflectance ratio (0.610/0.59), sensitive to the wavelength of the charge transfer shoulder, plotted against the gold content for the surface soils.

Secondary gold shows a weak relationship with a longer wavelength charge transfer shoulder (hematite-rich). This is demonstrated in Figure 15 which shows the soils with the higher gold contents are weakly related to the largest reflectance ratios (related to longer wavelength absorption edge). A similar relationship, albeit reversed, was found with the Beasley Creek study (Cudahy and others, 1992a). It is not clear why there are not corresponding changes with the iron crystal field absorption.

7.3 Clay

This section examines in greater detail the clay information available from the reflectance data, including the clay mineralogy and clay abundance.

The spectral data show two distinct groups of OH-related absorptions. The first group is mostly related to the soils from line 35600 mN (Figure 9b) which show weak but recognisable absorption doublets at 1.4 μm and 2.2 μm, minor absorptions at 2.32 μm and 2.38 μm and relatively shallow absorption at 1.9 μm. The second group are related to soils from lines 35040 and 35800 mN (Figures 9a and 9c) which show no evidence for the absorption doublets at 1.4 and 2.2 μm, nor the absorptions at 2.32 and 2.38 μm. Instead, these spectra are characterised by single absorptions at 1.4 μm and 2.2 μm, deep water-related absorption at 1.9 μm and absorption near 1.46 μm (causing right-handed asymmetry to the 1.4 μm absorption). These differences are related to changes with the clay mineralogy. The first group are typical of kaolinite whereas the second group are characteristic of smectite/palygorskite. Palygorskite is an Mg/Al-bearing, hydrated clay with similar spectral characteristics to smectite (Figure 6f).

The initial XRD analyses for the whole soils showed no evidence for smectite/palygorskite. In the light of the spectral results, more detailed XRD analyses of clay-concentrated samples were undertaken. These subsequent analyses found smectite but not palygorskite. This result suggests that "routine" XRD techniques are not as sensitive as the spectral method for discriminating some clay information.

The asymmetry of the 1.4 μm and 2.2 μm absorptions were examined to see if a quantitative measurement of the kaolinite to smectite ratio could be established. The asymmetry of these absorptions were determined using ratios of reflectances from 1.50 with 1.65 μm (1.4 μm absorption asymmetry) and 2.165 with 2.232 μm (2.2 μm absorption asymmetry). The results of these ratios are shown in Figure 16 which show the kaolinite-rich soils (line 35600 mN) are clearly separated from the smectite-rich soils (lines 35040 and 35800 mN). Therefore, either of these features could be used to provide an indication of the proportion of kaolinite to smectite. This information could be further assessed using the depth of the 1.9 μm water absorption as this parameter increases with increased smectite content. This is demonstrated in Figure 17 which shows correlation between the HQ-depth of the 1.9 μm absorption with the 1.4 and 2.2 μm absorption asymmetry ratios.

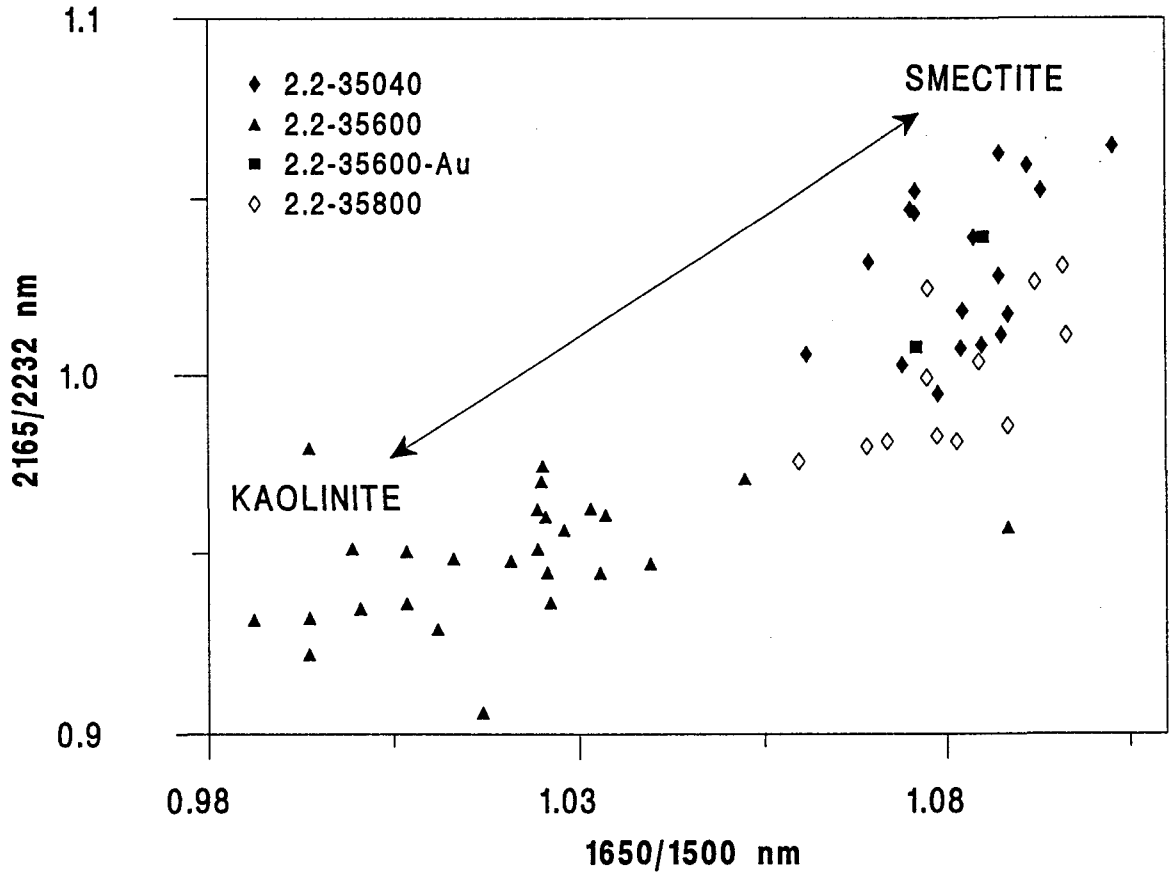

Figure 16: The reflectance ratios (1.65/1.50 and 2.165/2.232) sensitive to the asymmetry of the 1.4 and 2.2 absorptions plotted against each other. The fields for the theoretical smectite and kaolinite geometries are indicated.

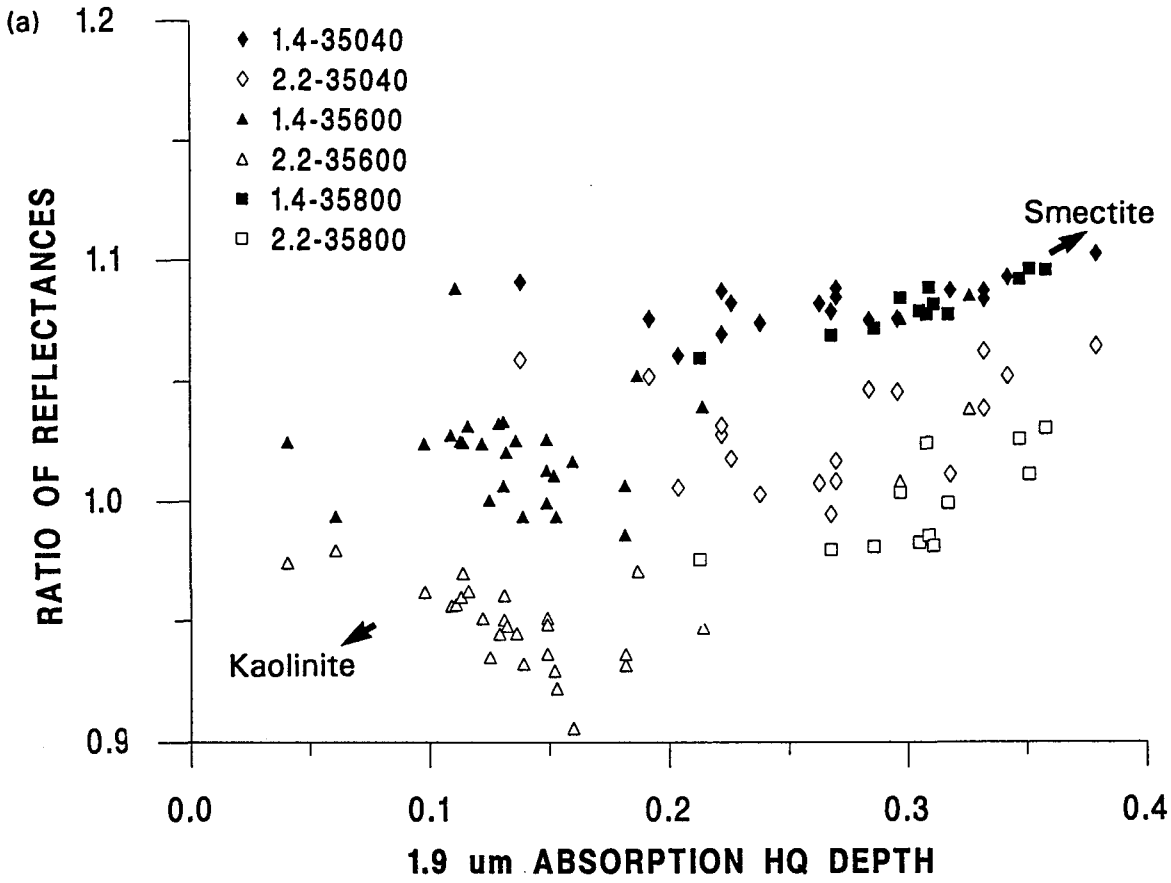

Figure 17: The ratio of reflectances at 1.65/1.5 μm and 2.165/2.232 μm plotted against the 1.9 HQ water absorption depths for (a) all the surface samples, and (b) for selected soils at 0-1 m, 1-3 m and >3 m depth.

The spectral data show a relationship between smectite and carbonate. This is demonstrated in Figure 18 which shows the CaO-rich (carbonate) samples are related to smectite-type 1.4 and 2.2 μm absorption-asymmetry ratios. Figures 10e an 10f show the carbonate-rich surface soils rich in smectite are "replaced" by more kaolinite-rich, material below 3 m as evidenced by the geometry 2.2 μm absorption. The significance of these results are discussed in Section 8.1.3.

Hypothetically, the clay content can be related to regolith development and possibly hydrothermal alteration. The depth of the 2.2 μm absorption was used as an approximation for the total Al_2O_3 content and measured using hull quotients. The results show correlation (Figure 19), though the smectite-rich soils have relatively shallow 2.2 μm absorptions and lower Al_2O_3 contents compared to the kaolinite-rich soils. This relationships does not mean there is less smectite in a given sample as smectite and kaolinite have different proportions of Al^{3+} in their respective crystal structures (discussed in Section 8.1.2).

There is no increase in the depth of the 2.2 μm absorption over gold mineralisation (Figure 20). Instead, the soils over gold mineralisation, along 35040 mN, show a slight decrease in the depth of the 2.2 μm absorption indicating smaller Al_2O_3 contents. There are too few data to draw any general conclusions from this result though this decrease is accompanied by the presence of amphibole (Section 7.1) which suggests weathering is incomplete at this locality.

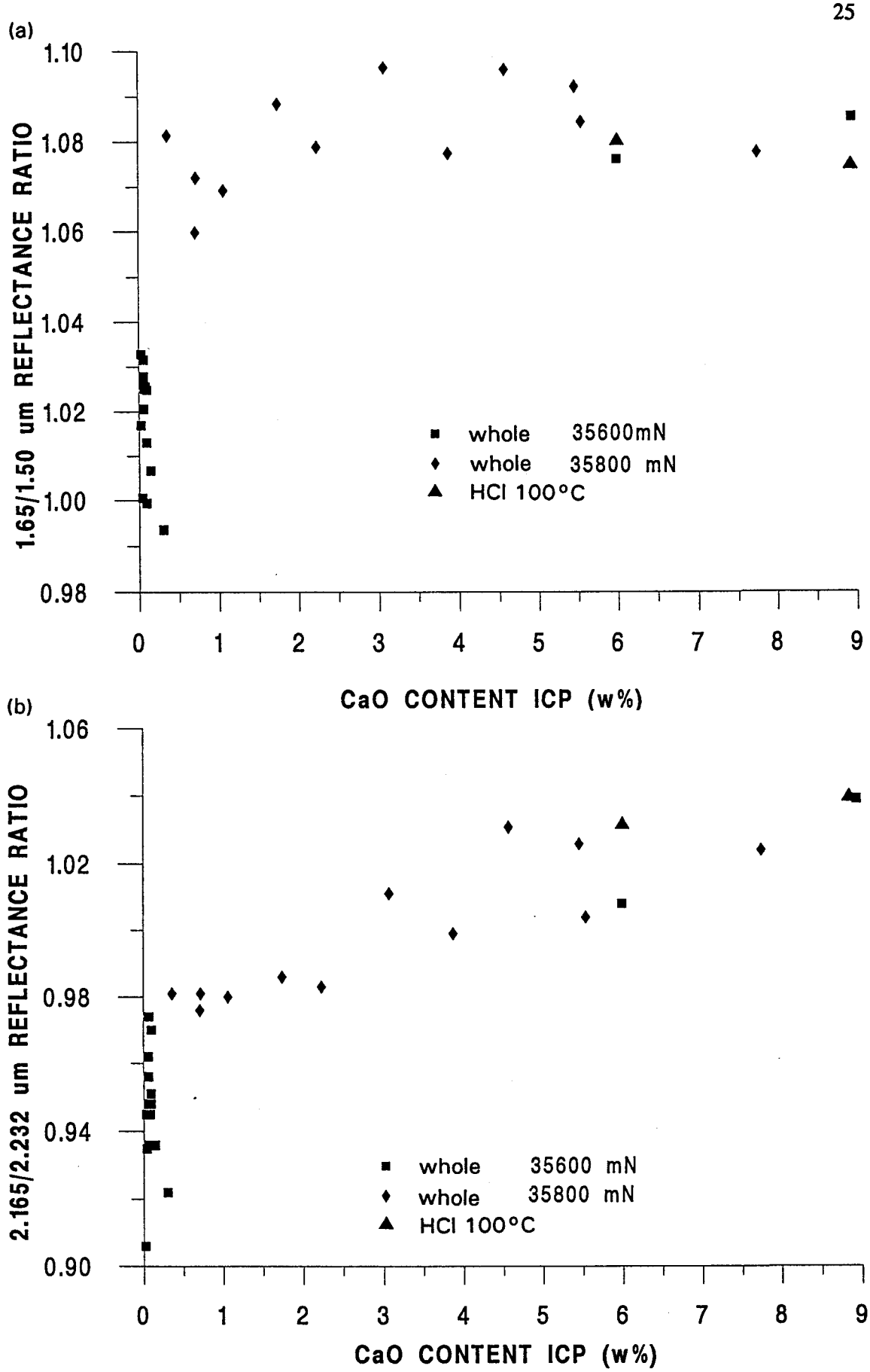

Figure 18: (a) The 1.65/1.50 reflectance ratio versus the CaO content for all the soils; and (b) the 2.165/2.232 reflectance ratio versus the CaO content for all the soils.

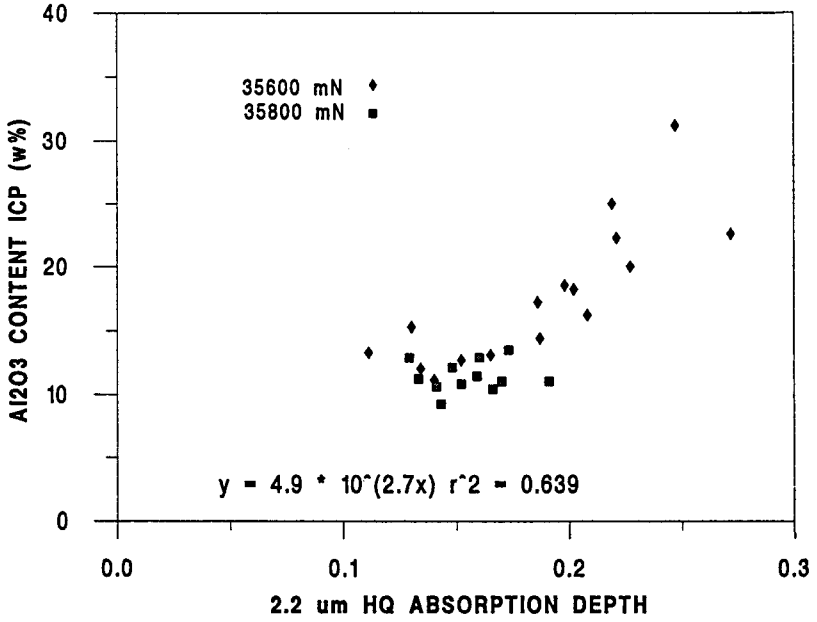

Figure 19: (a) The Al_2O_3 content versus the hull quotient depth of the 2.2 μm absorption (all samples).

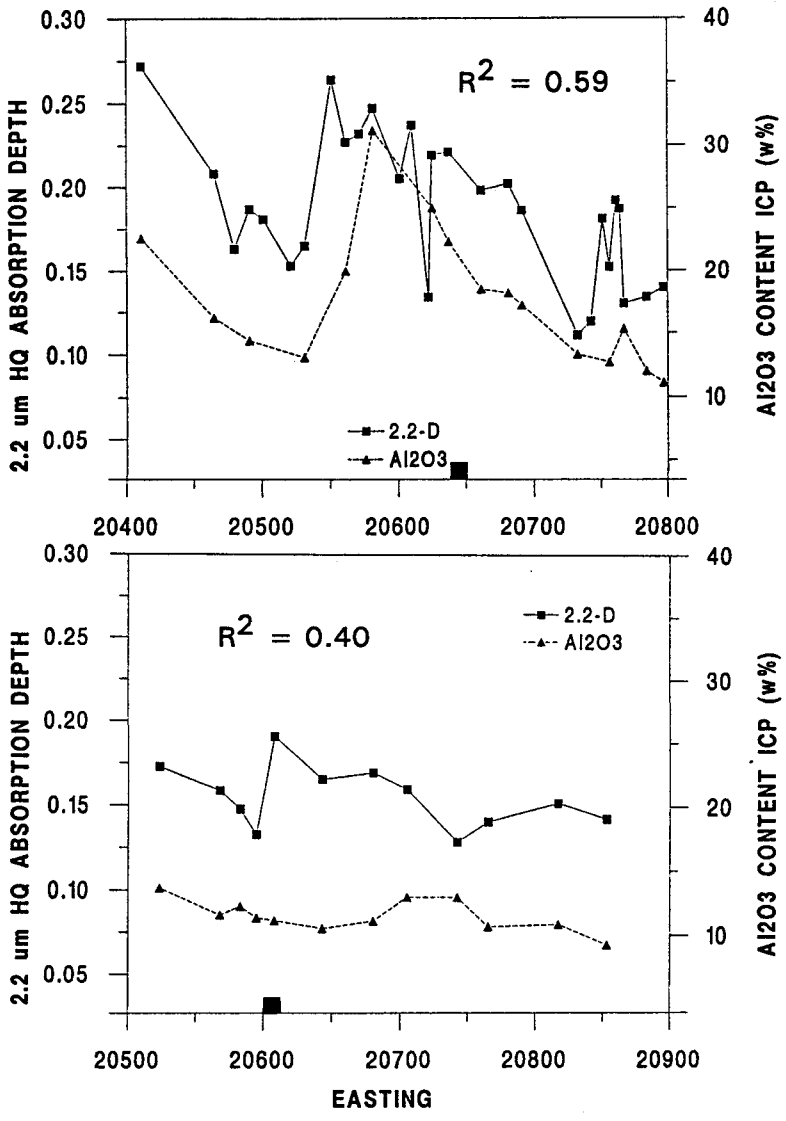

Figure 20: The hull quotient depth of the 2.2 μm absorption versus the traverse location for (a) 35600 mN; and (b) 35800 mN.

Secondary gold appears to be associated, in places, with pedogenic carbonate (Lintern, 1989), which in turn, is related to smectite. This association is demonstrated in Figure 16 which shows the soils rich in secondary gold along line 35600 mN plot in the smectite-field whereas the carbonate-poor soils plot in the kaolinite-field.

7.4 Carbonate

This section examines in greater detail the carbonate-related information apparent in the reflectance data. Lintern (1989) and Lintern and others (1990) found that primary gold mineralisation is not spatially associated with carbonate, though secondary gold, when developed, shows an association with pedogenic carbonate in the top metre.

The spectra of the soils rich in pedogenic carbonate (Appendix 4) do not show CO_3^{2-} absorptions at 1.864 μm, 1.939 μm and 2.332 μm (Figure 6g), even though these soils contain up to 13% CaO and 9.0% MgO, which equates to approximately 30% by weight of dolomite. Several experiments were conducted to determine why these carbonate absorptions are not present in the spectra. The first experiment was based on the hypothesis that aluminosilicates coat the surfaces of carbonate grains/nodules obscuring the carbonate from interaction with electromagnetic radiation. The second experiment aimed to establish the "threshold" carbonate concentration required in a mixture before the characteristic CO_3^{2-} absorptions became apparent in the reflectance spectra. The details of these experiments are described in Appendix 2 with the salient results are discussed below.

An imaging SEM was used to map the relative Ca, Al and Si contents of a cut, carbonate pisolith (15 mm diameter). The SEM image (Appendix 2, Figure 2.1) shows the outer 1-2 mm of the carbonate nodule comprises abundant Al and Si. This suggests aluminosilicates form a cortex over the carbonate interior. This provides an explanation for the lack of carbonate absorptions in spectra taken from carbonate nodules. However, a similar analysis of carbonate-rich soil showed abundant exposure of Ca- and Mg-bearing minerals (Appendix 2, Figure 2.2). Therefore, clay coatings appear not to be responsible for the lack of carbonate absorption in soil spectra.

An experiment involving laboratory mixtures of powdered calcite (<75 μm particle size) and carbonate-poor soil showed that approximately 40% by weight of carbonate is required in a mixture before the major CO_3^{2-} absorption at 2.32 μm absorption became apparent. The soils at Bounty have less than this "threshold" amount which provides an explanation for the lack of carbonate absorption in these soil spectra.

The reflectance spectra of carbonate-rich soils are associated with an increase in the albedo, especially in the visible. This relationship is demonstrated in Figure 21 which shows the largest reflectances at 0.5 μm are associated with the largest CaO contents. The increased albedo is not diagnostic of carbonate as an increase in clay content and/or a decrease in iron oxide content can also affect the visible brightness, though the affects of these other parameters can be assessed using other reflectance characteristics (Sections 7.2 and 7.3).

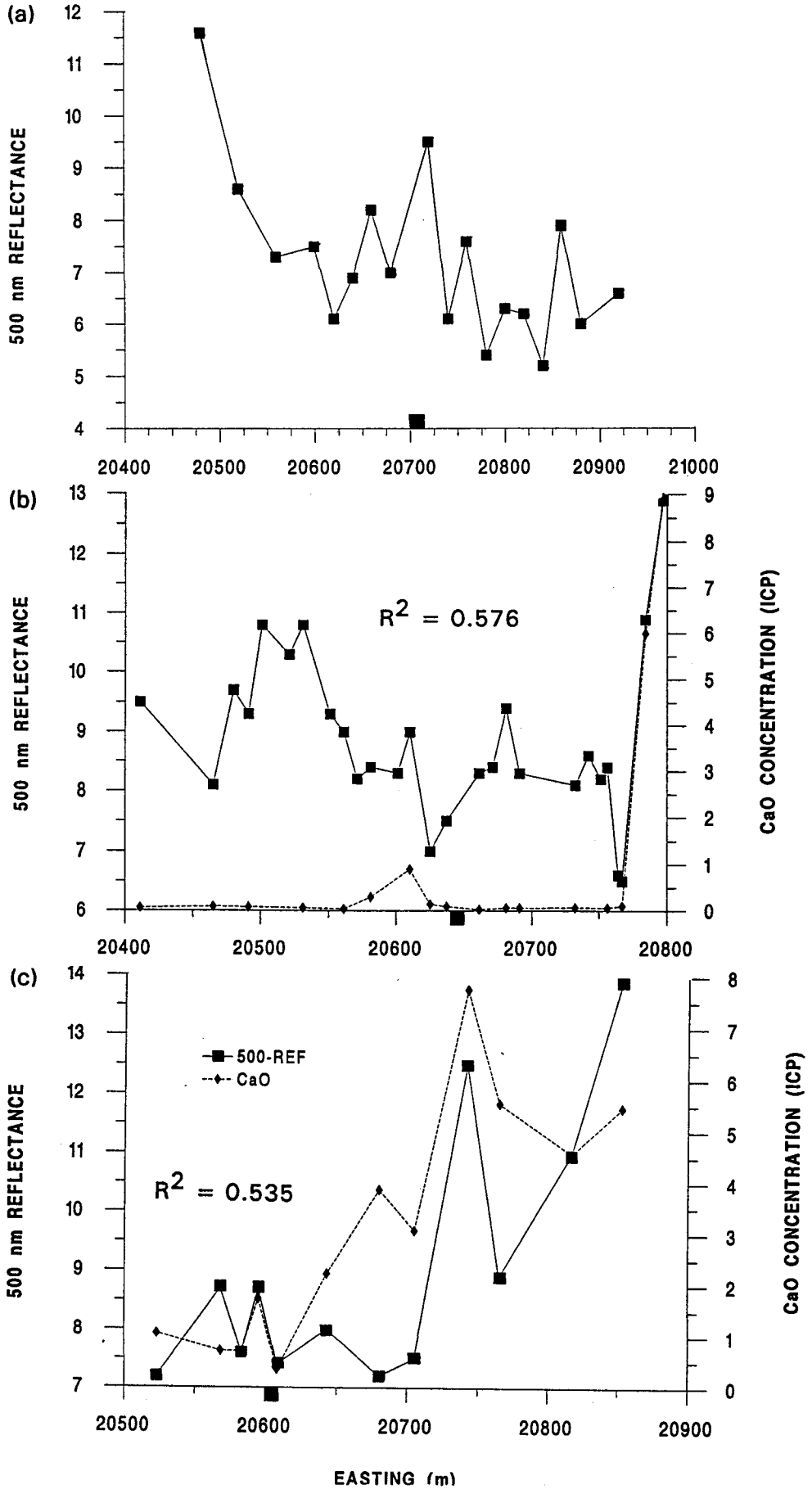

Figure 21: The reflectance at 0.5 μm and the CaO content versus the traverse location for the surface samples along (a) 35040 mN, (b) 35600 mN and (c) 35800 mN.

8.0 DISCUSSION

The reflectance data provide no evidence for "indicator" mineral absorptions associated with primary gold mineralisation> However, the data provide information related to the physicochemical character of the regolith, and possibly secondary gold. These aspects are discussed in more detail below.

8.1 Regolith Characteristics

The reflectance data provide information on the nature of ferric oxides (Section 7.2), clays (Section 7.3) and carbonate (7.4). Much of this information is consistent with the regolith model proposed by Cudahy (1992a) which relates spectral-physicochemical properties to four regolith processes, namely, lateritisation, aridity, erosion/deposition and pedogenesis. The model includes relationships involving the iron oxide and clay abundances, the hematite-goethite ratio, the degree of Al-substitution in the iron oxide lattice, clay mineralogy, clay crystallinity, Fe-substitution in the clay lattice and carbonate content. These physicochemical properties, except for Al-substitution, clay crystallinity and Fe-substitution in the clay lattice, were found to affect the reflectance spectra of the weathered materials in the Bounty/North Bounty study area.

The first and predictable conclusion that can be made from the spectral data is related to the lack of primary mineral absorptions (Fe^{2+}, Mg-OH) which indicates deep weathering of the parent rocks and little or no fresh rock or saprock at the surface. This is consistent with field mapping by Lintern and others (1990) and indicates the surficial materials are more derived from the upper parts of the laterite profile where iron oxides and clays dominate the mineralogy.

8.1.1 Iron Oxides

The reflectance data show information related to the hematite-goethite ratio and the iron oxide abundance (Section 7.2). The spectra of the carbonate-poor soils developed over lateritic duricrust show high ferric oxide content and enrichment in goethite. In contrast, the spectra of the carbonate-rich soils over exposed saprolite and transported cover show low ferric oxide content and enrichment in hematite. These associations are consistent with the regolith model (Cudahy, 1992a) as the soils over the iron-rich lateritic duricrust should be relatively rich in iron oxide compared to the soils over saprolite. The variations in the hematite-goethite ratio are possibly caused by changes in pH (related to the availability of Ca and Mg), as goethite can form in more acidic conditions and hematite forms in more neutral conditions (Schwertmann and Murad, 1983). This is consistent with the field mapping by Lintern and others (1990) who found the soils over lateritic duricrust are generally acidic. An alternative explanation is that the increased abundances of goethite over lateritic duricrust are related to goethite that formed in the matrix and rims around hematite-rich pisoliths of the lateritic duricrust (Anand and others, 1991; Cudahy, 1992a). This near surface concentration of goethite may also explain the change from goethite to hematite with depth in the weathered profile (Figures 10a and 10b). In areas stripped of lateritic duricrust, the hematite-rich soils are

"replaced" by more goethite-rich material at depth (Figures 10c, 10d, 10e and 10f), which is consistent with the regolith model.

8.1.2 Clays

The reflectance data show information related to variations in the clay mineralogy and clay abundance (Section 7.3). Kaolinite is evident in the spectra of soils overlying lateritic duricrust whereas smectite is evident in the spectra of soils overlying exposed saprolite. During lateritisation, well-crystalline kaolinite forms within the saprolite and poorly crystalline kaolinite forms in the lateritic duricrust (Cudahy, 1992a). Therefore, the smectite-rich soils over saprolite are anomalous. However, this can be explained by the post-lateritisation development of pedogenic carbonate (Sections 7.4 and 8.1.3) and smectite (Section 7.3) which overprinted the earlier-formed lateritic mineralogy. This explanation is consistent with the presence of more kaolinite-rich materials below the surface zone of smectite and pedogenic carbonate (Figure 10). McFarlane (1983) found a similar association between groundwater carbonates and smectite/palygorskite. Unfortunately, no samples were examined from areas of exposed saprolite poor in carbonate as these should theoretically comprise well-crystalline kaolinite.

According to the regolith model (Cudahy, 1992a), the clay abundance (related to the Al_2O_3 content) changes through the laterite profile with the largest clay abundances developed in the upper saprolite zone. However, the spectral data show that the smectite-rich soils over saprolite have shallow 2.2 μm Al-OH absorptions (lower Al_2O_3 content) compared to the kaolinite-rich soils over lateritic duricrust. This anomaly can be caused by any of three affects. Firstly, the total clay abundances are not directly related to the depth of the 2.2 μm absorption (related to the Al_2O_3 content) because there are different amounts of Al^{3+} in the kaolinite and smectite structures. This can be corrected by applying a gain factor of 2.5 (assuming similar unit cell sizes for kaolinite and smectite). The corrected results produces similar, if not deeper, 2.2 μm absorptions (total clay abundances) for the smectite-rich soils over exposed saprolite. Secondly, the addition of Ca and Mg causes a relative decrease in the other elements, including Al (relative decrease). Thirdly, some of the clay material in the soils over exposed saprolite has been removed, either chemically or mechanically (absolute decrease). The Beasley Creek study (Cudahy and others, 1992) found the soils overlying exposed saprolite were also poor in clay which was probably caused by the aeolian removal of clay-size particles and the deposition of coarser quartz grains.

8.1.3 Carbonates

Pedogenic carbonate has developed in areas of exposed saprolite and transported material within the upper few metres of the weathering profile (Lintern and others, 1990). These areas are generally located on gently inclined slopes where erosion has removed the acidic materials associated with lateritic duricrust. Therefore, the distribution of the pedogenic carbonate appears to be partly controlled by the nature of the exposed lateritic units indicating that the formation of pedogenic carbonate was post-lateritisation. This conclusion is supported by evidence from the SEM examination of soil rich in pedogenic carbonate (Appendix 2). This evidence includes the preservation of crystal growth facets

of Ca- and Mg-rich minerals which indicates little, if any, chemical corrosion of carbonate has occurred in a zone where leaching is expected. The results from this study have also demonstrated that pedogenic carbonate is associated with smectite (Section 7.3 and 8.1.2) and, possibly, hematite (Sections 7.2 and 8.1.1), such that the original laterite mineralogy has been significantly changed during later enrichment of Ca and Mg in the upper few metres of the weathering profile. These mineralogical and chronological relationships are consistent with the regolith model (Cudahy, 1992a).

It is not clear how Ca and Mg were concentrated in the top few metres of the soil profile. Lintern (1989) proposed several explanations. One of these was further developed by Lintern and Scott (1990), and involves the movement of Au, Mg and Ca from depth (approximately 20 m) to the surface through the action of deep plant roots. Gold, Ca and Mg are deposited in the soil through leaching from the plants and/or by the decomposition of plant material. Infiltrating soil water dissolves these mobile elements and takes them downward in solution where they may be taken up again by plant roots and so continue the cycle. However, this model does not explain the development of the gold-carbonate halo laterally displaced hundreds of metres from the zone of primary gold mineralisation at North Bounty (Figure 2). Therefore, the role of groundwater movement needs to be better understood.

8.2 Significance to Gold Exploration

The spectral data do not provide a simple mechanism for finding gold deposits such as Bounty/North Bounty. No "indicator" mineral absorptions are present that can be used to spectrally target primary or secondary gold. However, the reflectance data provide information relevant to the characteristics of the regolith relevant useful for geochemical strategies. Lintern (1989) found a spatial relationship exists between secondary gold and pedogenic carbonate, for some areas, and suggested that carbonate would be a useful sample medium for regional geochemical exploration. The spectra of soils, rich in pedogenic carbonates, do not show CO_3^{2-}-related absorptions, but can be recognised by increased albedo, especially in the visible, and carbonate appears to be intimately associated with smectite (smectite is spectrally detectable).

Spectral information and an appropriate regolith model could be used in a forward modelling and residual approach to highlight anomalous behaviour. For example, the few samples collected from over primary gold mineralisation show a weak increase in the depth of the 0.9 μm absorption related to a slight increase in the iron oxide content. If further work found that primary mineralisation was indeed related to an increase in iron oxide content, then the distribution and abundance of surface iron oxides could be tested quantitatively against a regolith model to normalise out the regolith-related iron oxide variations and so enhance anomalous information possibly associated with gold mineralisation.

9.0 CONCLUSIONS

The 0.4 to 2.5 μm reflectance properties of soils overlying the Bounty and North Bounty zones of gold mineralisation were measured and the information compared with ICP,

XRF, SEM and XRD physicochemical data to determine if gold mineralisation is associated with distinct spectral-physicochemical behaviour. The spectral results provided no distinctive characteristics related to primary gold mineralisation though the soils enriched in carbonate, and in places secondary gold, show characteristic spectral behaviour.

The spectra of the soils rich in pedogenic carbonate over exposed saprolite and transported materials show:

1. No evidence for CO_3^{2-} absorption;

2. Increased albedo, especially in the visible;

3. A longer wavelength charge transfer absorption shoulder and a shorter wavelength Fe^{3+} crystal field absorption indicating a greater proportion of hematite to goethite; and

4. Single absorptions at 1.4 and 2.2 μm, asymmetric absorption at 1.4 μm (caused by broad absorption at 1.46 μm) and deep absorption at 1.9 μm indicating smectite.

The spectra of the soils poor in carbonate over lateritic duricrust show:

1. A shorter wavelength charge transfer absorption shoulder and a longer wavelength Fe^{3+} crystal field absorption indicating greater a proportion of goethite to hematite; and

4. Absorptions doublets at 1.4 and 2.2 μm, shallow absorption at 1.9 μm, and minor absorptions at 2.31 and 2.38 μm indicating kaolinite.

The pedogenic carbonates are restricted to the upper few metres of the weathering profile with the spectra of the underlying materials showing weak kaolinite absorption doublets and deeper 0.9 μm absorption indicating increased iron oxide content.

In only one soil spectra was there evidence for primary mineral absorptions. This sample is probably related to mafic saprock and showed:

1. Mg-OH absorption at 2.306 and 2.384 μm related to amphibole (confirmed by XRD); and

2. Broad ferrous iron absorption at 1.1 μm.

These types of absorptions are more commonly found in the few spectra of relatively unweathered samples from deeper in the weathering profile (greater than 30 m depth).

The comparison of spectral information with physicochemical data showed:

1. The depth of the 0.9 μm absorption may be correlated with the Fe_2O_3 content;

2. The depth of the 2.2 μm absorption may be correlated with the Al_2O_3 content;

3. The asymmetry of the 1.4 and 2.2 μm absorptions are related to the CaO content;

4. The depth of the 1.9 μm water absorption is related to the CaO content;

5. The brightness at 0.5 μm is related to the CaO content

6. Approximately 40% by weight of carbonate in required in a mixture (<75 μm particle size) before the CO_3^{2-} absorption at 2.33 μm becomes recognisable in the spectrum.

The spectral-physicochemical information provides information on the characteristics of the regolith consistent with a model proposed by Cudahy (1992a). The results emphasise the importance of recognising overprinting regolith processes as these change earlier-formed mineral associations.

10.0 FURTHER WORK

There are several important areas for further work if spectral sensing techniques are to be used in a quantitative and thematic way for gold exploration in the weathered Yilgarn, including:

1. Establishing the wider significance of the few spectral-physicochemical relationships found in this study by examining a larger range of samples from weathered mineralisation and background areas. For example, how important is iron oxide abundance and mineralogy to gold?;

2. Establishing the spectral characteristics of carbonate-poor soils overlying exposed saprolite as these should hypothetically comprise well crystalline kaolinite and goethite;

3. Testing the spectral-physicochemical relationships proposed in the regolith model for complete vertical sections of the laterite profile, especially in areas of pedogenic carbonate and different parent rocks;

4. Determining quantitative relationships between spectral behaviour and physicochemical information, including clay crystallinity, iron oxide mineralogy, cation substitution in iron oxides and clays, and mineralogical abundances. The 8-14 μm wavelength region should also be assessed as this region can provide information on silicates, as well as carbonates, iron oxides and clays.

11.0 ACKNOWLEDGEMENTS

This study has been financially supported by industry and government sponsorship of the CSIRO/AMIRA P243 Remote Sensing for Gold Project in W.A.. Tim Munday edited an earlier draft and Angelo Vartesi drafted some of the figures. John Crabb managed the sample preparation and Mike Hart was responsible for the XRF and XRD measurements. Bruce Robinson and Terry Harrison assisted with the SEM analyses. Neil Beckingham assisted with the measurement and processing of the spectra and Cheryl Harris formatted the final document. To these people and sponsors we express our sincere thanks.

12.0 REFERENCES

ANAND, R. R., CHURCHWARD, H. M. and SMITH, R. E., 1991. Regolith/landform relationships and the petrological, mineralogical and geochemical characteristics of lags, Lawlers District, Western Australia. CSIRO IMEC Division of Exploration Geoscience Restricted Investigation Report No. 106R, 124 pages.

BISHOP, J.L., 1988. The effects of water, octahedral cation substitution and exchangeable cation composition on the shortwave infrared reflectance spectrum of montmorillonite. Masters Thesis, Stanford University, Department of Applied Earth Science, 65 pages.

BUCKINGHAM, W. F. and SOMMER, S. E. 1983. Mineralogical characterisation of rock surfaces formed by hydrothermal alteration and weathering - application to remote sensing. Economic Geology, Vol. 78, pp 664-674.

BUTT, C. R. M., 1982. Weathering and the Australian landscape. Geochemical exploration in deeply weathered terrain. Edited by R.E. Smith. CSIRO IMEC Division of Mineralogy Publication, Floreat Park, Perth, pp. 41-50.

CHIN, R. J, HICKMAN, A. H. and THOM, R. 1984. Hyden 1:250 000 Geological Series - Explanatory Notes. Geological Survey of Western Australia, Sheet SI/50-4, pp 21.

CLARK, R. N., KING, T. V. V., KLEJWA, M., SWAYZE, G. A. and VERGO, N., 1990. High spectral resolution reflectance spectroscopy of minerals. Journal of Geophysical Research, Vol. 95, No. B8, pp. 12653-12680.

CROWLEY, J. K. and VERGO, N., 1988. Near-infrared reflectance spectra of mixtures of mixtures of kaolin-group minerals: use in clay mineral studies. Clay and clay Minerals, Vol. 36, No. 4, pp. 310-316.

CUDAHY, T. J., 1992a. A model for the development of the Yilgarn Craton incorporating selected spectral information. CSIRO IMEC Division of Exploration Geoscience Restricted Investigation Report No. 243R, 35 pages.

CUDAHY, T. J., 1992b. Spectral properties of rocks and soils from the Laverton region, Western Australia, CSIRO IMEC Division of Exploration Geoscience Restricted Investigation Report No. 235R, 35 pages.

CUDAHY, T. J., 1992c. Spectral properties of iron oxides. CSIRO, Division of Exploration Geoscience. Restricted Investigation Report No. 244R, 50 pages.

CUDAHY, T. J., ROBERTSON, I. D. M. and GABELL, A. R., 1992a. Spectral properties of the soils and lags overlying the site of the Beasley Creek gold mine, Laverton region, Western, Australia. CSIRO IMEC Division of Exploration Geoscience Restricted Investigation Report No. 160R, 40 pages.

CUDAHY, T. J., SCOTT, K. M., LINTERN, M. J. and GABELL, A.R., 1992b. Investigation of weathered muscovite- and paragonite-bearing rocks and soils from the Panglo gold deposit, Ora Banda region, Western Australia, using reflectance data. CSIRO IMEC Division of Exploration Geoscience Restricted Investigation Report No. 234R, 60 pages.

DEER, W. A., HOWIE, R. A. and ZUSSMAN, J. 1977. An introduction to rock forming minerals. Longman Group Ltd. London, pp 528.

ELACHI, C., 1987. Introduction to the physics and techniques of remote sensing. John Wiley and Sons, 413 pages.

FARMER, V. C., 1974. The infrared spectra of minerals. Edited by V.C. Farmer. Mineralogical Society, 41 Queens Gate, London, pp. 331-364.

GREEN, A. A. and CRAIG, M. D., 1985. Analysis of aircraft spectrometer with logarithmic residuals. Proceedings of the AIS Workshop, Pasadena, JPL Publication 85-41, Jet Propulsion Laboratory, Pasadena California, U.S.A., pp. 111-119.

GOZZARD, J. R. and TAPLEY, I. J., 1992. Regolith-landform mapping in the Lawlers district, Report 2: Terrain classification mapping. CSIRO IMEC Division of Exploration Geoscience Restricted Investigation Report No. 240R, 96 pages.

HUNT, G. R. and SALISBURY, J. W., 1971. Visible and near infrared spectra of minerals and rocks: I Carbonates. Modern Geology. Vol. 2, pp 23-30.

HUNT, G. R., SALISBURY, J. W. and LENHOFF, C. J., 1971. Visible and near infrared spectra of minerals and rocks: III Oxides and Hydroxides. Modern Geology. Vol. 2, pp 195-205.

HUNT, G. R. and ASHLEY, R. P., 1979. Spectra of altered rocks in the visible and near infrared. Economic Geology, Vol. 74, pp. 1613-1629.

KEMP, E. M., 1978. Tertiary climatic evolution and vegetation history in the south-east Indian Ocean region: Palaeogeography, Palaeoclimatologyn Palaeoecology, Vol. 24, pp. 307-374.

LINTERN, M. J., 1989. Study of the distribution of gold in soils at Mt Hope, Western Australia. CSIRO Division of Exploration Geoscience Restricted Investigation Report 24R, 17 pages.

LINTERN, M. J., CHURCHWARD, H. M. and BUTT, C. R. M., 1990. Multi-element soil survey of the Mt Hope area, Western Australia. CSIRO Division of Exploration Geoscience Restricted Investigation Report 109R, 83 pages.

LINTERN, M. J. and SCOTT, K. M., 1989. The distribution of gold and other elements in soils and vegetation at Panglo, Western Australia. CSIRO Division of Exploration Geoscience Restricted Investigation Report 129R, 50 pages.

McFARLANE, M. J., 1983. Laterites: In Geochemical sediments and geomorphology: Precipitates and residua in the near-surface environment. Edited by Goudie and Pye. Academic Press, London, pp. 7-58.

MORRIS, R. V, LAUER, H. V., LAWSON, C. A., GIBSON, E. K., NACE, G.A. and STEWART, C., 1985. Spectral and other physiochemical properties of submicron powders of hematite (Fe_2O_3), maghemite (Fe_2O_3), magnetite (Fe_3O_4), goethite (FeOOH) and lepidocrocite (FeOOH). Journal of Geophysical Research, Vol. 90, No. B4, pp 3126-3144.

SALISBURY, J. W. and D'ARIA, D.M., (in press). Infrared (8-14 μm) remote sensing of soil particle size. Remote Sensing of Environment.

SCHWERTMANN, U. and MURAD, E., 1983. Effect of pH on the formation of goethite and hematite from ferrihydrite. Clays and Clay Minerals, Vol. 31, No. 4, pp. 277-284.

Appendix 1

Spectral Mnemonics and Abbreviations

Spectra Mnemonics

The V-SWIR spectra of each sample are assigned a unique 9 character mnemonic which describes all the attributes for that measurement. The format is:

$$X_1\ X_2\ X_3\ X_4\ X_5\ X_6\ .\ X_7\ X_8\ X_9$$

where X_1-X_6 *are alphabetic* characters and X_7-X_9 are *alpha-numeric* characters, and where:

X_1 is the project where "A" represents the P243 Gold Project;

X_2 is the *location* where "F" represents the Mt Hope area;

X_3 is the *type of measurement* where "L" represents laboratory in contrast to "F" for field;

X_4 *is the type of sample* where "S" is for soil;

X_5 is a *repeat measurement* where "B" is the first repeat;

X_6 is a *multiple sample* from the same locality or an additional treatment where "A" is the first treatment (e.g. soil plus HCl acid);

X_7-X_9 are the locality identity numbers.

Abbreviations

nm	nanometre (10^{-9} m)
μm	micrometre (10^{-6} m)
HQ	hull quotient
1.9-D	1.9 μm water absorption hull quotient depth
2.2-D	2.2 μm Al-OH absorption hull quotient depth

Appendix 2

Carbonate Experiments

Carbonate-Related Experiments

This section examines a number of problems associated with the carbonates, including:

1. Determining whether carbonate is exposed in natural materials (soils and nodules);
2. Determining the amountof carbonate required to produce CO_3^{2-} absorption in the 2.3 μm wavelength region; and
3. Determining whether the depths of iron oxide and Al-clay absorptions and the albedo of a sample are affected by changes in the abundance of carbonate.

SEM Studies of Natural Materials

This experiment aimed to determine why carbonate-rich soils and nodules lack CO_3^{2-} absorption in reflectance spectra. One possible reason for this is the development of clay- and/or iron oxide-rich coatings over the carbonate-rich grains/nodules. To test this hypothesis, an SEM was used to examine the elemental composition of soil particles and pisoliths.

A cut, carbonate pisolith, 15 mm in diameter, was probed for Ca, Al and Si using a CAMECA imaging SEM. The resultant SEM images (Figures 2.1a and 2.1b) show concentric bands rich and poor in Ca indicating variations in the development of carbonate. Figure 2.1a shows the outer 1-2 mm of the carbonate nodule are rich in Al and Si which indicates an outer layer of aluminosilicates obscuring the underlying carbonate-rich layers from interaction with EMR. This phenomenon would explain the lack of carbonate-related absorption in spectra taken from carbonate nodules.

The SEM examination was continued on carbonate-poor and carbonate-rich soils which showed fine-grained aluminosilicates (2-20 μm ion diameter) covering 10-40% of the surfaces of larger grains (Figures 2.2, 2.3 and 2.4). However, Ca and Mg are also clearly exposed at the surface indicated by the bulk and point SEM analyses. Therefore, the lack of carbonate-related absorption in the spectra of carbonate-rich soil cannot be explained by a surface coating of aluminosilicates. The SEM examination also showed the carbonate-rich sample from the North Bounty area comprised many angular grains, some with crystal growth facets (Figure 2.3). These growth facets are Ca-rich and Mg-rich and indicate little if any chemical corrosion has occurred.

Carbonate-Soil Mixtures

The main objective of this experiment was to determine the "threshold" concentration of exposed carbonate required before the CO_3^{2-} absorption at 2.33 μm became apparent in reflectance data. A pure calcite powder (<250 μm particle size) was added in 5% increments to a carbonate-poor soil (AFLSAA.019; <710 μm particle size with <1% naturally occurring CaO and MgO, 47.1% SiO_2, 12.7% Al_2O_3 and 34.6% Fe_2O_3). The

reflectance spectra of the carbonate-soil mixtures are plotted together in Figure 2.5 which shows the 2.332 μm CO_3^{2-} absorption is not clearly evident in the soil until a carbonate content of approximately 40% by weight. This is also demonstrated in Figure 2.6 which shows an exponential relationship exists between the hull quotient depth of the 2.3 μm CO_3^{2-} absorption and the carbonate content (weight %). The soils at Bounty comprise less than 40% carbonate which provides an explanation why the spectra of these samples did not produce recognisable CO_3^{2-} absorption at 2.33 μm.

With an increase in carbonate content there is also a relative decrease with the other minerals such as iron oxide and clay. The relative changes in the concentration of these other minerals was examined using the depths of associated absorptions. The affects on albedo were also examined. The depths of the 0.5 μm Fe^{3+} charge transfer absorption (related to iron oxide content), the 0.9 μm Fe^{3+} crystal field absorption (related to iron oxide content), 1.4 μm absorption (related to the number of OH bonds), 1.9 μm absorption (related to the number of water molecules) and the 2.2 μm absorption (related to the number of Al-OH bonds) decrease in depth with an increase in carbonate content (Figures 2.7, 2.8 and 2.9, respectively). These relationships generally approximate exponential functions. The albedo measured at 0.5 and 1.65 μm increases with carbonate content in a linear manner (Figure 2.10). Therefore, these parameters could be used as an indirect method by the concentration of an unknown material (in this case, carbonate) can be gauged.

These results suggest that even though the carbonate absorption at 2.3 μm may not be apparent in materials with less than 40% carbonate content, small amounts of carbonate will have a significant affect on the depths of the 0.5 μm, 0.9 μm and 2.2 μm absorptions as well as the albedo.

HCl Acid Treatment

The objective of this experiment was to determine whether the increased albedo of carbonate-rich samples is related to the carbonate. The experiment involved removing most of the carbonate from selected soils by adding 0.1 M HCl. Distiled water was added to the samples after effervescing ceased and the excess fluids decanted. The soils were then dried in an oven for 2 days at 100 °C before spectral measurement.

The spectral results of the soils before and after acid cleaning are presented in Figure 2.11. The brightness at 0.5 μm, for the carbonate-rich soils (AFLSAA.000 and AFLSAA.003) show a reduction of 4% reflectance after acid treatment making the brightness of these samples comparable with the carbonate-poor samples (AFLSAA.019, AFLSAA.033 and AFLSAA.063). The changes in brightness at 1.65 μm after acid treatment are more difficult to interpret as both the carbonate-rich and carbonate-poor soils show a reduction in brightness by up to 8% after acid treatment. This is inconsistent, for two reasons, with the relationships shown in Figure 2.10. Firstly, the changes in brightness at 1.65 μm should be approximately half that at 0.5 μm. Secondly, the carbonate-poor soils were not expected to show a reduction in brightness. The reasons for this are not clear.

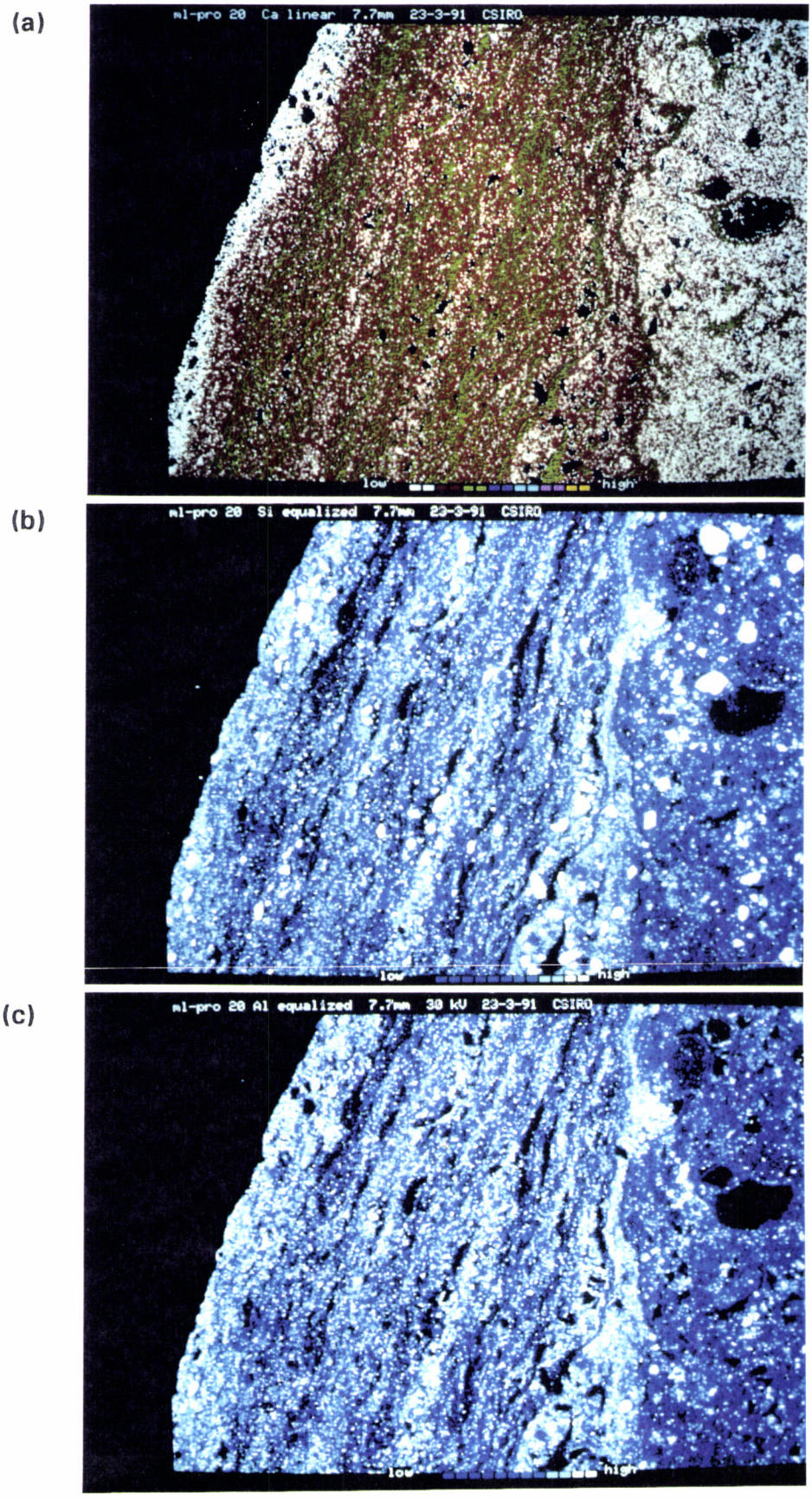

Figure 2.1: SEM image of a cut carbonate pisolith showing the distribution of (a) Ca, (b) Si and (c) Al. Large Ca contents are shown as reds and greens and small Ca contents are shown as white. The large Al and Si contents are shown as bright tones on the grey-scale images.

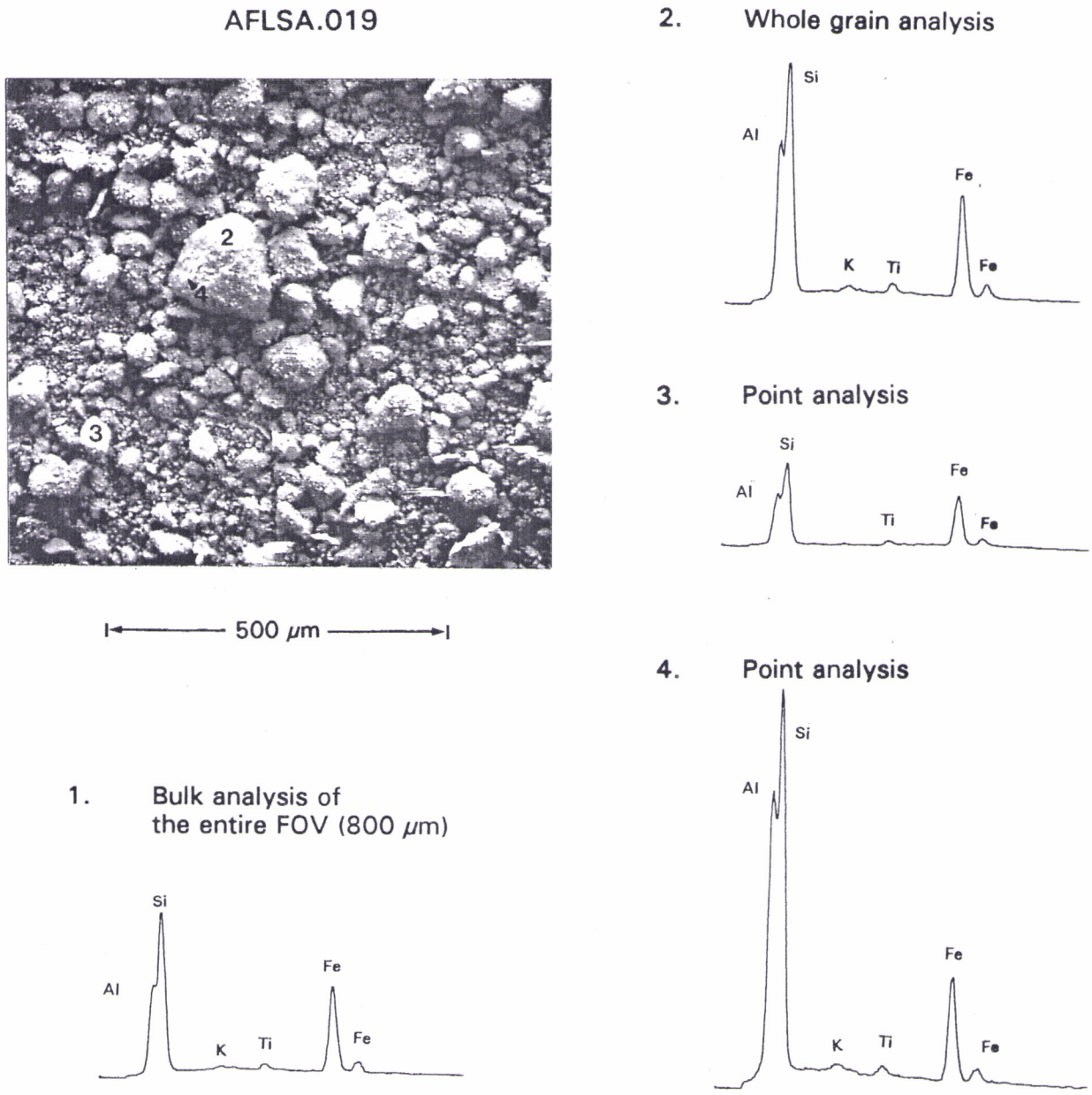

Figure 2.2: SEM photomicrograph and various analyses of a carbonate-poor soil from line 35600 mN.

AFLSA.000

500 μm

6. Whole grain analysis

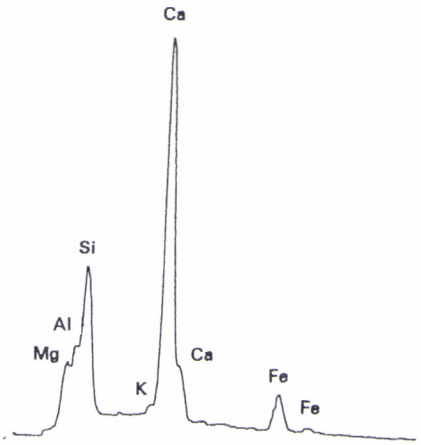

5. Bulk analysis of the entire FOV (800 μm)

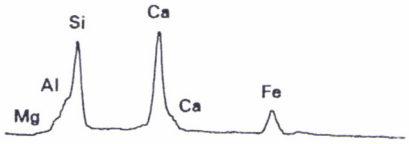

7. Bulk analysis grain with crystal growth facets

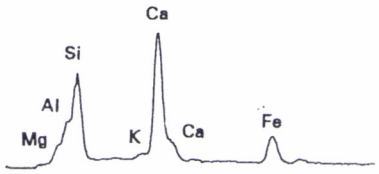

8. Point analysis of an elongate, subrounded grain

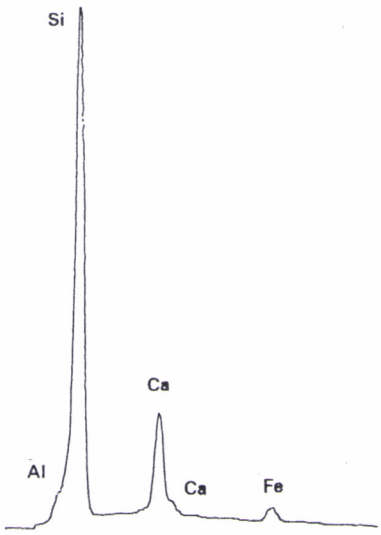

Figure 2.3: SEM photomicrograph and various analyses of a carbonate-rich soil from line 35600 mN.

AFLSA.000 (rounded quartz grain)

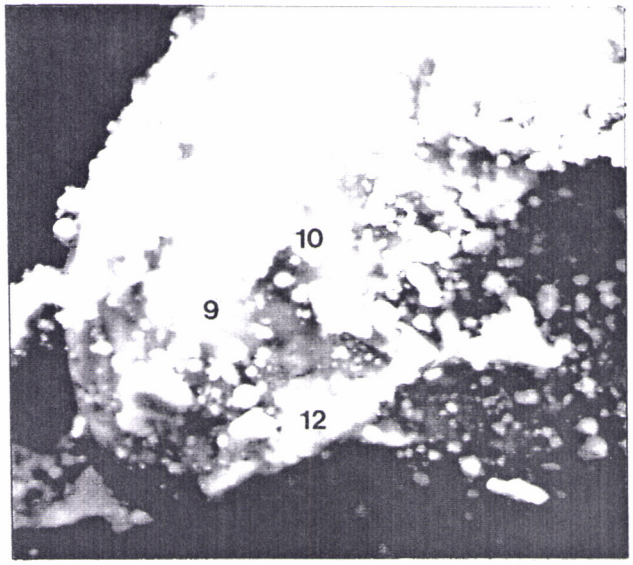

100 μm

9. Point analysis of a clean surface of the Si-rich grain

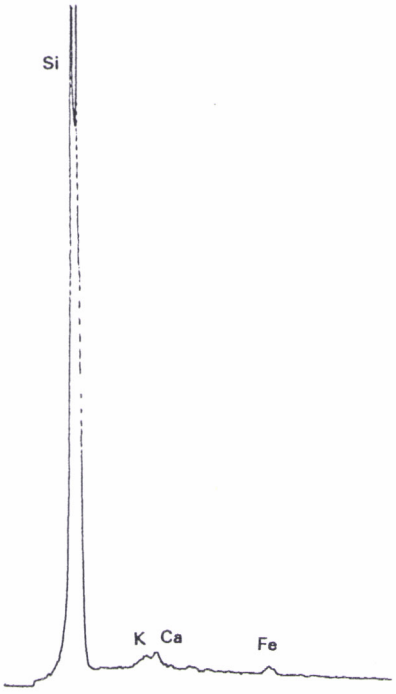

11. Bulk analysis of grain (100 μm dia.)

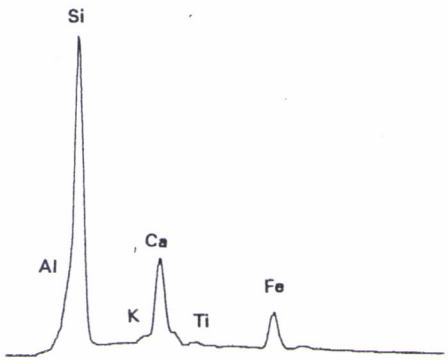

10. Point analysis

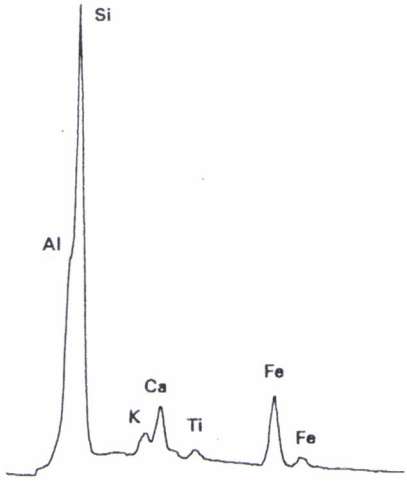

12. Point analysis of mineral accretion

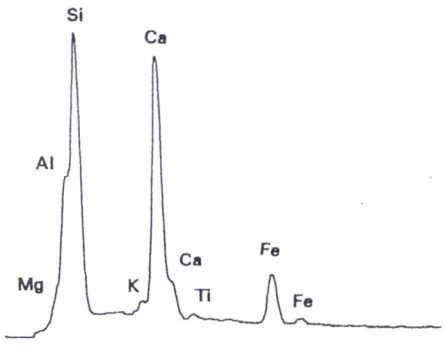

Figure 2.4: SEM photomicrograph and various analyses of a carbonate-rich grain from AFLSAA.000

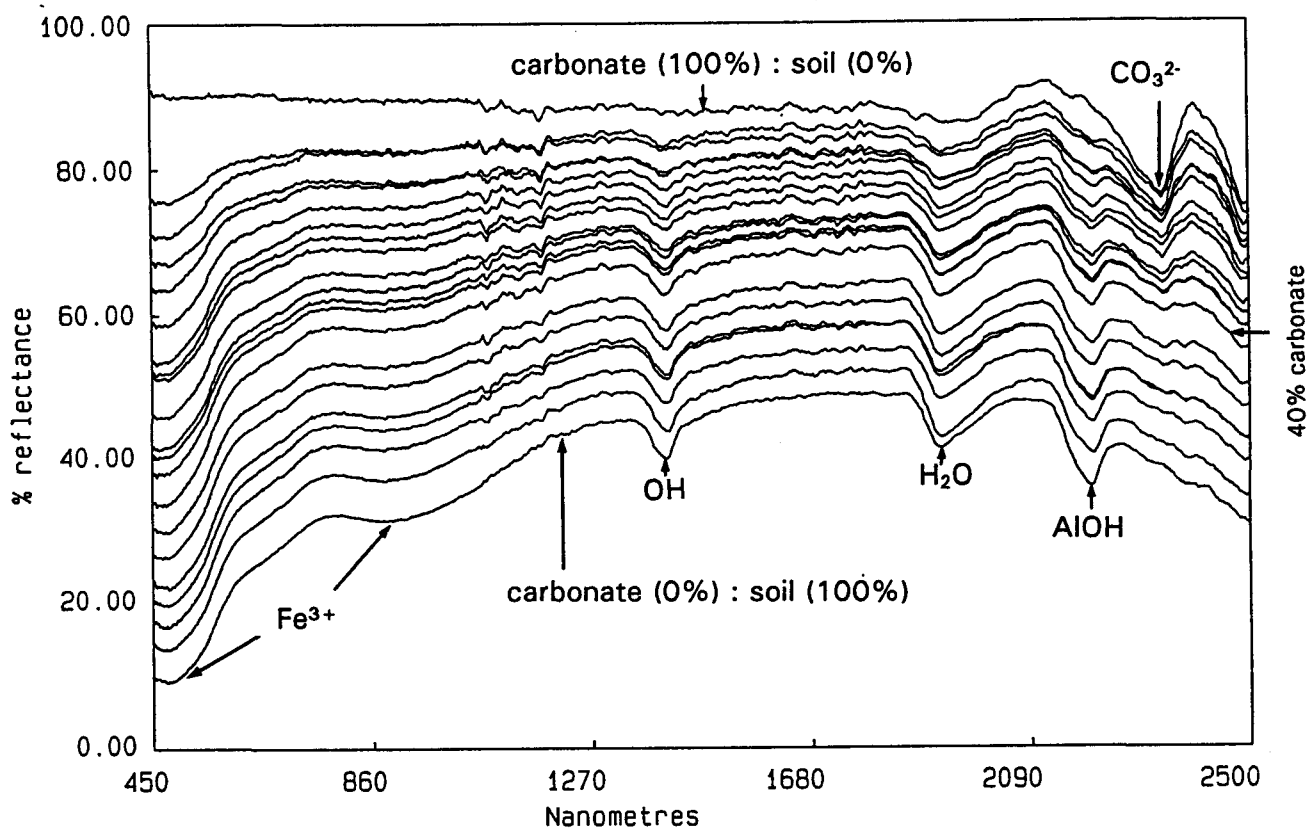

Figure 2.5: The reflectance spectra of carbonate-soil mixtures.

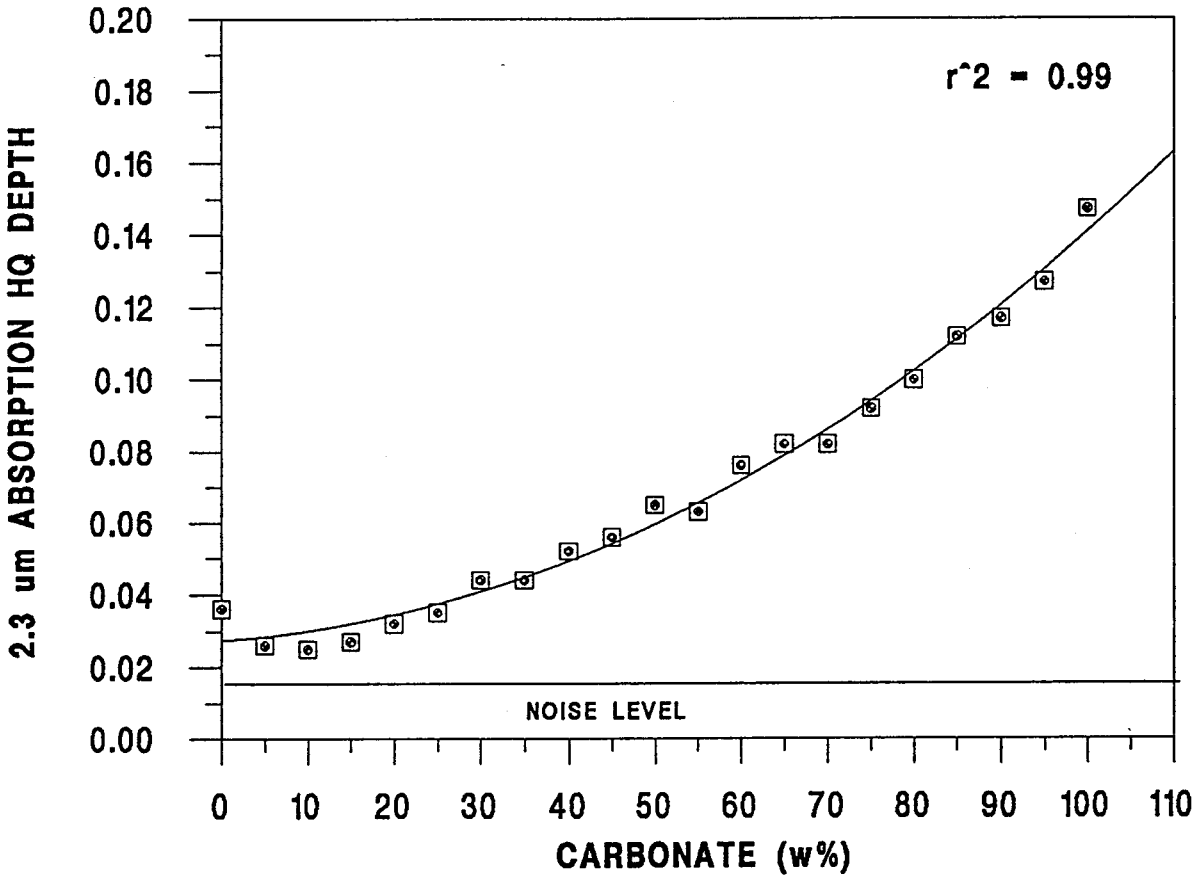

Figure 2.6: The hull quotient depth of the 2.33 μm absorption versus the carbonate content (weight %) for the calcite-soil mixtures.

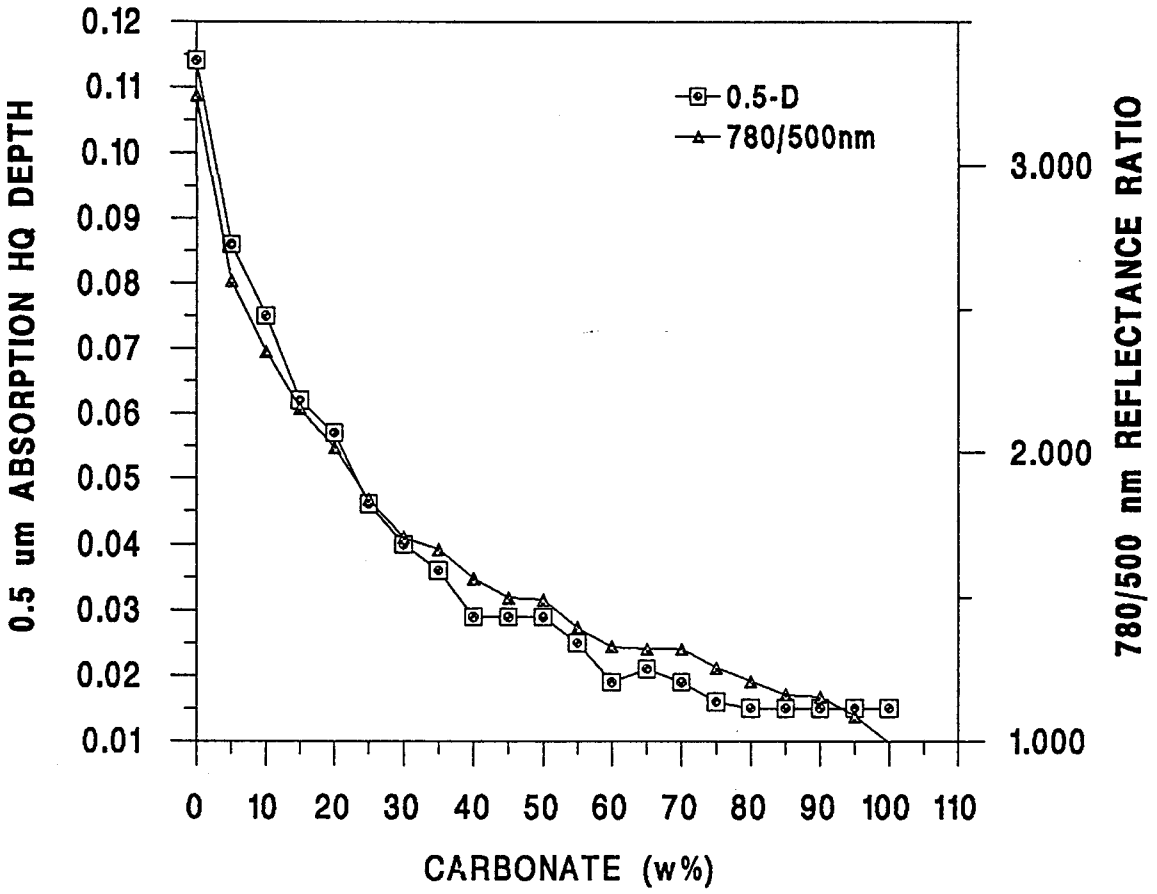

Figure 2.7: The hull quotient depth of the 0.5 μm absorption and a ratio of the reflectances at 0.78/0.50 μm plotted against the carbonate content (weight %) for the calcite-soil mixtures.

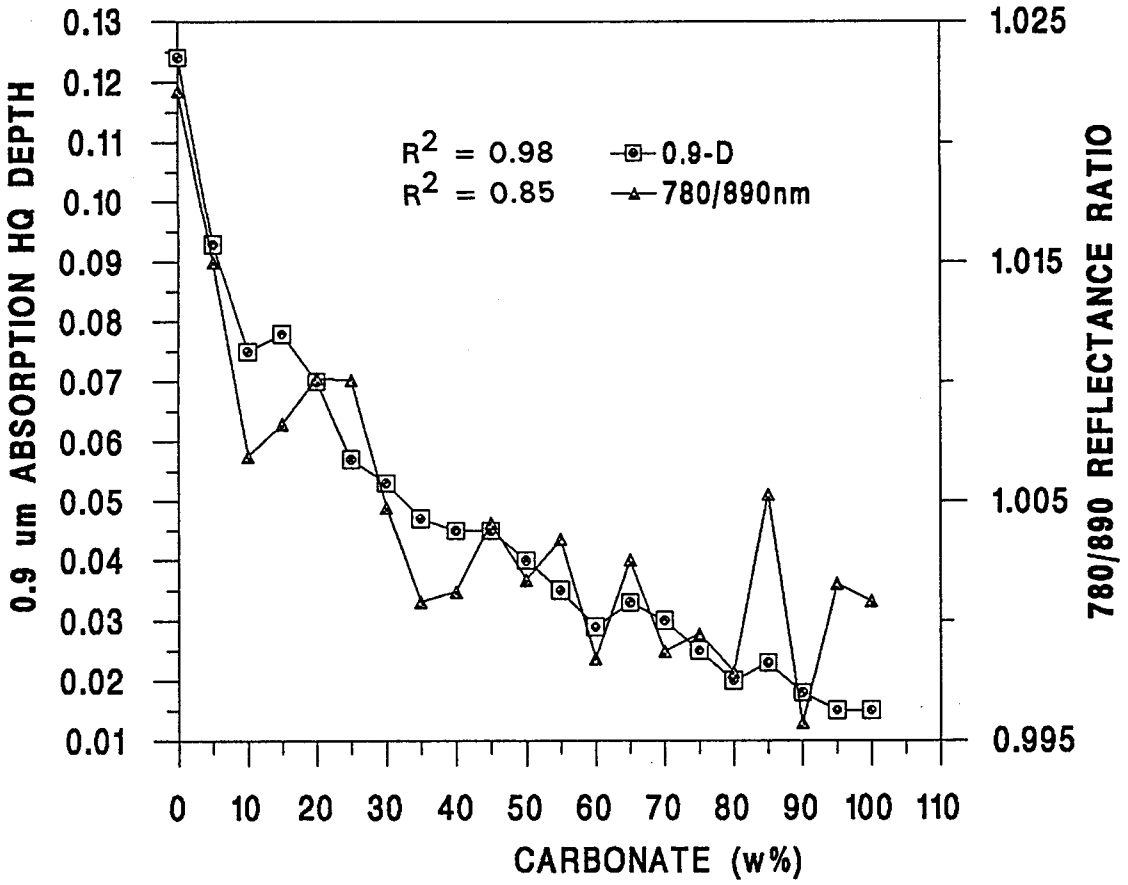

Figure 2.8: The hull quotient depth of the 0.9 μm absorption and a ratio of the reflectances at 0.78/0.89 μm plotted against the carbonate content (weight %) for the calcite-soil mixtures.

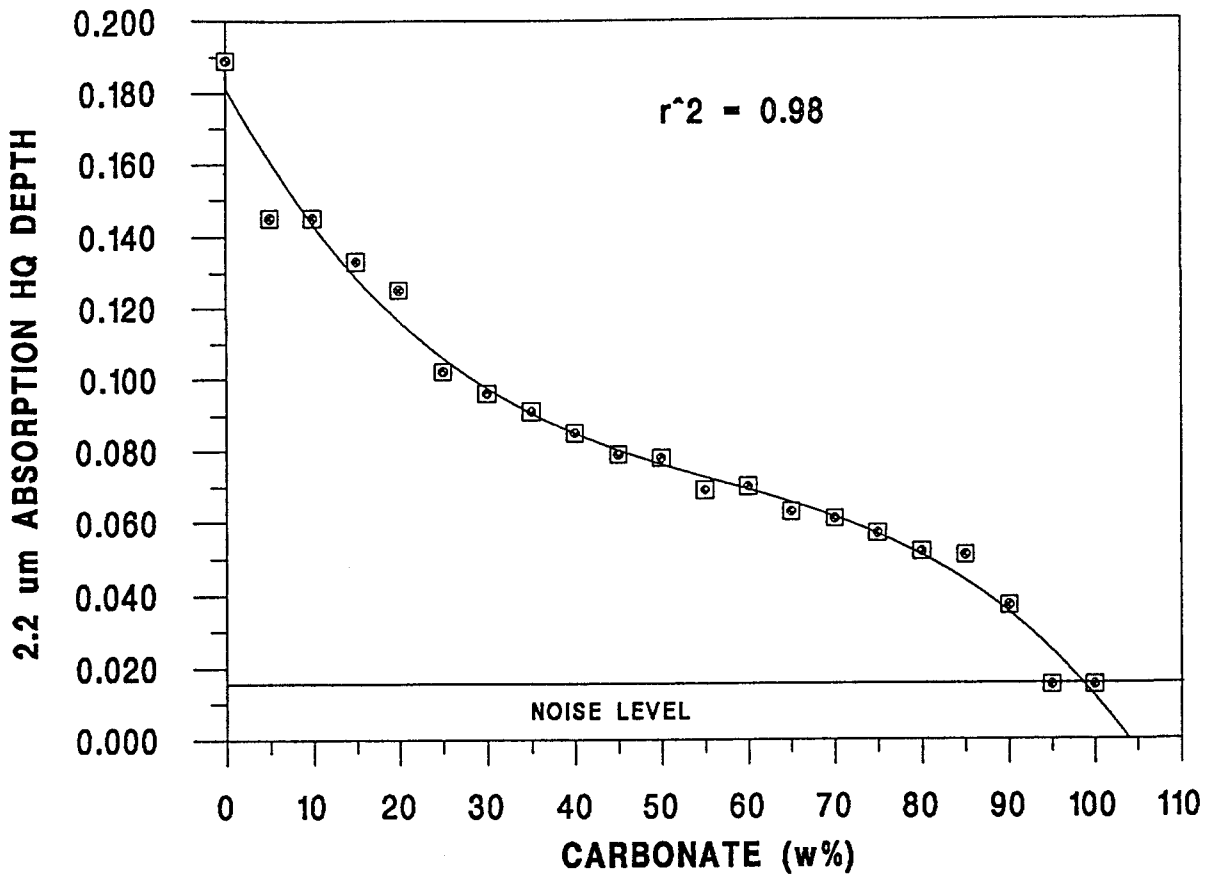

Figure 2.9: The hull quotient depth of the 2.2 μm absorption plotted against the carbonate content (weight %) for the calcite-soil mixtures.

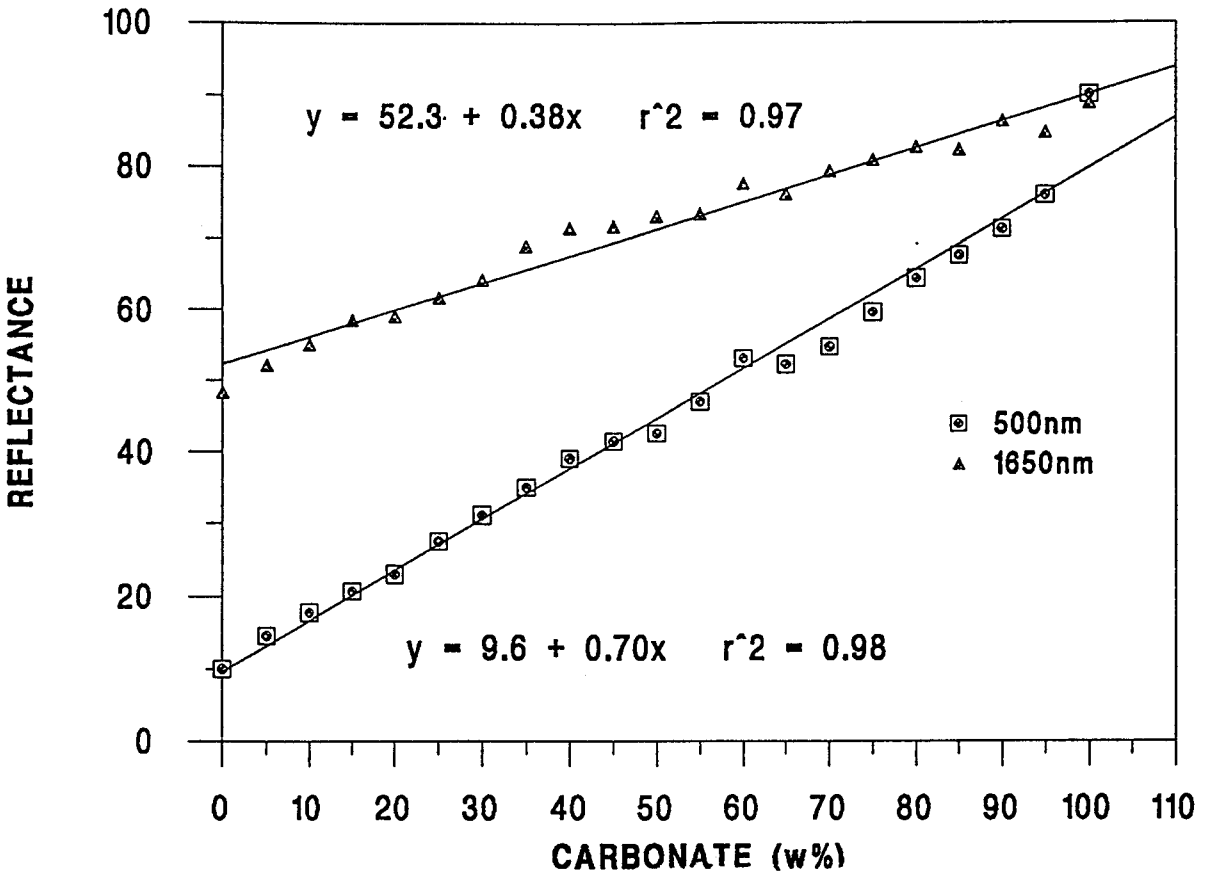

Figure 2.10: The reflectances at 0.5 μm and 1.65 μm plotted against the carbonate content (weight %) for the calcite-soil mixtures.

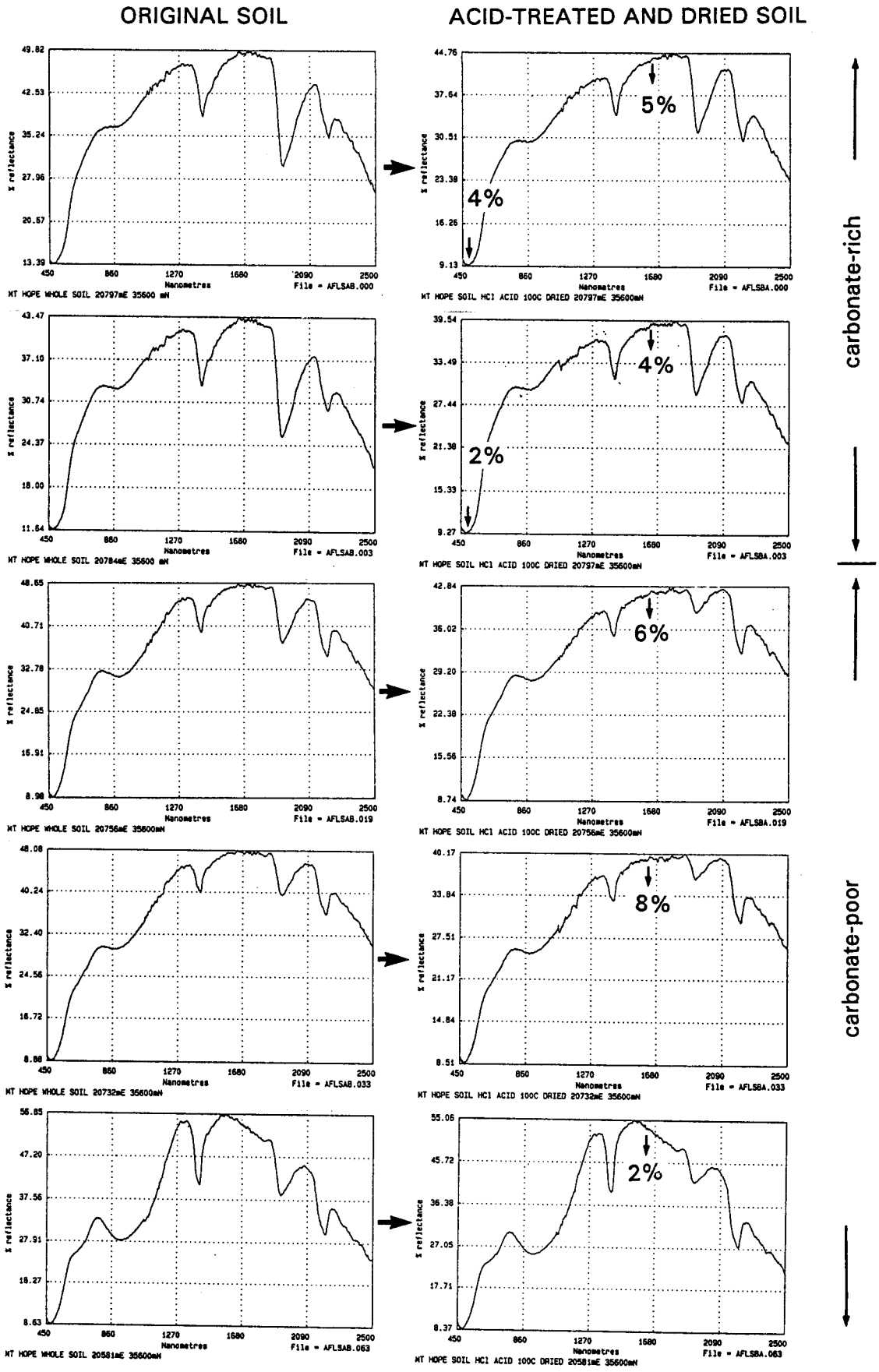

Figure 2.11: The reflectance spectra of carbonate-rich (AFLSAA.000 and AFLSAA.003) and carbonate-poor (AFLSAA.019, AFLSAA.033, and AFLSAA.063) soils from 35600 mN before and after HCl treatment.

Appendix 3

Description, Names, Grid Locations

MT HOPE SOIL IRIS REFLECTANCE DATA

FILENAME	DESCRIPTION	GRID REFERENCE
AFLSAA.000	WHOLE SOIL	20797mE 35600mN
AFLSAA.003	WHOLE SOIL	20784mE 35600mN
AFLSAA.006	WHOLE SOIL	20767mE 35600mN
AFLSAA.011	WHOLE SOIL	20764mE 35600mN
AFLSAA.014	WHOLE SOIL	20751mE 35600mN
AFLSAA.019	WHOLE SOIL	20756mE 35600mN
AFLSAA.031	WHOLE SOIL	20742mE 35600mN
AFLSAA.033	WHOLE SOIL	20732mE 35600mN
AFLSAA.036	WHOLE SOIL	20622mE 35600mN
AFLSAA.039	WHOLE SOIL	20711mE 35600mN
AFLSAA.042	WHOLE SOIL	20691mE 35600mN
AFLSAA.044	WHOLE SOIL	20681mE 35600mN
AFLSAA.046	WHOLE SOIL	20671mE 35600mN
AFLSAA.048	WHOLE SOIL	20661mE 35600mN
AFLSAA.050	WHOLE SOIL	20637mE 35600mN
AFLSAA.052	WHOLE SOIL	20625mE 35600mN
AFLSAA.057	WHOLE SOIL	20601mE 35600mN
AFLSAA.059	WHOLE SOIL	20610mE 35600mN
AFLSAA.061	WHOLE SOIL	20571mE 35600mN
AFLSAA.063	WHOLE SOIL	20581mE 35600mN
AFLSAA.067	WHOLE SOIL	20561mE 35600mN
AFLSAA.069	WHOLE SOIL	20551mE 35600mN
AFLSAA.071	WHOLE SOIL	20531mE 35600mN
AFLSAA.073	WHOLE SOIL	20521mE 35600mN
AFLSAA.075	WHOLE SOIL	20411mE 35600mN
AFLSAA.078	WHOLE SOIL	20501mE 35600mN
AFLSAA.080	WHOLE SOIL	20491mE 35600mN
AFLSAA.082	WHOLE SOIL	20480mE 35600mN
AFLSAA.085	WHOLE SOIL	20465mE 35600mN
AFLSAA.087	WHOLE SOIL	20853mE 35800mN
AFLSAA.090	WHOLE SOIL	20817mE 35800mN
AFLSAA.096	WHOLE SOIL	20765mE 35800mN
AFLSAA.099	WHOLE SOIL	20742mE 35800mN
AFLSAA.102	WHOLE SOIL	20705mE 35800mN
AFLSAA.105	WHOLE SOIL	20680mE 35800mN
AFLSAA.108	WHOLE SOIL	20643mE 35800mN
AFLSAA.111	WHOLE SOIL	20608mE 35800mN
AFLSAA.113	WHOLE SOIL	20595mE 35800mN
AFLSAA.116	WHOLE SOIL	20583mE 35800mN
AFLSAA.121	WHOLE SOIL	20568mE 35800mN
AFLSAA.125	WHOLE SOIL	20523mE 35800mN
AFLSAA.128	WHOLE SOIL	20645mE 34960mN
AFLSAA.133	WHOLE SOIL	20676mE 34960mN
AFLSAA.139	WHOLE SOIL	20688mE 34960mN
AFLSAA.145	WHOLE SOIL	20700mE 34960mN
AFLSAA.150	WHOLE SOIL	20710mE 34960mN
AFLSAA.201	SOIL (<2mm)	20480mE 35040mN
AFLSAA.202	SOIL (<2mm)	20520mE 35040mN
AFLSAA.203	SOIL (<2mm)	20560mE 35040mN
AFLSAA.204	SOIL (<2mm)	20600mE 35040mN
AFLSAA.205	SOIL (<2mm)	20620mE 35040mN
AFLSAA.206	SOIL (<2mm)	20640mE 35040mN
AFLSAA.207	SOIL (<2mm)	20660mE 35040mN
AFLSAA.208	SOIL (<2mm)	20680mE 35040mN
AFLSAA.217	SOIL (<2mm)	20720mE 35040mN
AFLSAA.218	SOIL (<2mm)	20740mE 35040mN

AFLSAA.209	SOIL (<2mm)	20760mE 35040mN
AFLSAA.210	SOIL (<2mm)	20780mE 35040mN
AFLSAA.211	SOIL (<2mm)	20800mE 35040mN
AFLSAA.212	SOIL (<2mm)	20820mE 35040mN
AFLSAA.213	SOIL (<2mm)	20840mE 35040mN
AFLSAA.214	SOIL (<2mm)	20860mE 35040mN
AFLSAA.215	SOIL (<2mm)	20880mE 35040mN
AFLSAA.216	SOIL (<2mm)	20920mE 35040mN
AFLSAB.000	WHOLE SOIL	20797mE 35600 mN
AFLSAB.003	WHOLE SOIL	20784mE 35600 mN
AFLSAB.019	WHOLE SOIL	20756mE 35600mN
AFLSAB.033	WHOLE SOIL	20732mE 35600mN
AFLSAB.063	WHOLE SOIL	20581mE 35600mN
AFLSBA.000	SOIL HCl ACID 100C DRIED	20797mE 35600mN
AFLSBB.000	SOIL HCl ACID 100C DRIED	20797mE 35600mN
AFLSBC.000	SOIL HCl ACID 100C DRIED	20797mE 35600mN
AFLSBD.000	SOIL HCl ACID 100C DRIED	20797mE 35600mN
AFLSBE.000	SOIL HCl ACID 100C DRIED	20797mE 35600mN
AFLSBA.003	SOIL HCl ACID 100C DRIED	20797mE 35600mN
AFLSBA.019	SOIL HCl ACID 100C DRIED	20756mE 35600mN
AFLSBA.033	SOIL HCl ACID 100C DRIED	20732mE 35600mN
AFLSBA.063	SOIL HCl ACID 100C DRIED	20581mE 35600mN
AFLSAC.000	WHOLE SOIL VARIANCE	20797mE 35600mN
AFLSAD.000	WHOLE SOIL VARIANCE	20797mE 35600mN
AFLSAE.000	WHOLE SOIL VARIANCE	20797mE 35600mN
AFLSAF.000	WHOLE SOIL VARIANCE	20797mE 35600mN
AFLSAG.000	WHOLE SOIL VARIANCE	20797mE 35600mN
AFLSAC.099	WHOLE SOIL VARIANCE	20742mE 35800mN
AFLSAD.099	WHOLE SOIL VARIANCE	20742mE 35800mN
AFLSAE.099	WHOLE SOIL VARIANCE	20742mE 35800mN
AFLSAF.099	WHOLE SOIL VARIANCE	20742mE 35800mN
AFLSBA.099	WHOLE SOIL CRUSHED	20742mE 35800mN
AFLSBB.099	WHOLE SOIL CRUSHED	20742mE 35800mN
AFLSCA.000	WHOLE SOIL CRUSHED	20797mE 35600mN
AFLSCB.000	WHOLE SOIL CRUSHED	20797mE 35600mN
AFLSBA.019	SOIL PLUS 0% CARBONATE	20756 mE 35600 mN
AFLSBB.019	SOIL PLUS 5% CARBONATE	20756 mE 35600 mN
AFLSBC.019	SOIL PLUS 10% CARBONATE	20756 mE 35600 mN
AFLSBD.019	SOIL PLUS 15% CARBONATE	20756 mE 35600 mN
AFLSBE.019	SOIL PLUS 20% CARBONATE	20756 mE 35600 mN
AFLSBF.019	SOIL PLUS 25% CARBONATE	20756 mE 35600 mN
AFLSBG.019	SOIL PLUS 30% CARBONATE	20756 mE 35600 mN
AFLSBH.019	SOIL PLUS 35% CARBONATE	20756 mE 35600 mN
AFLSBI.019	SOIL PLUS 40% CARBONATE	20756 mE 35600 mN
AFLSBJ.019	SOIL PLUS 45% CARBONATE	20756 mE 35600 mN
AFLSBK.019	SOIL PLUS 50% CARBONATE	20756 mE 35600 mN
AFLSBL.019	SOIL PLUS 55% CARBONATE	20756 mE 35600 mN
AFLSBM.019	SOIL PLUS 60% CARBONATE	20756 mE 35600 mN
AFLSBN.019	SOIL PLUS 65% CARBONATE	20756 mE 35600 mN
AFLSBO.019	SOIL PLUS 70% CARBONATE	20756 mE 35600 mN
AFLSBQ.019	SOIL PLUS 75% CARBONATE	20756 mE 35600 mN
AFLSBR.019	SOIL PLUS 80% CARBONATE	20756 mE 35600 mN
AFLSBS.019	SOIL PLUS 85% CARBONATE	20756 mE 35600 mN
AFLSBT.019	SOIL PLUS 90% CARBONATE	20756 mE 35600 mN
AFLSBU.019	SOIL PLUS 95% CARBONATE	20756 mE 35600 mN
AFLSBV.019	SOIL PLUS 100% CARBONATE	20756 mE 35600 mN
AFLSCK.019	SOIL PLUS 50% CARBONATE	20756 mE 35600 mN
AFLSDK.019	SOIL PLUS 50% CARBONATE	20756 mE 35600 mN
AFLSEK.019	SOIL PLUS 50% CARBONATE	20756 mE 35600 mN
AFLSFK.019	SOIL PLUS 50% CARBONATE	20756 mE 35600 mN

Appendix 4

Reflectance spectra, Tables of Oxide Contents and Spectral Information

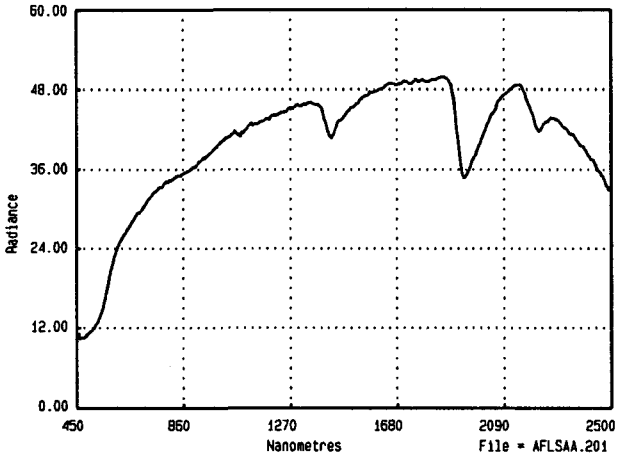

MT HOPE FORRESTANIA SOIL (<2mm) 20480mE 35040mN

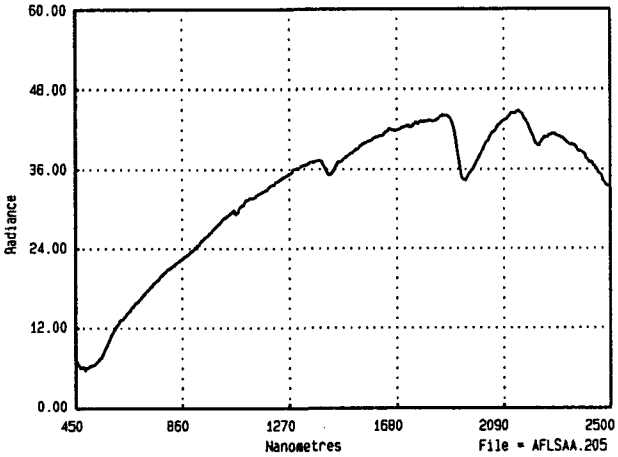

MT HOPE FORRESTANIA SOIL (<2mm) 20620mE 35040mN

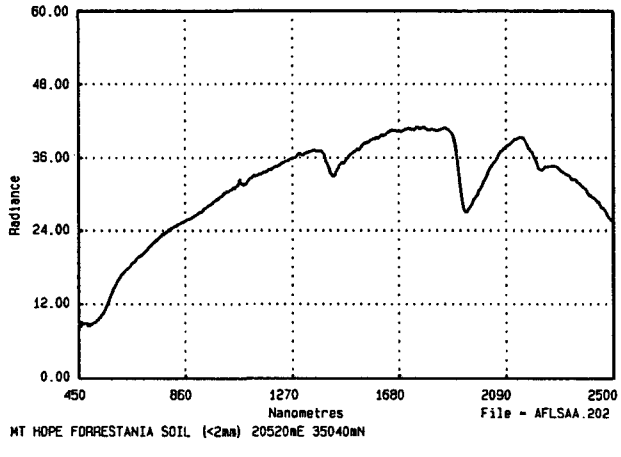

MT HOPE FORRESTANIA SOIL (<2mm) 20520mE 35040mN

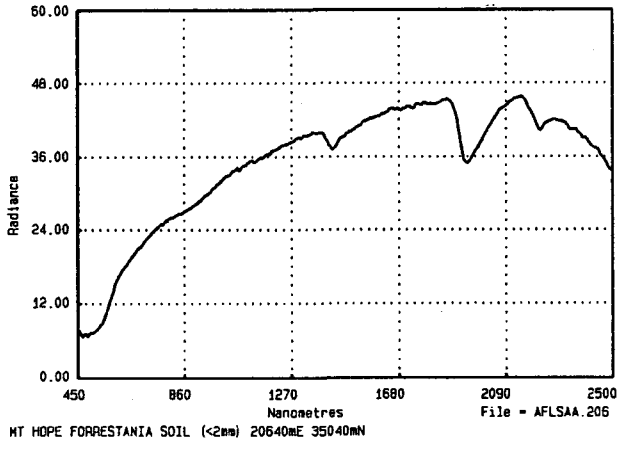

MT HOPE FORRESTANIA SOIL (<2mm) 20640mE 35040mN

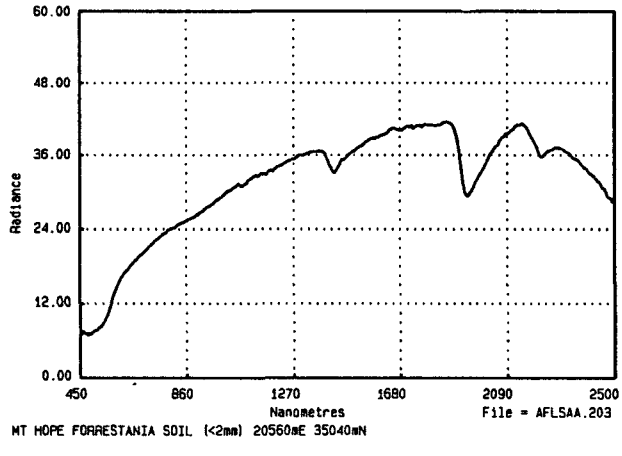

MT HOPE FORRESTANIA SOIL (<2mm) 20560mE 35040mN

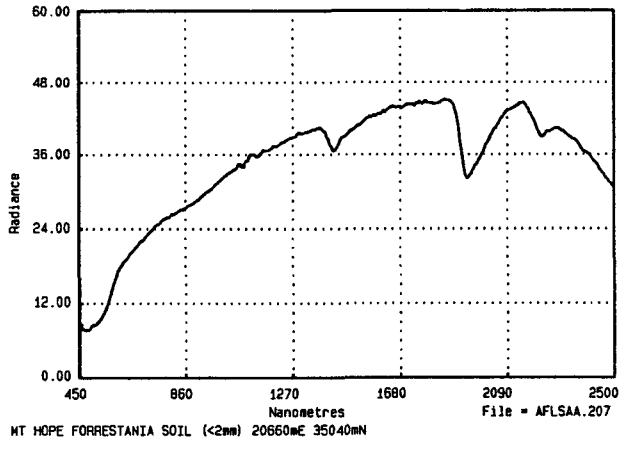

MT HOPE FORRESTANIA SOIL (<2mm) 20660mE 35040mN

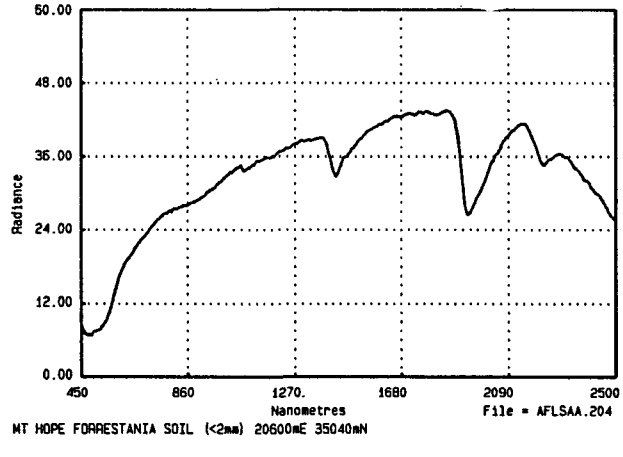

MT HOPE FORRESTANIA SOIL (<2mm) 20600mE 35040mN

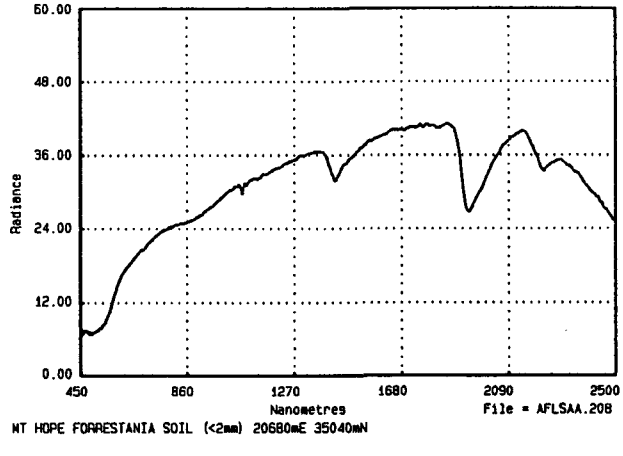

MT HOPE FORRESTANIA SOIL (<2mm) 20680mE 35040mN

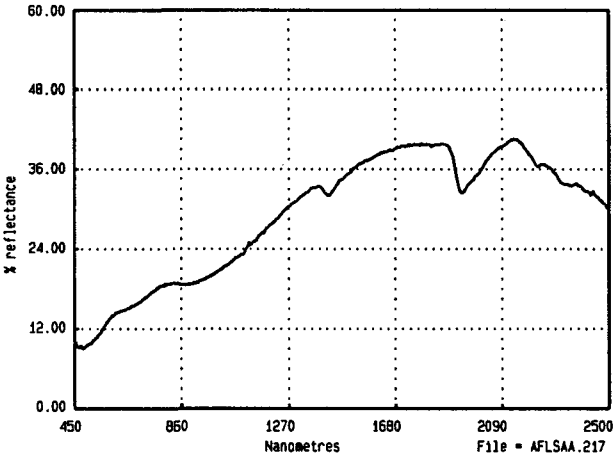

MT HOPE FORRESTANIA SOIL (<2mm) 20720mE 35040mN

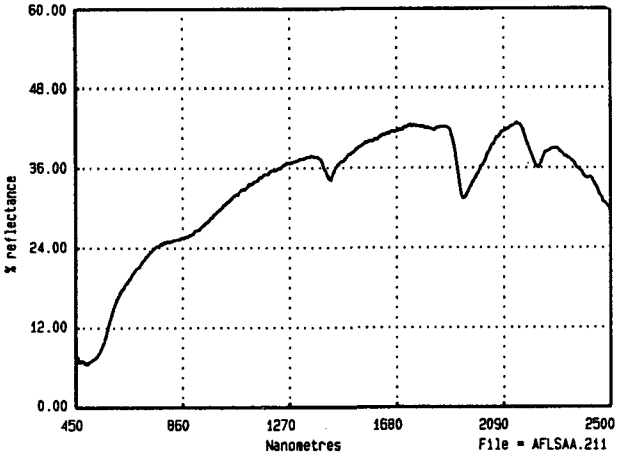

MT HOPE FORRESTANIA SOIL (<2mm) 20800mE 35040mN

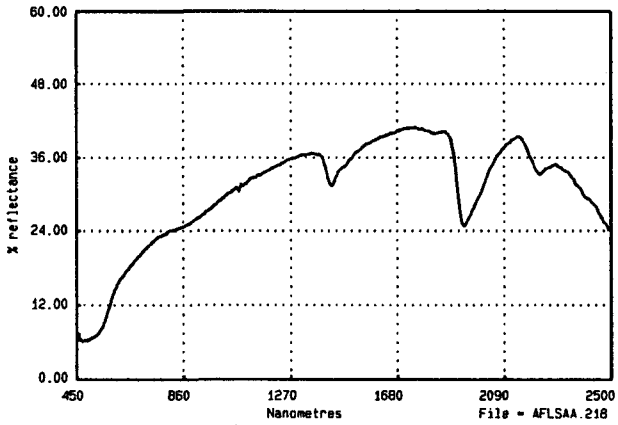

MT HOPE FORRESTANIA SOIL (<2mm) 20740mE 35040mN

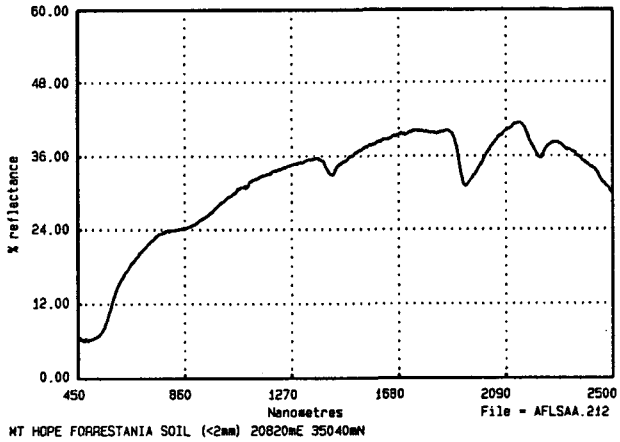

MT HOPE FORRESTANIA SOIL (<2mm) 20820mE 35040mN

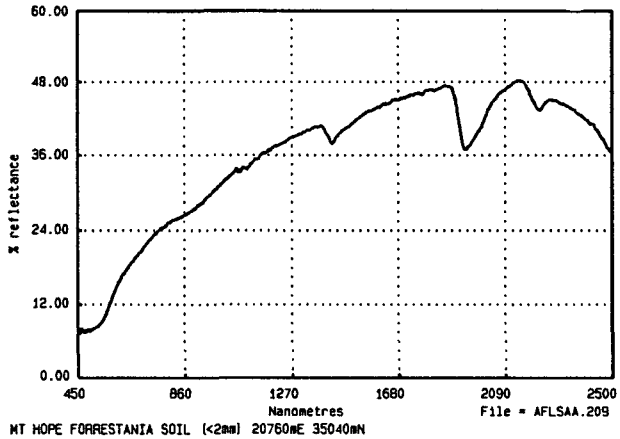

MT HOPE FORRESTANIA SOIL (<2mm) 20760mE 35040mN

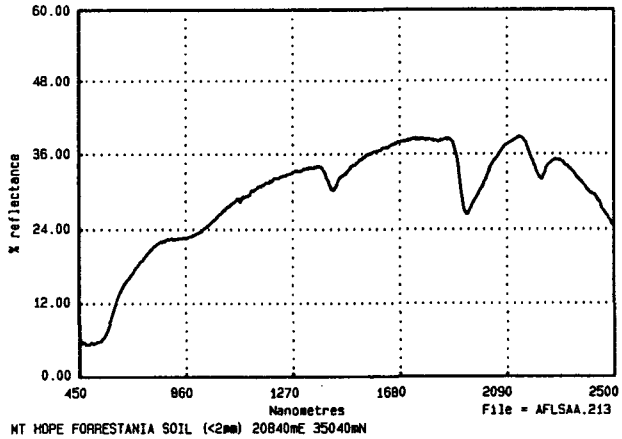

MT HOPE FORRESTANIA SOIL (<2mm) 20840mE 35040mN

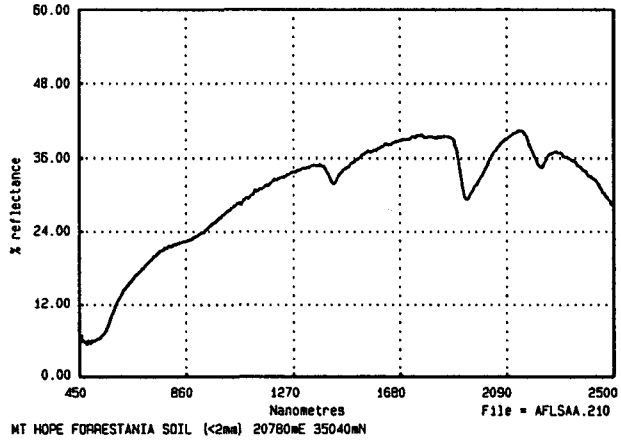

MT HOPE FORRESTANIA SOIL (<2mm) 20780mE 35040mN

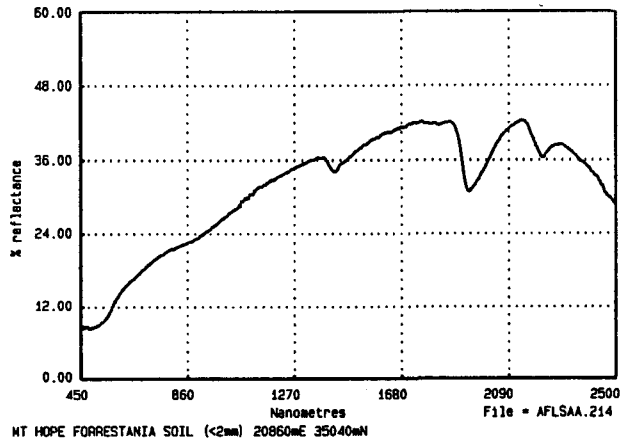

MT HOPE FORRESTANIA SOIL (<2mm) 20860mE 35040mN

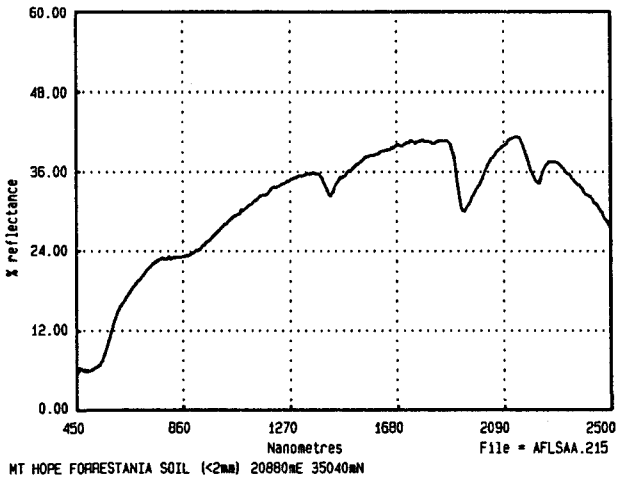

MT HOPE FORRESTANIA SOIL (<2mm) 20880mE 35040mN

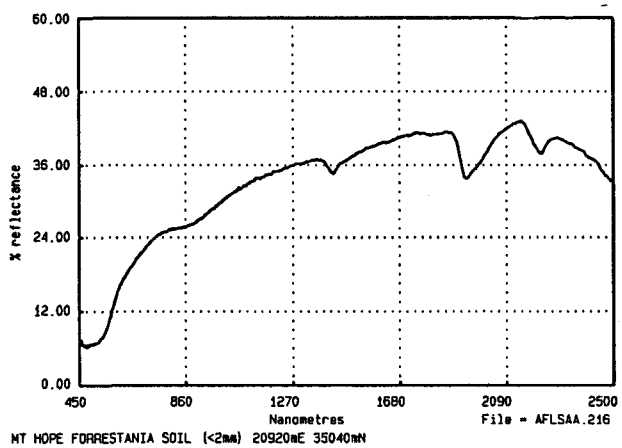

MT HOPE FORRESTANIA SOIL (<2mm) 20920mE 35040mN

MT HOPE SOILS

Line 35040 mN

Selected Absorption Wavelengths, Depths and Widths

-FILENAME-	EAST	NORTH	500nm	590nm	610nm	780nm	900nm	1340nm	1410nm	1500nm	1650nm	2123nm	2165nm	2208nm	2232nm
AFLSAA.201	20480	35040	11.641	22.458	25.050	34.197	37.069	47.612	42.386	47.434	51.030	50.017	47.107	43.573	45.043
AFLSAA.202	20520	35040	8.942	15.231	16.906	24.100	26.930	38.346	34.114	38.723	42.099	40.769	38.268	35.269	36.015
AFLSAA.203	20560	35040	7.718	14.807	16.591	23.930	26.714	37.787	34.312	38.642	41.877	42.784	39.861	37.183	38.372
AFLSAA.204	20600	35040	7.649	15.970	18.327	27.247	29.429	40.182	34.039	40.237	44.369	42.971	39.591	35.879	37.186
AFLSAA.205	20620	35040	6.296	11.287	12.732	20.242	24.084	38.137	36.598	40.259	43.766	46.556	43.748	41.182	42.558
AFLSAA.206	20640	35040	7.462	14.896	16.987	25.420	28.512	41.046	38.637	42.497	45.451	47.531	44.795	42.041	43.412
AFLSAA.207	20660	35040	8.754	16.429	18.326	26.061	28.955	41.448	38.013	42.437	45.627	46.289	43.387	40.487	41.447
AFLSAA.208	20680	35040	7.195	14.748	16.852	24.420	26.384	37.733	32.935	38.205	41.754	41.424	38.017	34.667	36.131
AFLSAA.217	20720	35040	9.710	13.757	14.424	18.505	18.697	32.490	32.006	36.075	38.812	40.463	38.505	36.340	36.601
AFLSAA.218	20740	35040	6.615	13.673	15.814	23.493	25.721	36.557	31.431	36.663	39.998	39.394	36.218	33.214	34.194
AFLSAA.209	20760	35040	7.833	14.072	15.913	24.667	27.424	40.099	37.915	41.675	45.102	48.240	45.653	43.336	44.844
AFLSAA.210	20780	35040	5.979	11.775	13.681	21.306	23.326	34.806	31.820	35.839	38.876	40.405	37.004	34.462	36.692
AFLSAA.211	20800	35040	6.896	14.305	16.423	24.462	26.061	37.594	34.261	38.391	41.539	42.586	38.731	36.015	38.438
AFLSAA.212	20820	35040	6.318	13.298	15.624	23.423	24.928	35.421	32.963	36.582	39.292	41.294	37.901	35.741	37.789
AFLSAA.213	20840	35040	5.635	11.805	14.241	22.207	23.267	33.795	30.169	34.573	37.596	38.550	34.852	32.001	34.461
AFLSAA.214	20860	35040	8.512	13.609	14.953	20.999	23.269	36.052	34.134	37.765	41.101	42.313	38.870	36.388	38.218
AFLSAA.215	20880	35040	5.865	12.844	15.139	22.970	23.814	35.725	32.337	36.707	39.603	41.217	36.800	34.271	36.997
AFLSAA.216	20920	35040	6.975	14.175	16.472	24.934	26.612	36.767	34.589	38.010	40.322	43.363	40.214	37.899	39.978

MT HOPE SOILS

Line 35040 mN

Selected Absorption Wavelengths, Depths and Widths

-FILENAME-	EAST	NORTH	Fe-S	Fe-A	0.9-D	0.9-W	1.4-D	1.4-W	1.9-D	1.9-W	2.2-D	2.2-W
AFLSAA.201	20480	35040	594	892	.029	48.967	.131	42.325	.296	73.193	.094	37.950
AFLSAA.202	20520	35040	592	924	.041	19.492	.135	42.883	.332	71.769	.078	34.163
AFLSAA.203	20560	35040	602	908	.030	23.883	.135	42.883	.332	71.769	.078	34.163
AFLSAA.204	20600	35040	598	898	.046	60.596	.182	43.799	.379	76.497	.113	40.034
AFLSAA.205	20620	35040	602	896	.031	19.817	.081	37.322	.222	66.975	.079	36.741
AFLSAA.206	20640	35040	596	898	.039	43.689	.089	43.812	.222	66.975	.082	39.067
AFLSAA.207	20660	35040	600	898	.038	88.609	.107	42.974	.284	74.337	.084	38.953
AFLSAA.208	20680	35040	600	898	.053	56.234	.153	41.436	.342	75.870	.113	40.034
AFLSAA.217	20720	35040	602	922	.135	45.752	.073	33.881	.192	71.333	.053	24.738
AFLSAA.218	20740	35040	612	878	.043	68.570	.169	42.254	.384	76.902	.103	43.124
AFLSAA.209	20760	35040	610	902	.046	61.401	.087	42.294	.226	71.777	.109	37.682
AFLSAA.210	20780	35040	602	904	.063	72.112	.114	39.603	.270	67.838	.108	36.674
AFLSAA.211	20800	35040	598	904	.068	78.466	.120	33.914	.263	71.766	.108	36.674
AFLSAA.212	20820	35040	600	900	.071	83.844	.099	34.349	.238	72.897	.116	37.974
AFLSAA.213	20840	35040	606	900	.083	86.593	.138	38.120	.318	66.895	.129	40.297
AFLSAA.214	20860	35040	598	904	.061	94.917	.090	39.881	.270	76.011	.103	40.132
AFLSAA.215	20880	35040	606	906	.092	86.355	.124	37.620	.268	72.276	.129	40.297
AFLSAA.216	20920	35040	600	898	.061	76.152	.087	36.122	.204	68.795	.095	41.170

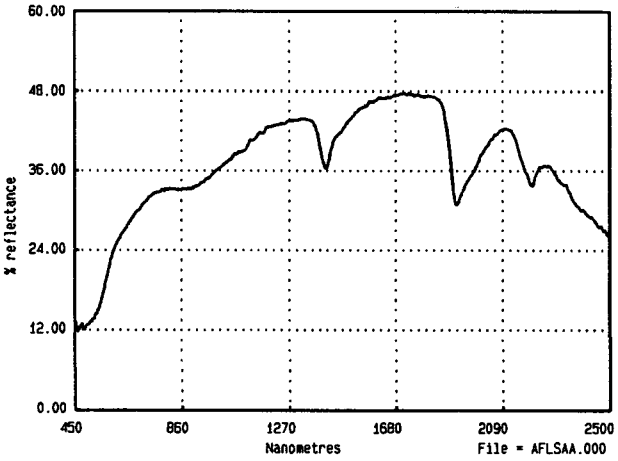

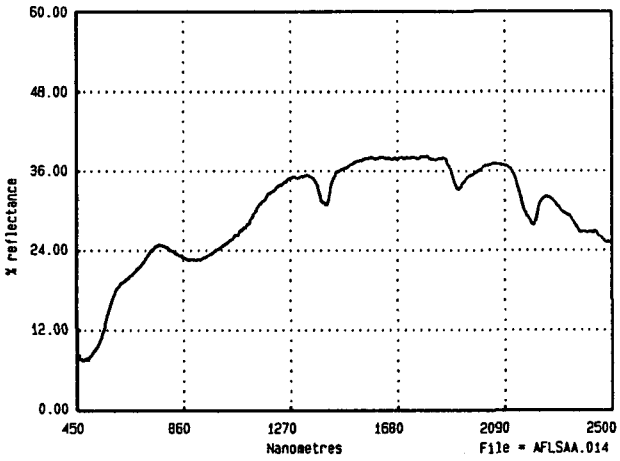

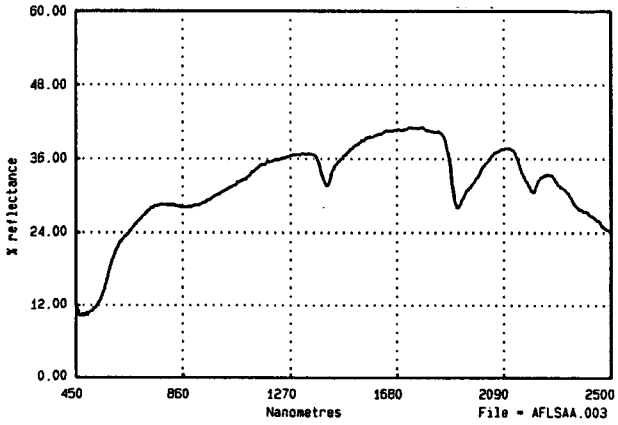

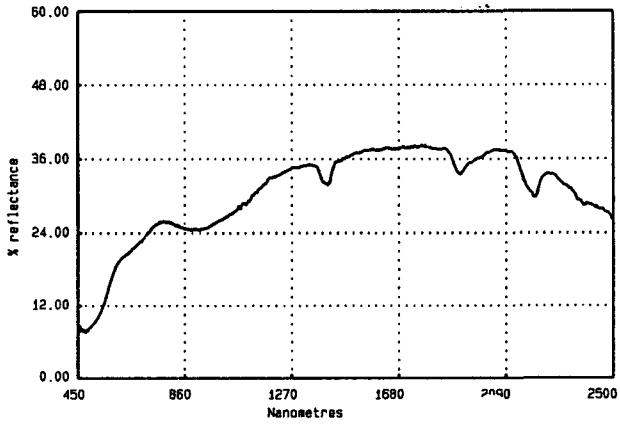

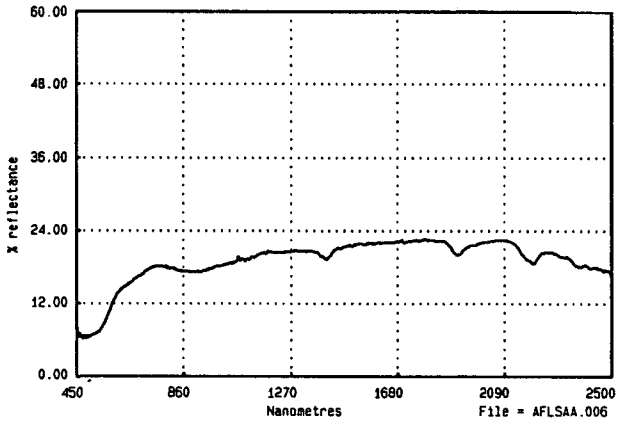

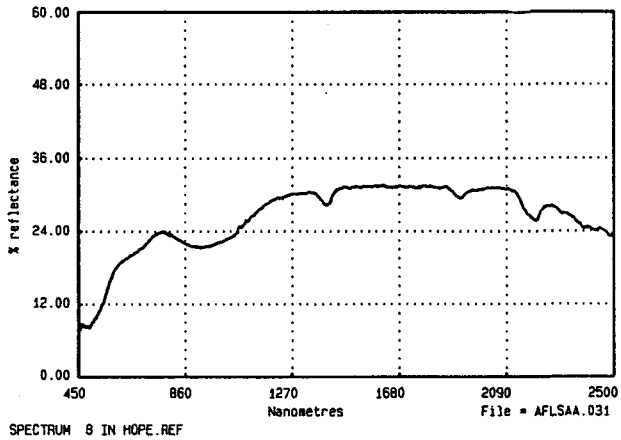

SPECTRUM 8 IN HOPE.REF

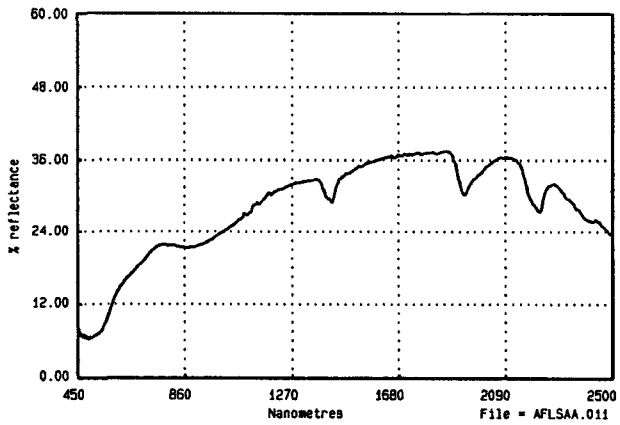

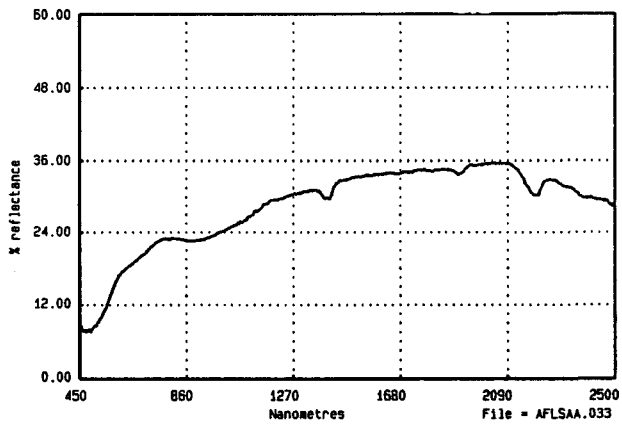

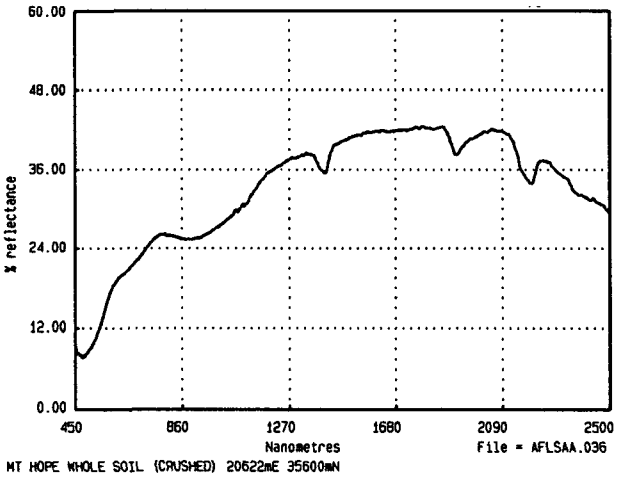

MT HOPE WHOLE SOIL (CRUSHED) 20622mE 35600mN

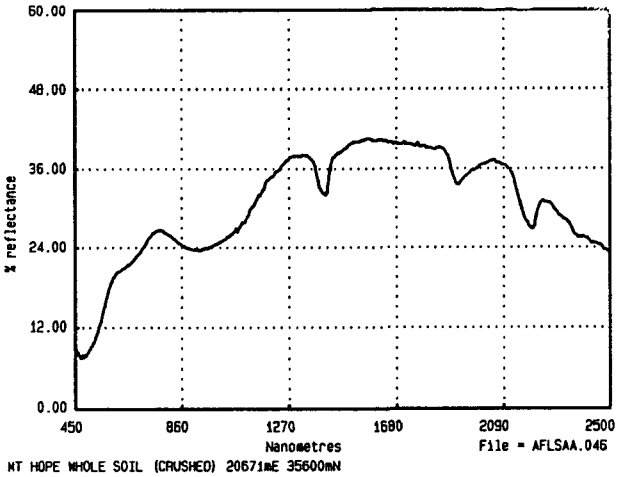

MT HOPE WHOLE SOIL (CRUSHED) 20671mE 35600mN

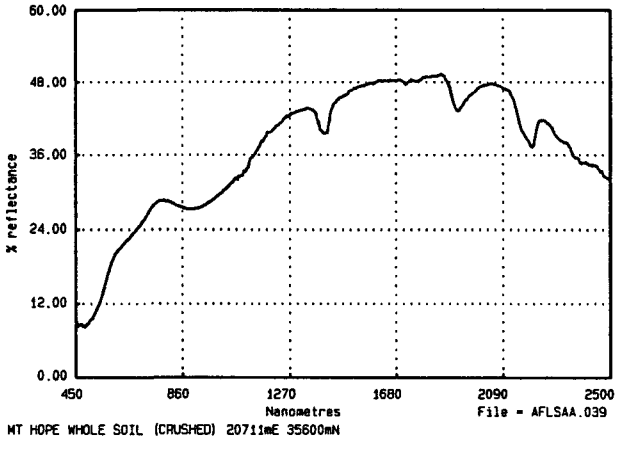

MT HOPE WHOLE SOIL (CRUSHED) 20711mE 35600mN

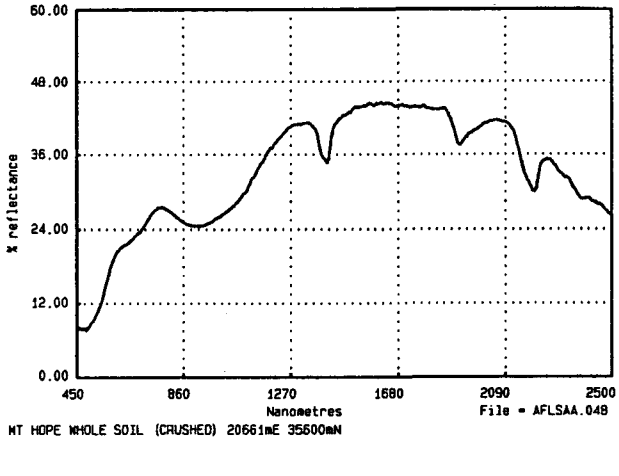

MT HOPE WHOLE SOIL (CRUSHED) 20661mE 35600mN

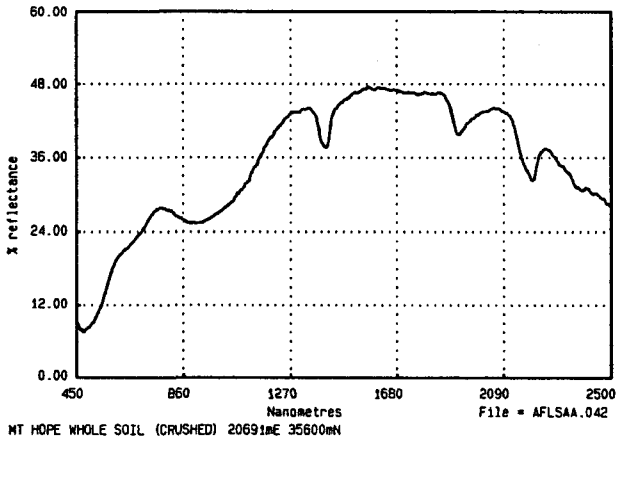

MT HOPE WHOLE SOIL (CRUSHED) 20691mE 35600mN

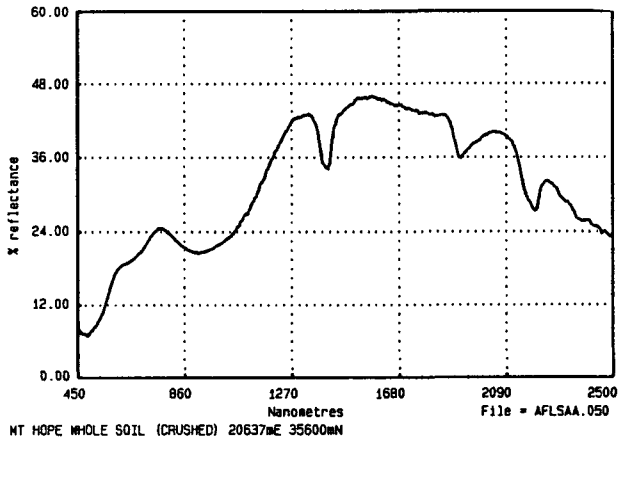

MT HOPE WHOLE SOIL (CRUSHED) 20637mE 35600mN

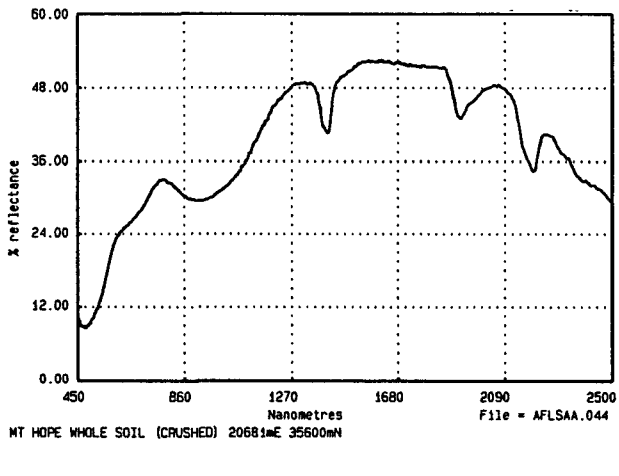

MT HOPE WHOLE SOIL (CRUSHED) 20681mE 35600mN

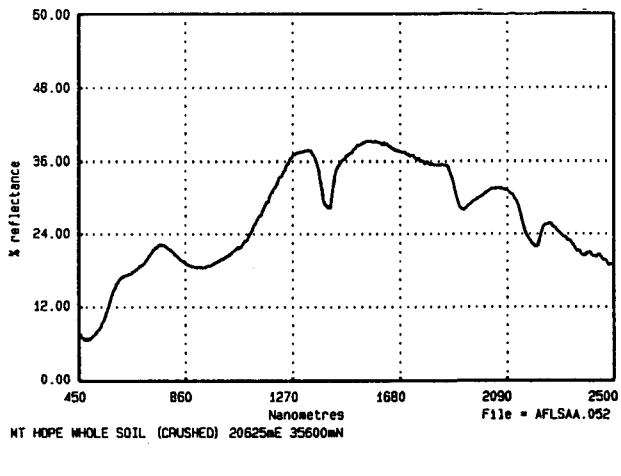

MT HOPE WHOLE SOIL (CRUSHED) 20625mE 35600mN

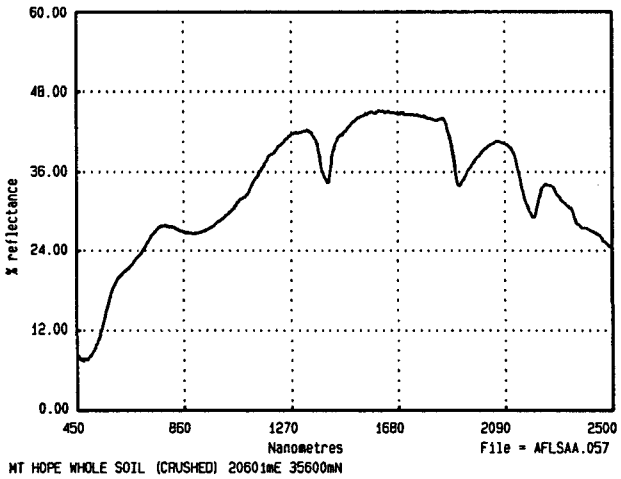

MT HOPE WHOLE SOIL (CRUSHED) 20601mE 35600mN

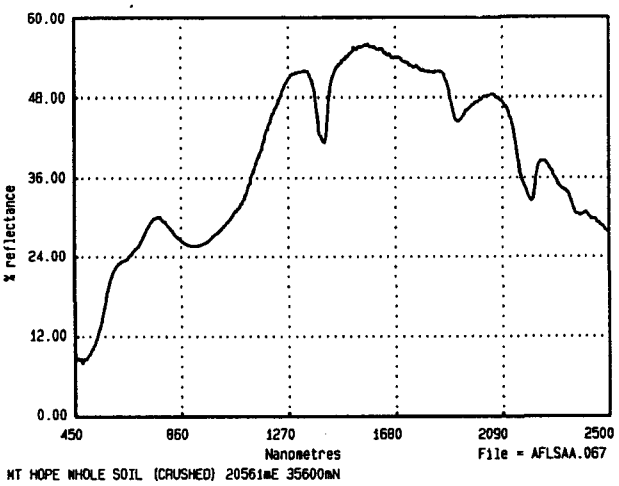

MT HOPE WHOLE SOIL (CRUSHED) 20561mE 35600mN

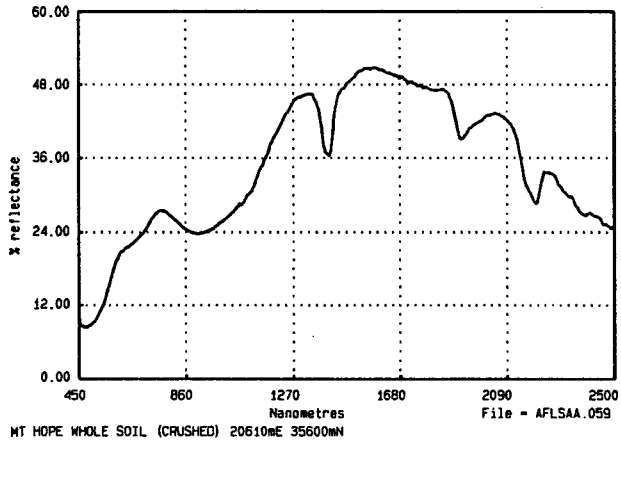

MT HOPE WHOLE SOIL (CRUSHED) 20610mE 35600mN

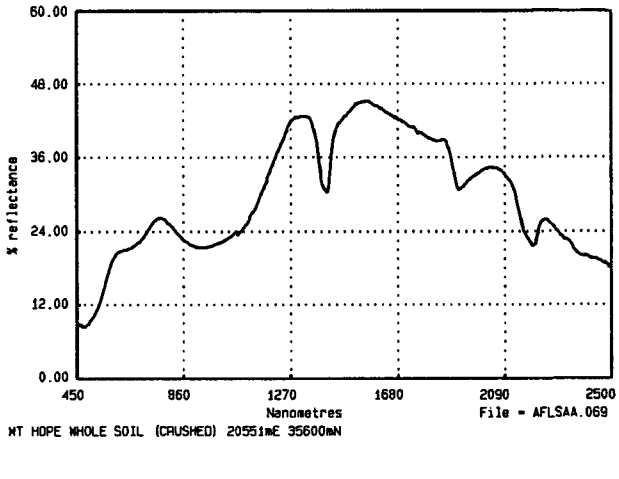

MT HOPE WHOLE SOIL (CRUSHED) 20551mE 35600mN

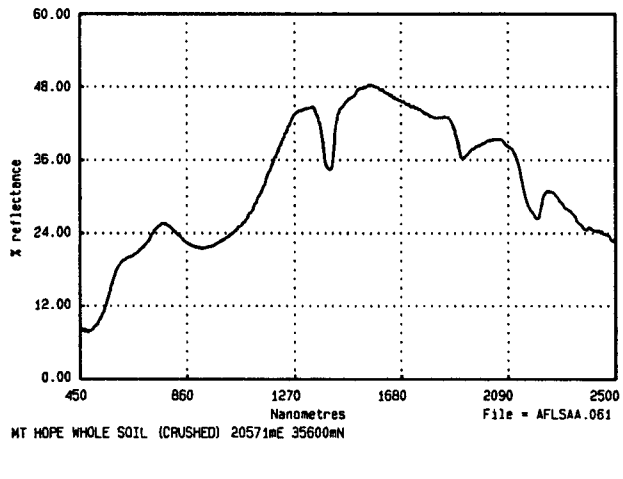

MT HOPE WHOLE SOIL (CRUSHED) 20571mE 35600mN

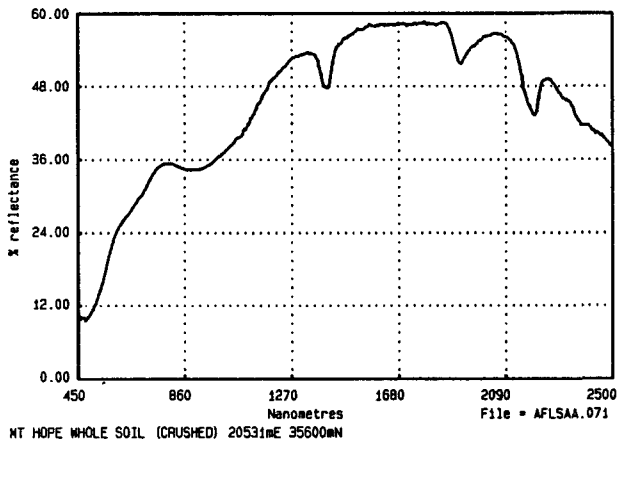

MT HOPE WHOLE SOIL (CRUSHED) 20531mE 35600mN

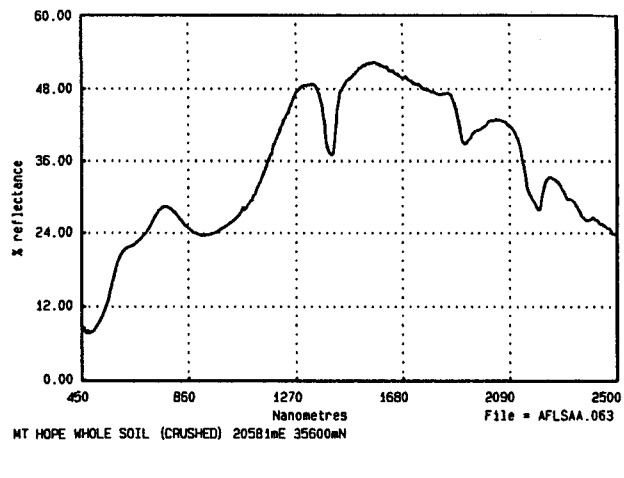

MT HOPE WHOLE SOIL (CRUSHED) 20581mE 35600mN

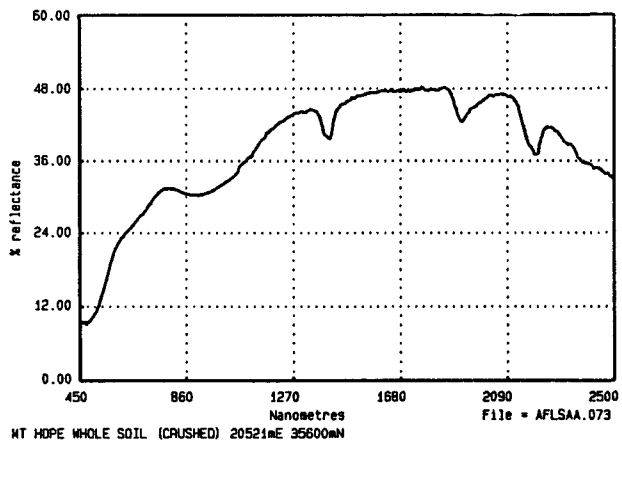

MT HOPE WHOLE SOIL (CRUSHED) 20521mE 35600mN

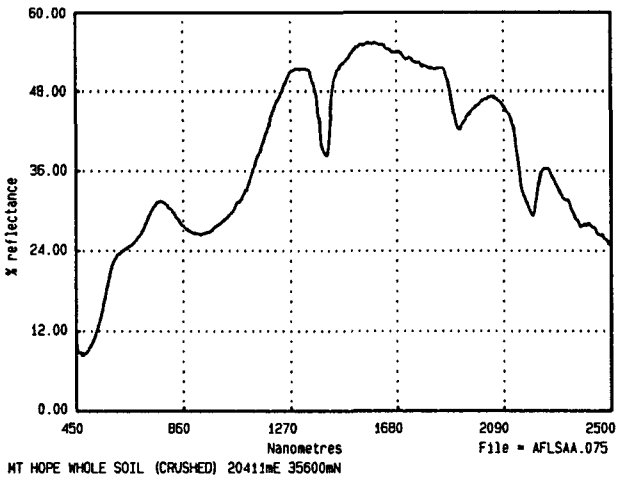

MT HOPE WHOLE SOIL (CRUSHED) 20411mE 35600mN

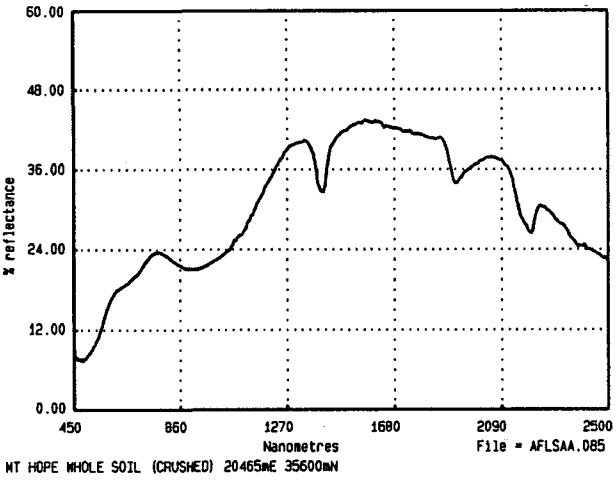

MT HOPE WHOLE SOIL (CRUSHED) 20465mE 35600mN

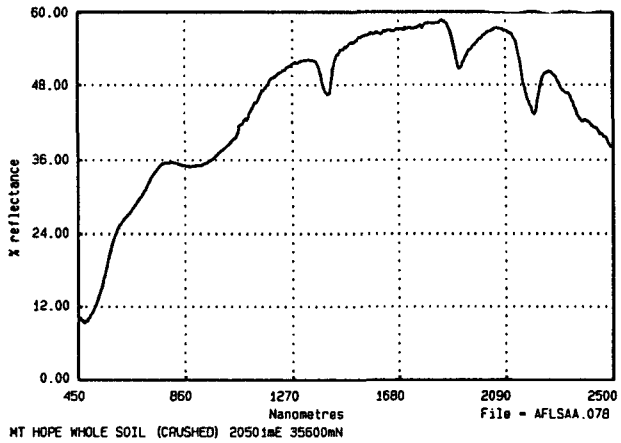

MT HOPE WHOLE SOIL (CRUSHED) 20501mE 35600mN

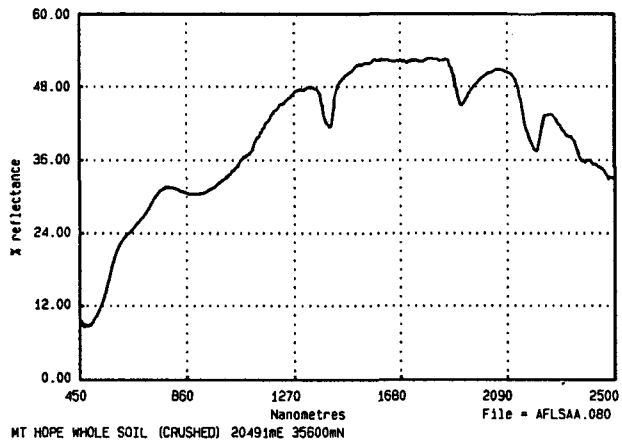

MT HOPE WHOLE SOIL (CRUSHED) 20491mE 35600mN

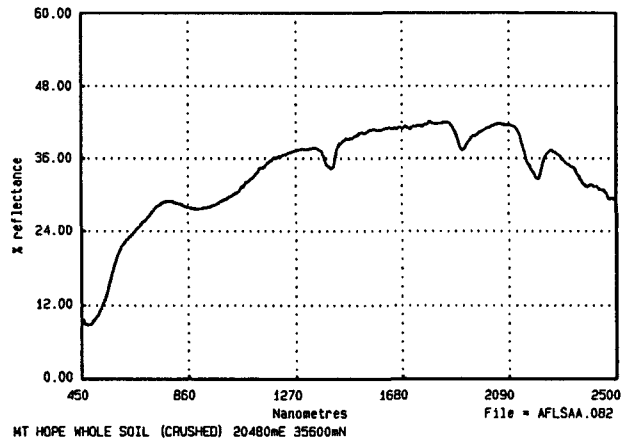

MT HOPE WHOLE SOIL (CRUSHED) 20480mE 35600mN

MT HOPE SOILS

Line 35600 mN

Selected Reflectances

-FILENAME-	EASTING	500nm	590nm	610nm	780nm	900nm	1340nm	1410nm	1455nm	1465nm	1500nm	1650nm	2123nm	2165nm	2208nm	2232nm
AFLSAA.000	20797	12.931	22.780	25.098	37.787	33.312	43.686	36.431	41.407	41.809	43.508	47.218	42.077	37.402	33.896	36.011
AFLSAA.003	20784	10.880	19.665	21.857	28.640	28.380	36.853	31.642	35.642	36.026	37.676	40.542	37.479	33.220	30.628	32.944
AFLSAA.006	20767	6.491	12.371	13.982	18.072	17.261	20.549	19.570	21.121	21.119	21.569	22.105	21.960	19.682	18.731	20.293
AFLSAA.011	20764	6.628	13.085	14.829	21.685	21.373	32.639	29.029	33.214	33.785	34.665	36.483	35.358	29.667	27.678	30.563
AFLSAA.019	20756	8.360	17.888	19.569	25.767	24.688	35.113	37.057	35.687	36.114	36.584	37.738	36.621	31.876	30.310	33.124
AFLSAA.014	20751	8.184	16.958	18.698	24.702	22.569	35.201	31.063	36.073	36.278	37.034	37.934	35.680	30.062	28.460	31.608
AFLSAA.031	20742	8.579	17.774	18.868	24.007	21.270	30.379	28.517	31.027	31.218	31.275	31.076	30.483	27.093	25.896	27.662
AFLSAA.033	20732	8.069	15.930	17.281	22.866	22.651	31.037	30.004	32.646	32.814	33.138	33.968	34.714	31.752	30.372	32.588
AFLSAA.042	20691	8.344	18.367	19.997	27.839	25.452	44.001	37.832	44.669	44.998	46.177	47.129	42.063	34.966	32.675	36.892
AFLSAA.044	20681	9.403	22.530	24.133	33.065	29.629	48.739	40.846	49.616	49.878	50.853	52.177	45.901	37.490	34.817	40.040
AFLSAA.046	20761	8.436	18.777	20.268	26.677	23.720	37.892	32.010	38.388	38.480	39.661	39.925	35.166	29.153	27.074	30.674
AFLSAA.048	20661	8.295	19.023	20.648	27.480	24.620	41.162	35.073	41.938	42.336	42.939	44.348	39.776	32.765	30.421	34.690
AFLSAA.050	20637	7.502	16.850	18.246	24.471	20.668	42.861	34.486	43.056	43.386	44.769	44.744	37.620	29.963	27.513	31.501
AFLSAA.052	20625	7.003	15.186	16.693	22.051	18.509	37.358	28.245	36.100	36.329	37.777	38.030	29.609	23.746	22.005	25.368
AFLSAA.036	20622	8.675	17.848	19.263	26.052	25.425	38.263	35.757	39.864	40.162	40.702	41.687	40.705	35.696	34.018	37.105
AFLSAA.059	20610	9.037	18.928	20.738	27.342	23.822	46.472	36.801	47.252	47.463	49.149	49.683	39.776	31.390	28.951	33.785
AFLSAA.057	20601	8.252	18.504	19.967	27.702	26.581	42.005	34.402	41.460	41.456	43.217	44.928	38.831	31.878	29.507	33.662
AFLSAA.063	20581	8.380	19.447	21.166	28.256	23.760	48.556	37.319	48.703	49.339	50.714	50.391	39.326	30.438	28.161	33.011
AFLSAA.061	20571	8.245	18.049	19.435	25.453	21.640	44.743	34.703	44.882	45.455	46.559	46.264	36.152	28.538	26.533	30.616
AFLSAA.067	20561	8.996	20.782	22.602	29.993	25.714	51.804	41.615	52.533	52.970	54.268	54.297	44.896	35.635	32.896	38.128
AFLSAA.069	20551	9.295	19.603	20.672	26.081	21.739	42.397	30.612	41.701	42.032	43.638	43.033	31.112	23.896	21.934	25.652
AFLSAA.071	20531	10.819	23.365	25.231	35.366	34.393	53.468	48.007	55.035	55.831	56.666	58.244	54.693	46.666	43.718	48.796
AFLSAA.073	20521	10.347	21.655	23.175	31.223	30.356	44.518	39.860	45.417	45.539	46.396	47.571	45.826	39.499	37.163	41.144
AFLSAA.078	20501	10.824	23.643	25.611	35.479	35.012	52.084	46.623	53.812	53.811	55.167	57.020	55.742	47.336	43.874	49.278
AFLSAA.080	20491	9.297	20.911	22.759	31.659	30.412	47.932	41.608	49.166	49.650	50.909	52.212	48.774	40.738	37.787	43.124
AFLSAA.082	20480	9.659	20.376	22.003	28.843	27.706	37.686	34.483	38.937	39.322	37.723	41.051	40.672	34.997	32.829	36.571
AFLSAA.085	20465	8.051	16.437	17.766	23.663	21.002	40.162	33.128	40.658	41.027	41.980	42.525	35.524	28.750	26.655	30.312
AFLSAA.075	20411	9.538	22.049	23.508	31.367	26.520	51.111	38.674	51.287	51.970	53.396	54.295	42.818	32.353	29.854	35.713

MT HOPE SOILS

Line 35600 mN

Selected Absorption Wavelengths, Depths and Widths

-FILENAME-	EAST	NORTH	Fe-S	Fe-A	0.9-D	0.9-W	1.4-D	1.4-W	1.9-D	1.9-W	2.2-D	2.2-W
AFLSAA.000	20797	35600	604	922	.077	114.397	.192	39.188	.326	68.033	.140	37.959
AFLSAA.003	20784	35600	616	926	.089	124.983	.171	38.463	.297	67.285	.134	37.931
AFLSAA.006	20767	35600	612	920	.106	088.559	.106	31.368	.114	41.754	.130	40.642
AFLSAA.011	20764	35600	624	932	.136	124.371	.149	30.968	.187	45.892	.187	42.256
AFLSAA.019	20756	35600	598	946	.144	135.678	.117	30.044	.116	45.893	.152	41.821
AFLSAA.014	20751	35600	600	938	.196	146.968	.154	34.166	.122	41.871	.181	42.949
AFLSAA.031	20742	35600	590	956	.182	131.508	.085	30.862	.061	35.554	.119	44.457
AFLSAA.033	20732	35600	600	942	.104	120.794	.084	25.674	.041	33.921	.111	49.918
AFLSAA.042	20691	35600	600	920	.230	153.414	.170	31.083	.132	47.846	.186	44.267
AFLSAA.044	20681	35600	592	962	.230	151.367	.196	32.080	.149	45.668	.202	45.106
AFLSAA.046	20761	35600	592	974	.228	156.075	.183	32.804	.131	45.371	.192	46.451
AFLSAA.048	20661	35600	596	958	.235	156.168	.186	29.078	.129	42.751	.198	40.493
AFLSAA.050	20637	35600	600	978	.329	168.316	.230	30.602	.149	50.757	.221	43.826
AFLSAA.052	20625	35600	598	962	.328	168.815	.263	32.508	.182	60.572	.219	47.111
AFLSAA.036	20622	35600	592	950	.140	136.694	.105	29.878	.098	41.583	.134	43.821
AFLSAA.059	20610	35600	594	958	.294	168.137	.247	31.134	.152	48.830	.237	48.537
AFLSAA.057	20601	35600	590	962	.169	146.195	.206	34.202	.214	53.774	.205	44.726
AFLSAA.063	20581	35600	596	982	.333	167.284	.263	34.619	.153	46.751	.247	46.138
AFLSAA.061	20571	35600	594	988	.327	166.321	.252	30.970	.139	46.251	.232	48.852
AFLSAA.067	20561	35600	598	962	.313	168.149	.231	34.755	.125	48.458	.227	48.488
AFLSAA.069	20551	35600	588	999	.346	154.695	.305	35.448	.182	51.116	.264	46.458
AFLSAA.071	20531	35600	590	958	.157	145.109	.139	31.766	.109	42.336	.165	44.354
AFLSAA.073	20521	35600	584	960	.142	135.224	.129	30.746	.113	44.547	.153	41.252
AFLSAA.078	20501	35600	590	952	.135	132.166	.139	29.454	.131	43.446	.181	42.275
AFLSAA.080	20491	35600	596	956	.161	143.116	.167	32.205	.136	48.260	.187	40.523
AFLSAA.082	20480	35600	596	950	.122	127.797	.121	31.607	.111	40.425	.163	40.241
AFLSAA.085	20465	35600	596	982	.275	166.213	.212	29.273	.149	50.152	.208	42.706
AFLSAA.075	20411	35600	592	978	.313	167.503	.281	34.202	.160	51.937	.272	48.518

MT HOPE SOILS

Line 35600 mN

Selected ICP Analyses

-FILENAME-	EAST	SiO2	Al2O3	Fe2O3	CaO	Au
AFLSAA.000	20797	49.3	11.1	6.8	8.93	0.998
AFLSAA.003	20784	51.1	12.0	12.3	5.99	0.290
AFLSAA.006	20767	46.8	15.3	32.7	0.10	0.290
AFLSAA.011	20764					
AFLSAA.019	20756	47.1	12.7	34.6	0.06	0.092
AFLSAA.014	20751					
AFLSAA.031	20742					
AFLSAA.033	20732	51.3	13.3	27.1	0.07	0.240
AFLSAA.042	20691	55.8	17.2	27.5	0.06	0.040
AFLSAA.044	20681	58.9	18.2	29.6	0.06	0.060
AFLSAA.046	20761					
AFLSAA.048	20661	58.7	18.5	26.6	0.03	0.180
AFLSAA.050	20637	43.3	22.3	32.8	0.09	0.018
AFLSAA.052	20625	41.7	25.0	25.2	0.14	0.016
AFLSAA.036	20622					
AFLSAA.059	20610					
AFLSAA.057	20601					
AFLSAA.063	20581	36.2	31.2	15.4	0.30	0.020
AFLSAA.061	20571					
AFLSAA.067	20561	33.6	20.0	33.1	0.04	0.016
AFLSAA.069	20551					
AFLSAA.071	20531	53.0	13.1	19.6	0.06	0.012
AFLSAA.073	20521					
AFLSAA.078	20501					
AFLSAA.080	20491	51.8	14.4	20.5	0.08	0.032
AFLSAA.082	20480					
AFLSAA.085	20465	53.4	16.2	22.9	0.09	0.026
AFLSAA.075	20411	43.6	22.6	20.8	0.02	0.144

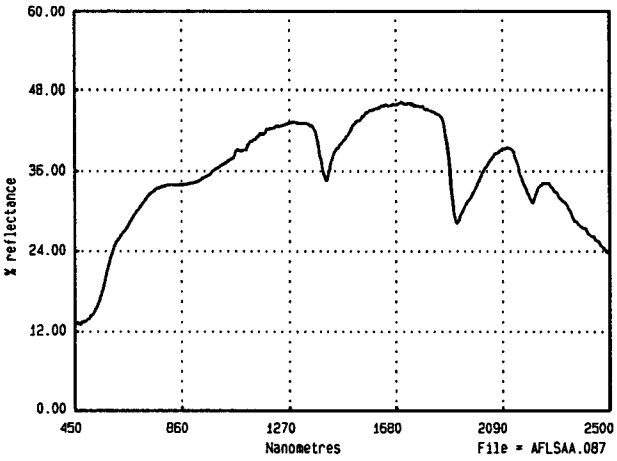
60.00
48.00
36.00
24.00
12.00
0.00
% reflectance
450
860
1270
1680
2090
2500
Nanometres
File = AFLSAA.087

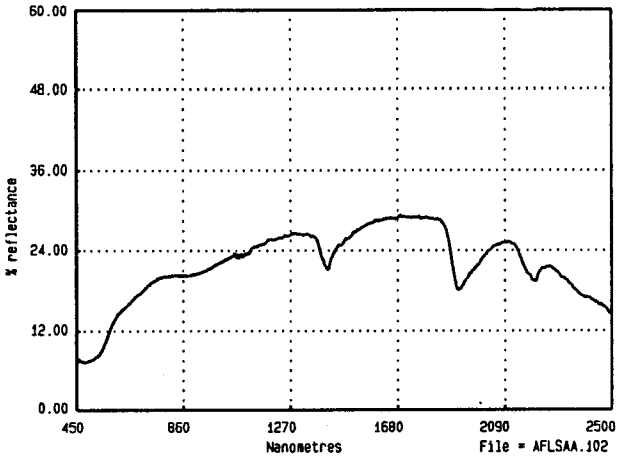
60.00
48.00
36.00
24.00
12.00
0.00
% reflectance
450
860
1270
1680
2090
2500
Nanometres
File = AFLSAA.102

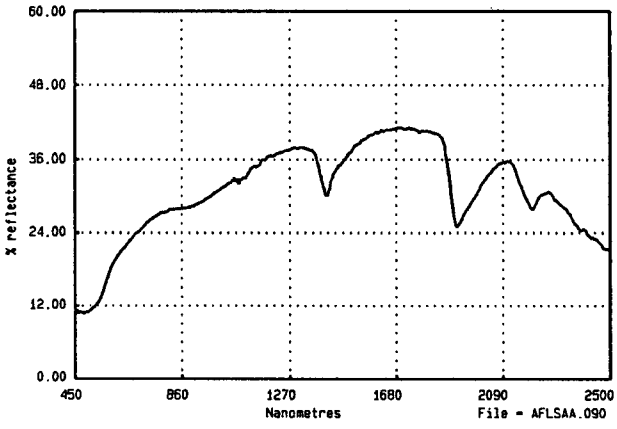
60.00
48.00
36.00
24.00
12.00
0.00
% reflectance
450
860
1270
1680
2090
2500
Nanometres
File = AFLSAA.090

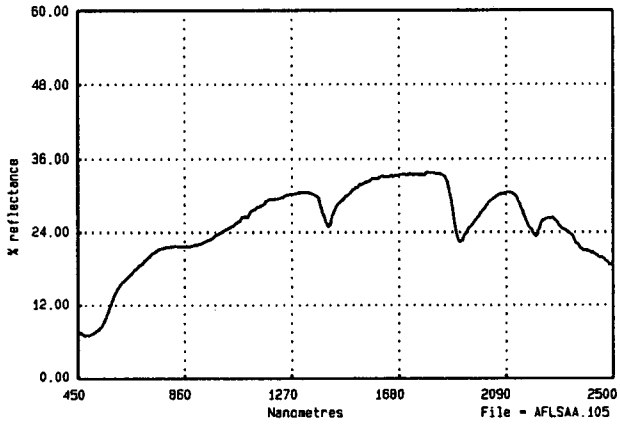
60.00
48.00
36.00
24.00
12.00
0.00
% reflectance
450
860
1270
1680
2090
2500
Nanometres
File = AFLSAA.105

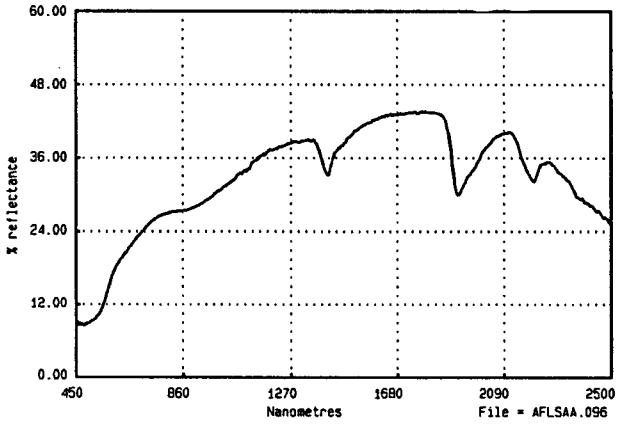
60.00
48.00
36.00
24.00
12.00
0.00
% reflectance
450
860
1270
1680
2090
2500
Nanometres
File = AFLSAA.096

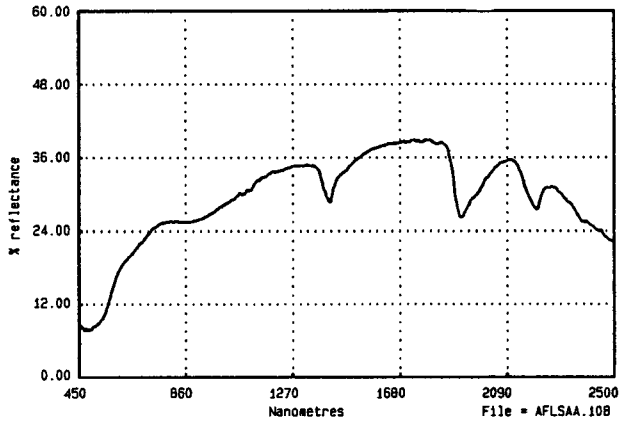
60.00
48.00
36.00
24.00
12.00
0.00
% reflectance
450
860
1270
1680
2090
2500
Nanometres
File = AFLSAA.108

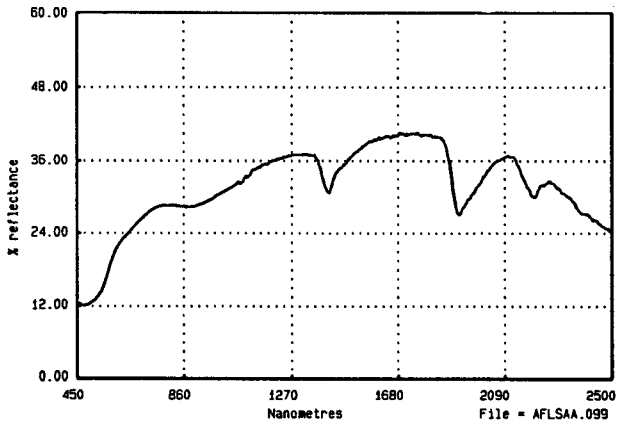
60.00
48.00
36.00
24.00
12.00
0.00
% reflectance
450
860
1270
1680
2090
2500
Nanometres
File = AFLSAA.099

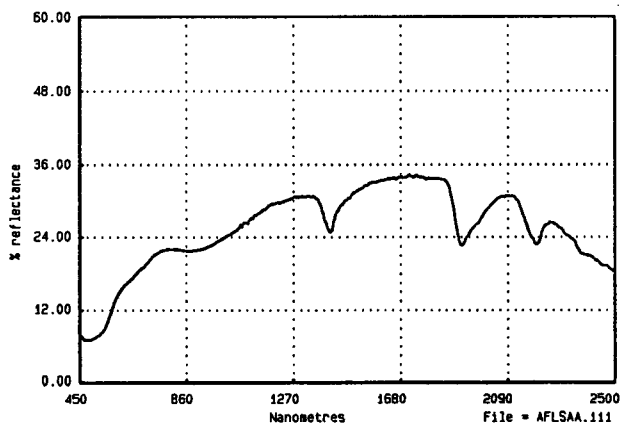
60.00
48.00
36.00
24.00
12.00
0.00
% reflectance
450
860
1270
1680
2090
2500
Nanometres
File = AFLSAA.111

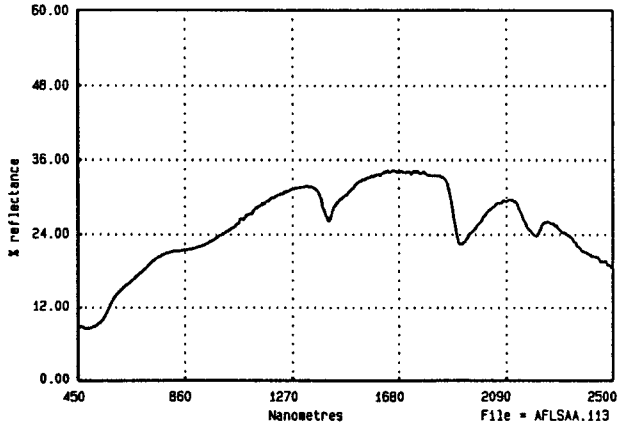
60.00
48.00
36.00
24.00
12.00
0.00
% reflectance
450
860
1270
1680
2090
2500
Nanometres
File = AFLSAA.113

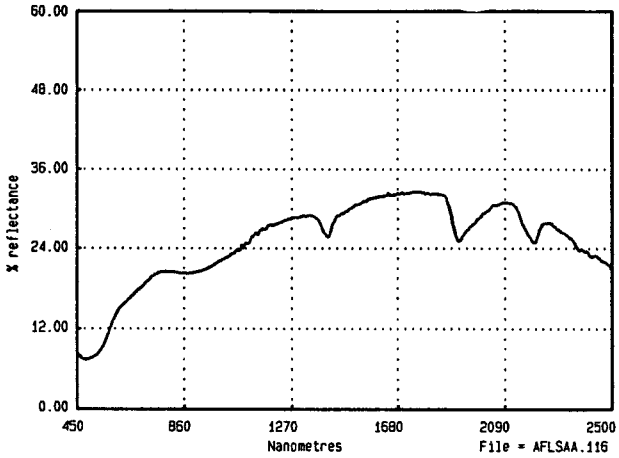
60.00
48.00
36.00
24.00
12.00
0.00
% reflectance
450
860
1270
1680
2090
2500
Nanometres
File = AFLSAA.116

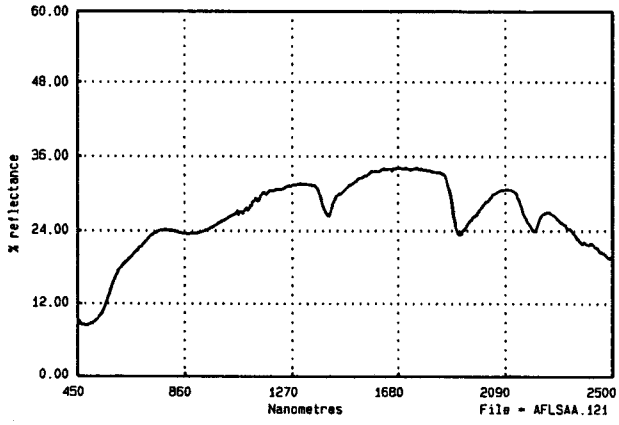
60.00
48.00
36.00
24.00
12.00
0.00
% reflectance
450
860
1270
1680
2090
2500
Nanometres
File = AFLSAA.121

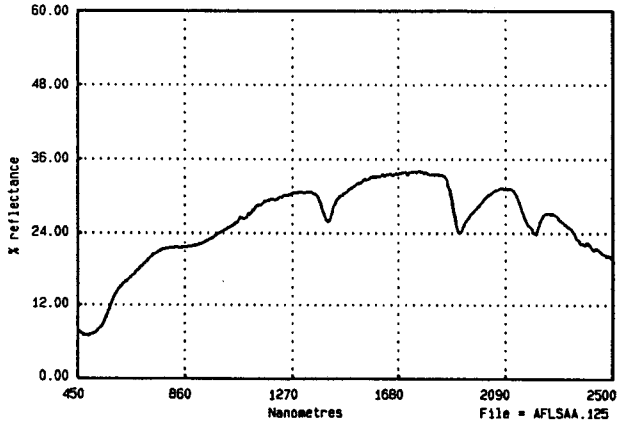
60.00
48.00
36.00
24.00
12.00
0.00
% reflectance
450
860
1270
1680
2090
2500
Nanometres
File = AFLSAA.125

MT HOPE SOILS

Line 35800

Selected Absorption Wavelengths, Depths and Widths

-FILENAME-	EAST	NORTH	Fe-S	Fe-A	0.9-D	0.9-W	1.4-D	1.4-W	1.9-D	1.9-W	2.2-D	2.2-W
AFLSAA.087	20853	35800	600	924	.064	105.746	.212	29.273	.347	73.474	.143	39.607
AFLSAA.090	20817	35800	588	920	.061	098.593	.226	39.317	.358	73.489	.152	43.257
AFLSAA.096	20765	35800	596	926	.075	120.357	.179	37.310	.297	66.597	.141	42.380
AFLSAA.099	20742	35800	596	928	.082	121.230	.198	39.755	.308	70.172	.129	38.929
AFLSAA.102	20705	35800	592	926	.068	095.804	.228	39.305	.351	68.098	.160	37.016
AFLSAA.105	20680	35800	600	928	.092	123.841	.209	36.421	.317	65.597	.170	39.862
AFLSAA.108	20643	35800	596	922	.085	116.495	.205	33.357	.305	67.191	.166	43.965
AFLSAA.111	20608	35800	592	932	.110	133.008	.222	37.049	.311	64.545	.191	44.143
AFLSAA.113	20595	35800	590	940	.079	114.601	.196	38.634	.309	70.467	.133	40.384
AFLSAA.116	20583	35800	598	930	.111	119.210	.146	34.213	.213	58.827	.148	40.995
AFLSAA.121	20568	35800	594	924	.105	121.807	.188	33.374	.286	68.000	.159	39.419
AFLSAA.125	20523	35800	594	926	.085	109.581	.184	33.056	.268	57.028	.173	42.909

MT HOPE SOILS

Line 35800 mN

Selected Reflectances

-FILENAME-	EAST	NORTH	500nm	590nm	610nm	780nm	900nm	1340nm	1410nm	1500nm	1650nm	2123nm	2165nm	2208nm	2232nm
AFLSAA.087	20853	35800	13.946	23.470	25.579	33.700	34.178	42.915	43.563	41.770	45.616	39.341	34.638	31.415	33.756
AFLSAA.090	20817	35800	11.011	18.456	20.120	27.428	28.484	37.510	30.145	37.137	40.698	35.449	30.969	27.939	30.046
AFLSAA.096	20765	35800	8.922	17.015	18.871	26.589	27.841	38.808	33.178	39.754	43.108	39.844	35.065	32.126	34.934
AFLSAA.099	20742	35800	12.519	20.502	22.311	28.596	28.475	36.985	30.807	36.941	39.806	36.662	32.728	30.012	31.950
AFLSAA.102	20705	35800	7.478	13.237	14.618	20.005	20.449	26.360	21.224	26.294	28.827	24.948	21.547	19.363	21.307
AFLSAA.105	20680	35800	7.159	13.674	15.245	21.456	21.944	30.291	24.896	30.955	33.351	30.104	25.978	23.436	25.999
AFLSAA.108	20643	35800	7.950	16.126	18.179	25.386	25.682	34.592	28.889	35.320	38.101	35.104	30.236	27.588	30.765
AFLSAA.111	20608	35800	7.367	13.984	15.552	21.974	21.878	30.652	24.787	31.233	33.777	30.204	25.407	23.056	25.890
AFLSAA.113	20595	35800	8.672	13.778	14.777	20.767	21.898	31.702	26.194	31.419	34.193	29.379	25.480	23.810	25.848
AFLSAA.116	20583	35800	7.649	13.549	15.024	20.462	20.838	29.074	25.776	30.211	32.017	30.640	26.983	24.970	27.658
AFLSAA.121	20568	35800	8.744	16.135	17.865	24.099	23.609	31.447	26.465	31.724	34.009	30.332	26.189	24.140	26.690
AFLSAA.125	20523	35800	7.177	13.489	15.007	21.482	22.073	30.707	25.948	31.396	33.568	30.677	26.196	23.784	26.734

MT HOPE SOILS

Line 35800 mN

Selected ICP Analyses

-FILENAME-	EASTING	SiO2	Al2O3	Fe2O3	CaO	Na2O	K2O	S	Au
AFLSAA.087	20853	58.30	9.24	3.88	5.46	0.46	0.48	0.047	0.152
AFLSAA.090	20817	61.30	10.80	4.34	4.57	0.46	0.48	0.050	0.152
AFLSAA.096	20765	65.70	10.60	4.78	5.54	0.53	0.48	0.035	0.208
AFLSAA.099	20742	66.0	12.90	5.04	7.74	0.46	0.60	0.068	0.204
AFLSAA.102	20705	65.80	12.90	5.06	3.07	0.30	0.60	0.036	0.224
AFLSAA.105	20680	69.0	11.0	4.72	3.87	0.38	0.36	0.028	0.100
AFLSAA.108	20643	68.0	10.40	4.28	2.23	0.30	0.36	0.045	0.086
AFLSAA.111	20608	77.60	11.00	8.83	0.36	0.00	0.24	0.018	0.020
AFLSAA.113	20595	63.10	11.20	4.76	1.74	0.30	0.48	0.039	0.030
AFLSAA.116	20583	70.70	12.10	9.10	0.71	0.15	0.36	0.062	0.020
AFLSAA.121	20568	76.00	11.40	7.02	0.72	0.15	0.36	0.039	0.030
AFLSAA.125	20523	69.90	13.50	5.37	1.06	0.37	0.36	0.018	0.022

MT HOPE SOILS

STANDARDS

Selected Reflectances
Before Acid Treatment and Drying in an Oven at 100 °C

-FILENAME-	EAST	500nm	590nm	610nm	780nm	900nm	1340nm	1410nm	1455nm	1465nm	1500nm	1650nm	2123nm	2165nm	2208nm	2232nm
AFLSAC.000	20797	13.229	23.596	25.918	33.228	33.331	40.370	32.299	35.406	36.236	37.842	41.397	35.655	31.491	27.899	29.849
AFLSAD.000	20797	13.436	23.496	25.841	33.414	33.480	41.883	33.779	00.000	37.956	39.738	43.244	37.421	27.178	29.143	31.361
AFLSAE.000	20797	11.851	19.312	21.190	27.783	28.511	35.729	28.705	32.017	31.881	33.844	37.457	32.298	28.680	25.750	27.667
AFLSAF.000	20797	15.171	25.732	28.168	35.244	35.175	42.997	31.081	38.332	38.820	40.709	44.278	37.000	32.527	29.334	31.301
AFLSAG.000	20797	13.826	23.900	26.270	34.720	35.207	43.501	32.470	38.679	38.634	40.747	45.120	38.190	34.240	30.623	32.647
AFLSAC.099	20742	12.752	21.304	23.293	30.336	30.113	37.286	28.978	32.754	32.996	34.876	38.663	33.110	28.931	25.900	27.513
AFLSAD.099	20742	11.887	20.303	22.031	29.204	29.757	36.584	31.309	32.511	32.724	34.566	38.023	32.455	28.211	25.149	37.076
AFLSAE.099	20742	15.707	25.447	27.629	34.270	33.494	38.571	28.993	34.422	34.992	36.442	39.720	34.663	30.762	27.984	29.735
AFLSAF.099	20742	13.826	23.235	25.540	33.109	33.170	40.748	34.632	36.505	36.855	38.621	42.366	35.978	31.599	28.213	30.279

Selected Reflectances
After Acid Treatment and Drying in an Oven at 100 °C

-FILENAME-	EAST	500nm	590nm	610nm	780nm	900nm	1340nm	1410nm	1455nm	1465nm	1500nm	1650nm	2123nm	2165nm	2208nm	2232nm
AFLSBA.000	20797	9.684	19.419	22.019	29.949	30.193	40.622	34.726	39.757	39.823	41.139	44.053	41.708	34.561	30.125	33.101
AFLSBB.000	20797	9.196	18.062	20.239	26.481	26.202	34.151	28.540	32.908	32.769	34.341	37.065	33.839	28.003	24.126	26.768
AFLSBC.000	20797	8.841	17.433	19.644	25.886	25.572	32.945	26.875	31.436	31.726	32.922	35.689	31.465	25.405	21.715	24.364
AFLSBD.000	20797	8.850	17.343	19.566	25.765	25.470	32.821	27.000	31.546	31.474	32.920	35.423	31.312	25.431	21.716	24.164
AFLSBE.000	20797	8.440	16.624	18.840	24.832	24.602	33.505	27.740	32.305	32.338	33.865	36.740	33.520	27.134	23.362	25.829

MT HOPE SOILS

STANDARDS

Selected Absorption Wavelengths, Depths and Widths Before Acid Treatment and Drying in an Oven at 100 °C

-FILENAME-	EAST	NORTH	Fe-S	Fe-A	0.9-D	0.9-W	1.4-D	1.4-W	1.9-D	1.9-W	2.2-D	2.2-W
AFLSAC.000	20797	35600	604	902	0.058	75.205	0.212	45.034	0.372	81.322	0.148	40.265
AFLSAD.000	20797	35600	600	922	0.076	84.318	0.209	43.492	0.369	81.956	0.152	38.111
AFLSAE.000	20797	35600	602	916	0.058	82.165	0.211	47.070	0.367	77.385	0.135	40.882
AFLSAF.000	20797	35600	606	924	0.069	85.259	0.210	47.782	0.367	76.086	0.140	41.779
AFLSAG.000	20797	35600	604	918	0.058	78.397	0.220	50.563	0.386	78.542	0.139	39.967
AFLSAC.099	20742	35800	606	920	0.072	88.422	0.243	46.720	0.386	81.151	0.148	41.827
AFLSAD.099	20742	35800	604	912	0.060	74.417	0.233	46.330	0.377	79.214	0.156	40.955
AFLSAE.099	20742	35800	602	920	0.062	90.232	0.211	47.634	0.331	76.208	0.133	42.372
AFLSAF.099	20742	35800	606	926	0.070	93.542	0.222	48.366	0.368	75.394	0.145	42.693

Selected Absorption Wavelengths, Depths and Widths After Acid Treatment and Drying in an Oven at 100 °C

-FILENAME-	EAST	NORTH	Fe-S	Fe-A	0.9-D	0.9-W	1.4-D	1.4-W	1.9-D	1.9-W	2.2-D	2.2-W
AFLSBA.000	20797	35600	610	916	0.086	111.547	0.179	34.801	0.284	66.203	0.211	43.618
AFLSBB.000	20797	35600	608	912	0.086	108.314	0.191	40.619	0.313	69.664	0.209	45.468
AFLSBC.000	20797	35600	608	908	0.087	104.862	0.209	35.757	0.340	70.229	0.233	39.488
AFLSBD.000	20797	35600	610	908	0.087	99.116	0.210	35.755	0.341	74.324	0.228	45.993
AFLSBE.000	20797	35600	608	916	0.105	103.122	0.207	36.267	0.351	71.824	0.229	48.314

MT HOPE SOIL

HCl ACID AND OVEN DRIED SOILS FROM LINE 35600 mN

Selected Absorption Wavelengths, Depths and Widths

-FILENAME-	EAST	NORTH	Fe-S	Fe-A	0.9-D	0.9-W	1.4-D	1.4-W	1.9-D	1.9-W	2.2-D	2.2-W
AFLSBA.000	20797	35600	0.610	0.916	0.086	111.547	0.179	34.801	0.284	66.203	0.211	43.618
AFLSBA.003	20784	35600	0.610	0.916	0.064	90.006	0.171	35.042	0.251	63.283	0.179	39.354
AFLSBA.019	20756	35600	0.598	0.946	0.114	141.067	0.124	33.261	0.092	54.340	0.174	43.771
AFLSBA.033	20732	35600	0.600	0.958	0.127	150.692	0.127	33.583	0.093	56.337	0.178	39.502
AFLSBA.063	20581	35600	0.59	0.984	0.329	166.421	0.264	36.008	0.131	60.882	0.279	46.885

Selected Reflectances

-FILENAME-	EAST	NORTH	500nm	590nm	610nm	780nm	900nm	1340nm	1410nm	1455nm	1465nm	1500nm	1650nm	2123nm	2165nm	2208nm	2232
AFLSBA.000	20797	35600	9.684	19.419	22.019	29.949	30.193	40.622	34.726	39.757	39.823	41.139	44.053	41.708	34.561	30.125	33.101
AFLSBA.003	20784	35600	9.657	19.338	21.866	29.925	29.832	36.443	34.260	35.755	35.886	36.931	39.193	37.120	31.295	27.877	30.450
AFLSBA.019	20756	35600	9.511	19.389	21.152	28.681	27.947	39.023	35.302	39.593	39.411	40.154	42.066	41.610	35.204	32.521	36.136
AFLSBA.033	20732	35600	9.153	17.641	19.165	25.694	25.198	36.821	33.064	37.230	36.975	38.098	39.640	38.748	32.512	30.006	33.449
AFLSBA.063	20581	35600	9.283	20.914	22.574	30.066	25.499	51.994	39.460	52.054	52.485	53.705	52.952	41.332	30.861	27.669	32.629

MT HOPE SOILS

SELECTED WHOLE SOILS FROM LINE 35600 mN

Selected Absorption Wavelengths, Depths and Widths

-FILENAME-	EAST	NORTH	Fe-S	Fe-A	0.9-D	0.9-W	1.4-D	1.4-W	1.9-D	1.9-W	2.2-D	2.2-W
AFLSAB.000	20797	35600	0.608	0.922	0.065	95.831	0.201	45.326	0.363	75.317	0.142	37.518
AFLSAB.003	20784	35600	0.608	0.916	0.073	108.558	0.214	47.216	0.372	76.697	0.148	44.233
AFLSAB.019	20756	35600	0.604	0.988	0.135	134.697	0.153	33.846	0.204	63.l370	0.167	43.589
AFLSAB.033	20732	35600	0.604	0.946	0.127	143.225	0.128	29.908	0.153	68.233	0.146	42.321
AFLSAB.063	20581	35600	0.600	0.988	0.308	168.354	0.268	33.779	0.216	60.354	0.242	43.857

Selected Reflectances

-FILENAME-	EAST	NORTH	500nm	590nm	610nm	780nm	900nm	1340nm	1410nm	1455nm	1465nm	1500nm	1650nm	2123nm	2165nm	2208nm	2232nm
AFLSAB.000	20797	35600	14.163	25.126	27.556	36.225	36.969	47.322	38.750	42.812	42.963	45.342	49.454	44.269	39.164	35.038	37.688
AFLSAB.003	20784	35600	12.200	22.197	24.697	33.094	32.931	41.241	33.279	37.124	37.220	39.225	43l.365	37.745	32.864	29.740	31.944
AFLSAB.019	20756	35600	10.004	21.634	23.753	32.412	31.l311	45.778	39.686	44.450	44.35	45.870	48.377	45.308	38.415	35.354	39.672
AFLSAB.033	20732	35600	9.759	19.795	21.637	29.869	29.854	45.318	40.162	44.807	44.940	46.035	47.963	45.062	38.918	36.351	40.030
AFLSAB.063	20581	35600	9.767	22.580	24.426	33.044	28.246	54.727	41.009	52.510	52.322	54.648	55.498	43.211	33.402	30.235	35.455

MT HOPE SOIL

Carbonate Experiment

SAMPLE	CALCITE	0.5-D	0.9-D	2.2-D	2.33-D	500nm	780nm	890nm	1650nm
AFLSBA.019	0	0.114	0.124	0.189	0.036	9.896	32.067	31.373	48.292
AFLSBB.019	5	0.086	0.093	0.145	0.026	14.483	37.668	37.112	52.169
AFLSBC.019	10	0.075	0.075	0.145	0.025	17.684	41.630	41.345	54.969
AFLSBD.019	15	0.062	0.078	0.133	0.027	20.649	44.465	44.101	58.453
AFLSBE.019	20	0.057	0.070	0.125	0.032	23.012	46.385	45.920	58.970
AFLSBF.019	25	0.046	0.057	0.102	0.035	27.488	50.440	49.937	61.564
AFLSBG.019	30	0.040	0.053	0.096	0.044	31.130	53.082	52.832	64.114
AFLSBH.019	35	0.036	0.047	0.091	0.044	34.928	58.157	58.111	68.794
AFLSBI.019	40	0.029	0.045	0.085	0.052	39.018	61.046	60.973	71.302
AFLSBJ.019	45	0.029	0.045	0.079	0.056	41.401	61.981	61.730	71.572
AFLSBK.019	50	0.029	0.040	0.078	0.065	42.536	63.430	63.323	73.031
AFLSBL.019	55	0.025	0.035	0.069	0.063	46.994	65.587	65.366	73.313
AFLSBM.019	60	0.019	0.029	0.070	0.076	53.027	70.481	70.591	77.480
AFLSBN.019	65	0.021	0.033	0.063	0.082	52.211	68.919	68.746	76.103
AFLSBO.019	70	0.019	0.030	0.061	0.082	54.653	72.168	72.260	79.275
AFLSBQ.019	75	0.016	0.025	0.057	0.092	59.560	74.707	74.748	80.853
AFLSBR.019	80	0.015	0.020	0.052	0.100	64.325	77.656	77.823	82.547
AFLSBS.019	85	0.015	0.023	0.051	0.112	67.571	78.502	78.089	82.259
AFLSBT.019	90	0.015	0.018	0.037	0.117	71.257	82.227	82.580	86.249
AFLSBU.019	95	0.015	0.015	0.015	0.127	75.936	82.575	82.449	84.641
AFLSBV.019	100	0.015	0.015	0.015	0.147	89.960	89.512	89.440	88.818

Mt HOPE

SUBSURFACE SOILS

-FILENAME-	EAST	NORTH	Depth (m)	Fe-S (nm)	FeA (nm)	1.50 (μm)	1.65 (μm)	1.4R	2.17 (μm)	2.23 (μm)	2.2R	1.9-D HQ
AFLSAA.128	20645	34960	00-01	592	884	40.4	43.6	1.08	39.1	36.8	1.06	0.313
AFLSAA.129	20645	34960	01-02	593	910	37.9	41.7	1.1	35.1	32.6	1.08	0.360
AFLSAA.130	20645	34960	03-04	605	882	45.5	49.0	1.08	41.8	40.3	1.04	0.303
AFLSAA.131	20645	34960	05-06	611	876	55.2	58.6	1.06	49.5	46.4	1.07	0.294
AFLSAA.132	20645	34960	35-36	-	-	38.5	41.7	1.08	45.0	43.8	1.03	-
AFLSAA.133	20676	34960	01-02	601	887	38.9	42.9	1.10	34.2	32.0	1.07	0.386
AFLSAA.134	20676	34960	01-02	600	888	56.9	60.5	1.06	44.0	42.3	1.04	0.314
AFLSAA.135	20676	34960	03-04	609	857	58.0	64.1	1.11	46.5	44.0	1.06	0.375
AFLSAA.136	20676	34960	05-06	609	863	63.3	69.8	1.10	49.6	46.5	1.07	0.376
AFLSAA.137	20676	34960	56-57	-	-	14.7	15.3	1.04	16.0	15.7	1.02	-
AFLSAA.089	20853	35800	03-04	595	900	22.9	25.1	1.10	17.2	17.5	0.98	0.371
AFLSAA.092	20817	35800	03-04	595	903	24.7	26.4	1.07	18.6	18.6	1.00	0.159
AFLSAA.098	20765	35800	03-04	598	896	31.7	34.7	1.09	23.9	24.3	0.98	0.369
AFLSAA.101	20742	35800	03-04	592	909	32.6	33.1	1.01	21.9	21.9	1.00	0.287
AFLSAA.104	20705	35800	03-04	595	902	29.9	32.7	1.09	22.5	23.0	0.98	0.373
AFLSAA.107	20680	35800	03-04	596	910	23.3	23.6	1.01	16.5	16.3	1.01	0.273
AFLSAA.001	20797	35600	02-03	600	900	23.7	27.4	1.16	15.5	15.3	1.01	0.498
AFLSAA.002	20797	35600	04-05	596	922	27.1	27.7	1.02	20.1	20.5	0.98	0.232
AFLSAA.004	20784	35600	02-03	600	901	24.1	26.4	1.09	18.4	18.8	0.98	0.373
AFLSAA.005	20784	35600	04-05	596	920	34.0	34.6	1.02	22.2	22.7	1.00	0.219

Mt HOPE

SUBSURFACE SOILS

-FILENAME-	EAST	NORTH	Depth (m)	Fe-S (nm)	FeA (nm)	1.50 (μm)	1.65 (μm)	1.4R	2.17 (μm)	2.23 (μm)	2.2R	1.9-D HQ
AFLSAA.128	20645	34960	00-01	592	884	40.4	43.6	1.08	39.1	36.8	1.06	0.313
AFLSAA.129	20645	34960	01-02	593	910	37.9	41.7	1.1	35.1	32.6	1.08	0.360
AFLSAA.130	20645	34960	03-04	605	882	45.5	49.0	1.08	41.8	40.3	1.04	0.303
AFLSAA.131	20645	34960	05-06	611	876	55.2	58.6	1.06	49.5	46.4	1.07	0.294
AFLSAA.132	20645	34960	35-36	-	-	38.5	41.7	1.08	45.0	43.8	1.03	-
AFLSAA.133	20676	34960	01-02	601	887	38.9	42.9	1.10	34.2	32.0	1.07	0.386
AFLSAA.134	20676	34960	01-02	600	888	56.9	60.5	1.06	44.0	42.3	1.04	0.314
AFLSAA.135	20676	34960	03-04	609	857	58.0	64.1	1.11	46.5	44.0	1.06	0.375
AFLSAA.136	20676	34960	05-06	609	863	63.3	69.8	1.10	49.6	46.5	1.07	0.376
AFLSAA.137	20676	34960	56-57	-	-	14.7	15.3	1.04	16.0	15.7	1.02	-
AFLSAA.089	20853	35800	03-04	595	900	22.9	25.1	1.10	17.2	17.5	0.98	0.371
AFLSAA.092	20817	35800	03-04	595	903	24.7	26.4	1.07	18.6	18.6	1.00	0.159
AFLSAA.098	20765	35800	03-04	598	896	31.7	34.7	1.09	23.9	24.3	0.98	0.369
AFLSAA.101	20742	35800	03-04	592	909	32.6	33.1	1.01	21.9	21.9	1.00	0.287
AFLSAA.104	20705	35800	03-04	595	902	29.9	32.7	1.09	22.5	23.0	0.98	0.373
AFLSAA.107	20680	35800	03-04	596	910	23.3	23.6	1.01	16.5	16.3	1.01	0.273
AFLSAA.001	20797	35600	02-03	600	900	23.7	27.4	1.16	15.5	15.3	1.01	0.498
AFLSAA.002	20797	35600	04-05	596	922	27.1	27.7	1.02	20.1	20.5	0.98	0.232
AFLSAA.004	20784	35600	02-03	600	901	24.1	26.4	1.09	18.4	18.8	0.98	0.373
AFLSAA.005	20784	35600	04-05	596	920	34.0	34.6	1.02	22.2	22.7	1.00	0.219